International
Progress Report

IPR-02-09

Äspö Hard Rock Laboratory

Two – phase flow in fractured crystalline rock

Investigations in Niche 2175

Lutz Liedtke
Irena Engelhardt
Marco Fiene
BGR

Klaus-Peter Kröhn
Herbert Kull
GRS

Hartmut Jakobs
CAB

Carsten Thorenz
Universität Hannover

December 2001

Svensk Kärnbränslehantering AB
Swedish Nuclear Fuel
and Waste Management Co
Box 5864
SE-102 40 Stockholm Sweden
Tel 08-459 84 00
+46 8 459 84 00
Fax 08-661 57 19
+46 8 661 57 19

Äspö Hard Rock
Laboratory

Report no.
IPR-02-09

No.
F60

Author
L. Liedtke, I. Engelhardt, M. Fiene, K.P. Kröhn, H. Kull, H. Jakobs, C. Thorenz

Date
Dec. 2001

Checked by

Date

Approved
Christer Svemar

Date
2004-03-09

Äspö Hard Rock Laboratory

Two – phase flow in fractured crystalline rock

Investigations in Niche 2175

Lutz Liedtke
Irena Engelhardt
Marco Fiene
BGR

Klaus-Peter Kröhn
Herbert Kull
GRS

Hartmut Jakobs
CAB

Carsten Thorenz
Universität Hannover

December 2001

Keywords: Two – phase flow, single – phase flow, modelling, hydraulic tests, fractured rock, Äspö

Foreword

This report describes performance and results of a joint project on two-phase flow in fractured rock carried out in the HRL Äspö under the leadership of BGR and GRS. Contributions were made by CAB of University Braunschweig, University Hanover, and WRE of Royal Institute of Technology, Stockholm. The authors acknowledge that the constitutive relationships for the simulations in Chapter 3.4.5 were provided by Jerker Jarsjö, WRE of Royal Institute of Technology. The work was supported by the Federal Ministry of Economics and Technology (BMWi) and the Swedish Nuclear Fuel and Waste Management Co (SKB).

The general objectives of the project were to advance the understanding of two-phase flow phenomena in saturated fractured rock and to improve the numerical tools for simulating and predicting the relevant processes associated with a geological repository for radioactive waste in crystalline rock. The work consisted of in situ investigations carried out in the HRL Äspö and of studies aimed at modelling two-phase flow behaviour in water saturated fractured rock.

The authors gratefully acknowledge the funding and the support for this project by their funding organisations. In particular, the authors express their appreciation to the staff of the HRL Äspö for the always friendly and helpful assistance throughout the project.

TABLE OF CONTENTS

EXECUTIVE SUMMARY

Background and scope

The Two-Phase Flow project was carried out at the HRL Äspö in the frame of the Project agreement between SKB (Sweden) and BMWi (Germany) under the leadership of BGR and GRS. Contributions to the development of numerical models were made by WRE of KTH, University Hanover, and CAB of TU Braunschweig. The project started on 1 January 1997 and it lasted until 30 June 2000. In 1996, a pre-study had been carried out which was aimed at selecting a suitable test site in the HRL Äspö. The general objectives were to improve the understanding of two-phase flow phenomena and processes in water saturated fractured rock and to advance conceptual models and computer programmes used to simulate two-phase flow associated with a geological repository located in crystalline rock.

Two-phase flow conditions in a repository and its surrounding host rock can result from a number of different gas generation/pressurization processes:

- corrosion of metallic materials,
- radiolysis effects,
- microbial processes,
- groundwater degassing due to pressure decrease,
- trapping air after closure of the repository.

The amount of gases generated in the repository and the significance of gases to repository performance depends on the disposal concepts, i.e., the host rock, the disposed waste, and the emplacement configuration. However, it has become apparent that in many concepts gas migration and two-phase flow may occur and these mechanisms may have an impact on the performance of the engineered and the natural barriers in and around a deep geological repository. Therefore, considerable efforts have been made in the past to understand two-phase flow processes and to provide modelling tools that will allow to simulate these processes and to assess their impact on repository performance. In the actual Two-Phase Flow project, the attempt was made to advance numerical models and to evaluate their predictive capability in combination with in situ experiments in which two-phase flow conditions were generated and investigated.

The in situ investigations were carried out in the HRL Äspö in a niche which had been selected in a pre-investigation project. The niche is situated between 354 and 360 metres below surface at tunnel metre 2715. In order to provide the conditions for single- and two-phase flow experiments, in the rock surrounding the niche the equipment was installed that was needed for conducting the experiments and suitable test configurations were selected. The in situ work consisted of the following steps:

- Determination of basic geological and hydraulic parameters
  - detailed geological mapping / macro scale
  - structural analysis / micro scale
- Determination of single-phase flow parameters
- Determination of two-phase flow and transport parameters

The in situ investigations also addressed more practical issues related to two-phase flow studies. Because experiments in this field still are difficult to conduct, the aim was to develop and improve the equipment for quantifying two-phase flow parameters and to advance the knowledge for performing such experiments.

In the modelling part of the project, different models were used to simulate the in situ experiments. The aim was to evaluate the capability of the models to predict two-phase flow in a saturated fractured crystalline rock and to improve the models on the basis of the experience gained during the project performance. The modelling work consisted of development and implementation of:

- 3D model for single-phase water flow (including transport aspects)
- 3D model for single-phase gas flow (including transport aspects)
- 3D model for two-phase gas-water flow
- 3D computer programme for gas flow and transport

The following codes were used: The finite-element code ROCKFLOW_SM2 version 2.22.03 was used to calculate single-phase groundwater flow. The code calculates hydraulic heads using the continuity equation for uncompressible fluids in combination with Darcy's law. The code MUFTE_thermo version 4 was used to calculate two-phase flow processes. In this code, evaporation, condensation, solution and dissolution are taken into account. Darcy's law is incorporated with the coupled continuity equations for the liquid and the gaseous phase. The other codes used for two-phase flow simulations were TOUGH2 with the EOS (equation-of state) modules 1 and 3 and the module MMTM of ROCKFLOW.

Results

In the experiments in the rock surrounding niche 2175, no threshold pressure for gas injection was detected. The reason for this finding is the high permeability ($k > 10^{-10}$ m^2) along the main flow path. On the other hand, in the experiments gas could not be forced from the fractures into the rock matrix because of the very high entry pressure of the undisturbed rock matrix. Therefore, it can be concluded that in a granitic rock like that surrounding the experimental site, gas transport will occur only in fractures where gas transport is not restricted by capillary pressure.

In preparing the experiments, different methods were applied for identifying open fractures. The highest level of correlation was achieved between borehole scanning results and seismic results. The potential of video surveys was limited due to the conditions in water-filled boreholes, and by analysing drill-cores it was not possible to determine the aperture width of open fractures. The advantage of the Borehole Image Processing System (BIPS) was found to be that by this method data fracture aperture and fracture orientation can be made available.

Modelling of the actual regional flow field shows that the rock matrix at Äspö does not contribute significantly to the groundwater flow and that the flow into the niche can be considered to be at steady-state. Water flow in the Äspö granite is therefore adequately represented by two-dimensional steady-state fracture flow.

Three models were developed to describe two-phase flow processes in the in situ experiments. One model provided predictions according to the designed test conditions and the other two models interpreted the GWTR6 gas water tracer test. Despite the use of different numerical codes and different input data the spreading of the gas phase could be reproduced in terms of breakthrough time and steady-state flow rates. Qualitative comparison of the calculated saturation distribution reveals additional similarities.

A new approach which virtually eliminates numerical dispersion from a fracture into the matrix was developed and tested. It allows more realistic representations of two-phase flow phenomena in a fractured porous medium like granitic rock than conventional continuum models. This applies especially to the entry of gas from a fracture into the rock matrix.

Theoretical work has been done concerning the means of upscaling two-phase flow parameters. The advantage of this approach is that the saturation dependent parameters are a function of measurable geostatistic data from the fractures. While the applicability of this method for practical purposes remains a subject for further investigations the necessary equations are derived and the influence of the new approach is demonstrated with the help of a principle example.

Conclusions

The results of the modelling exercise confirmed the following conclusions of earlier investigations into the groundwater flow in the Äspö host rock: The granite contains large scale fracture systems which are well interconnected. This overall fracture systems reaches from the Baltic sea down to the horizon of the Äspö HRL. In the test field, fracture apertures are too big to form a serious obstacle against gas flow. On the other hand, the entry pressure of the undisturbed matrix is very high. Therefore, it can be concluded that gas located in a fracture cannot enter the matrix even at gas generation rates as expected under the operating conditions of a repository. Thus, in a granitic rock like that at Äspö, gas transport is restricted to the fractures where gas flow is not hindered by capillary pressure. Gas production in a repository will therefore not raise the gas pressure in the host rock significantly above the hydrostatic level. Since it is not clear how and in what quantities gas will reach the host rock, further investigations will have to concentrate more on hydraulic conditions in the buffer material.

Abbreviations

BGR	Bundesanstalt für Geowissenschaften und Rohstoffe, Hannover
BMBF	Bundesministerium für Bildung und Forschung
BMWi	Bundesministerium für Wirtschaft und Technologie
CAB	Institut für Computeranwendungen im Bauingenieurwesen, Technische Universität Braunschweig
EDZ	Excavation damaged/disturbed zone
GRS	Gesellschaft für Reaktor- und Anlagensicherheit GmbH, Köln
GTHP	Gas Threshold Pressure (gas entry pressure)
HLW	High Level Waste
HRL	Hard Rock Laboratory
ILW	Intermediate Level Waste
KTH	Kungliga Tekniska Högskolan, Stockholm
KXP06	Specification of type and number of a borehole in the niche 2715
MUFTE THERMO	Fluid simulator code (Institut für Wasserbau, Universität Stuttgart)
MUFTE UG	Multiphase_Flow_Transport_Energy Model_Unstructured_Grid
NE1	Master fault zone at Äspö site, north-east orientated
PtWT+E	Projektträger für Wassertechnologie und Entsorgung , Forschungszentrum Karlsruhe
REV	Representative Element Volume
ROCKFLOW	Fluid simulator code (Institut für Wasserbau, Universität Hannover)
SKB	Svensk Kärnbränslehantering AB, Stockholm
TPF	Two-phase flow
V2	Subvertical ENE-WSW orientated master fault system in niche 2715
WELTEST 200	Fluid-flow simulator code (Schlumberger/Geoquest)
WNW-ESE	Westnorthwest – eastsoutheast (orientation)

1 Introduction

1.1 Background

In performance assessments for radioactive waste disposal, transport of radionuclides from the repository to the biosphere is a central issue. It is generally accepted that after repository closure groundwater is the only transport medium. Normally, at the repository horizon, several hundreds of metres below the water table, the rock formation is saturated and groundwater migrates under single-phase flow conditions. However, during repository construction and operation, gases will be produced and an elevated gas pressure may be built up. Therefore, at least in the rock surrounding the repository, two-phase gas-water flow may occur, and the presence of gas may considerably alter the hydraulic and transport properties of the rock. The main gas generation or pressurization mechanisms in a repository are

- corrosion of metallic materials,
- radiolysis effects,
- microbial processes,
- groundwater degassing due to pressure release,
- trapping air after closure of the repository.

Materials that may undergo corrosion in a repository are all the metallic components in waste packages and waste packagings as well as the structural components used for repository construction and operation. The corrosion rates strongly depend on the metal, e.g., iron, steel, copper, and on the corroding medium, e.g., groundwater, brine, oxygen. Corroding media may also originate from the waste product and the backfill. Physical parameters affecting corrosion are temperature, pressure, and radiation. A large number of corrosion studies have been carried out in the past (Rodwell, et al., 1999), most of them addressing container integrity over the long periods of time considered in safety analyses. In many of these studies also gas generation rates have been measured. The measurement results indicate large ranges in gas generation rates.

Radiolysis is the term for the decomposition of chemical substances due to radiation. Gas generation by radiolysis is characterized by the G value which gives the volume of gas generated in the mass of irradiated matter per absorbed energy dose. In a repository, radiolysis can be distinguished between internal radiolysis inside the waste packages and external radiolysis in the surrounding backfill material and host rock including groundwater or brine. Gas generation by internal radiolysis occurs mainly in LAW- and MAW packages. In LAW, because of the low energy dose, in comparison to gas generation by corrosion radiolysis can be neglected as a gas generation source. Only in MAW radiolytic gas generation may be significant. Due to the strong influence of the energy dose on gas generation, external radiolysis mainly will be significant in the vicinity of unshielded HAW canisters. In concepts including emplacement of shielded disposal canisters, radiolysis normally will be insignificant.

Gas generation by microbial degradation depends on a large variety of conditions. In the repository, microbes can exist in the groundwater even at great depths, and they can be brought into the repository in the waste packages, by the ventilation air, or by the operating personnel. Other preconditions for microbial activities are the availability of water and of organic material. Environmental conditions influencing microbial activity are pH value, temperature, oxygen supply, water salinity. The major gas components generated by microbes are CO_2 and CH_4, depending on the availability of oxygen. So far, only a few experiments have been carried out in this field and therefore it is difficult to quantitatively describe microbial gas generation.

Degassing is to be expected in deep groundwater systems where gases are dissolved under the hydrostatic pressure prevailing at the relevant depth. If due to tunnel construction and drilling the hydraulic pressure decreases to below the bubble pressure, degassing will occur and the gases will be released. The volume of the released gases depends on the gas content in the water and on the type of dissolved gases (oxygen, nitrogen, carbondioxyde, etc.) and their partial pressure. Therefore, gas-release predictions in quantitative terms require the knowledge of the relevant local conditions at the repository site.

From the discussion above it becomes obvious that both the amount of gases produced in the repository and the significance of the various gas generation mechanisms strongly depend on the repository concept. For example, in a repository in which thick walled copper canisters are disposed of, both gas generation by corrosion and by radiolysis will be very low, and mechanisms like microbial activity and degassing may become more important. In contrast, in a repository containing a large number of iron containers, gas generation by corrosion will be highly important. Another important boundary condition is the host rock in which the repository will be constructed and operated. However, independent of the repository concept, gas generation is an issue that has to be considered in repository performance assessments.

The significance of the effects of gas generation for repository safety is different in the disposal concepts. Effects on the movement of contaminated groundwater or on the transport of radionuclides to the biosphere will be important in water-saturated fractured host rock where potential mechanisms can be the pushing of water through open pathways due to gas bubbles or transport of groundwater in a stream of gas bubbles. Under these conditions, two-phase flow processes in the repository barriers will be significant. Another issue is the presence and encapsulation of oxygen near to the emplaced waste canisters, leading to enhanced corrosion and thereby impairing the container integrity. Overpressurization may become a problem in repositories in very tight host rock (e.g. rock salt). If the gases cannot escape and the gas pressure exceeds certain levels, fracturing of the barriers or the host rock may occur creating pathways through which radionuclides can be transported or through which after pressure decrease groundwater can enter into the repository.

Investigations into the two-phase flow of water/gas fluids through porous media have been carried out in the past in various engineering disciplines including chemical and civil engineering, exploration of natural resources like oil and gas, and soil science. For calculating the phenomena associated with two-phase flow, a number of constitutive relations have been set up based on basic laws developed earlier.

Darcy's law is generally used to describe slow single-phase flow through a porous medium. For modelling two-phase flow, various additional effects have to be taken into account. In gas flow in low-permeability media or at low pressures, the permeability increases according to the Klinkenberg relation and the Knudsen diffusion may become significant. The solubility of a gaseous phase in the liquid phase is described by Henry's law. The relationships between capillary pressure and water saturation are represented by the Brooks-Corey or the van Genuchten models in which capillary pressure is a function of the effective liquid saturation. Both models are used for calculating the capillary pressure and the relative permeability, and their application to various types of porous media has been validated by laboratory experiments (Marschall et.al, 1999). Originally, these constitutional relations predominantly have been developed for continuum flow conditions dominating in soil. Where, like in the work presented in this report, two-phase gas-water flow occurs in fractures, additional difficulties arise and the predictive capability of the models developed for flow in soil is limited (Jarsjö et al., 2001). To address these difficulties, attempts have been made to model single- and two-phase flow in fractured porous media. They are presented in detail in Chapter 3.

A number of studies have been conducted not only for developing flow models in various rock types, but also for calibrating these models by comparisons of modelling results with experimental findings. Such studies have been made notably in Underground Research Laboratories operated for investigating phenomena associated with radioactive waste disposal. As far as fracture flow is concerned, research has been carried out in Stripa (Olsson, 1992), Grimsel (Marschall et al, 1999), and Äspö (Jarsjö, Destouni, 1998). A comprehensive compilation of the aspects of gas generation, gas migration and two-phase flow that are relevant to geological disposal is given in Rodwell et al.(1999).

The work in the actual Two-Phase Flow project addressed the questions of how gases in a repository in water-saturated fractured rock will affect groundwater flow and radionuclide transport by creating two-phase flow conditions, and how gases will flow through water-saturated fractures. The work consisted of in situ investigations, carried out in a niche about 355 metres below the surface in the HRL Äspö (Chapter 2 of this report), and of modelling activities aimed at evaluating the capability of existing models by comparing modelling results with the results from the in situ investigations (Chapter 3).

1.2 Project objectives and scope

The objectives of the Two-Phase Flow project were

- to develop further models for simultaneous gas and water flow in fractured rock and to calibrate the models against the results of field tests,
- to generate a data base on important phenomena associated with two-phase flow in fractured rock,
- to develop and test the equipment for quantifying two-phase flow parameters,
- to gain experience in conducting two-phase flow experiments in pressurized water-saturated fractured rock.

To achieve these objectives, the niche at tunnel metre 2175 in the HRL Äspö was prepared for field experiments, and experiments were carried out in order to determine at first single-phase flow parameters and then two-phase flow parameters. In parallel, modelling was performed aimed at improving computer models for calculating single- and two-phase flow. The modelling results were compared with the results of the experiments carried out in the niche.

1.3 Project organization

The Two-Phase Flow project was carried out in the frame of the Project Agreement between BMWi (Germany) and SKB (Sweden) covering the cooperation in the Äspö Hard Rock Laboratory. This agreement was concluded for the years 1995 to 1998 in July 1995 and extended for the years 1999 to 2002 in December 1998. The project started on 1 January 1997 and it lasted until 30 June 2000. In 1996, a pre-study was carried out which was aimed at selecting a suitable test site in the HRL Äspö and at preparing the site (niche 2175) for conducting the experiments (Flach et al., 1997).

The project was a joint undertaking carried out under the leadership of GRS and BGR and funded by BMWi. GRS and BGR conducted both in situ experiments in the HRL Äspö and modelling activities. Contributions to the modelling work of the project were made by KTH (funded by SKB), University of Hanover, and CAB of Technical University of Braunschweig.

The work was subdivided into the following tasks:

I: In situ experiments in Niche 2175, presented in Chapter 2

- Ia: Determining the geological and hydraulic parameters
  - detailed geological mapping / macro scale
  - structural analysis / micro sacle
- Ib: Determining single-phase flow parameters
- Ic: Determining two-phase flow and transport parameters

II: Model development, presented in Chapter 3

- IIa: 3D model for single-phase water flow (including transport aspects)
- IIb: 3D model for single-phase gas flow (including transport aspects)
- IIc: 3D model for two-phase gas-water flow
- IId: 3D programme for gas flow and transport

2 In situ investigations

2.1 Overview

The primary objective of the in situ experiments was to provide field data required for calibration of numerical models used for simulating one- and two-phase flow. The following goals were set up:

- to develop a geological structural analysis in the micro scale of fracture systems and the petrophysical properties of the rock mass,
- to determine the distribution of hydraulic pressure and effective flow parameter values for a single fracture and the surrounding rock mass including the gas threshold pressure measurements on fracture and matrix,
- to determine the two-phase flow and transport parameters.

2.2 Geology

Äspö is dominated by a 1.75 billion year old intrusion of the Småland granite and is thus part of the Precambrian basement of Sweden (Rhén et al., 1997). The Småland granite intrusion contains major inclusions of older, dark, fine-grained rocks of volcanic origin (greenstones) and basic rocks (gabbro and diorite). Around 1.4 billion years ago, a red granite intruded the basement in the form of veins. These veins have an average size of 1.5 to 5 m. However, veins with a thickness of 30 m have also been mapped.

The slight foliation of the rock in a NE to ENE direction is attributed to the first deformations. The main fracture zones have an orthogonal network with strike directions of N-S, E-W and NE-SW.

The tunnel cuts through four different types of rock. The dominant rock types are the Äspö diorite and the Småland granite. The greenstone and the fine-grained granite only occur in small amounts in the tunnel.

The Äspö diorite is a dark-grey to red-grey, medium-grained granodiorite with red potash feldspar inclusions. The potash feldspar crystals have a length of approx. 0.5 to 1.0 cm. However, crystals up to 4 cm have been found. The diorite has been dated to around 1.803 billion years, and is thus of similar age as the Småland granite.

The Småland granite or Ävrö granite is medium-grained, porphyritic and has a composition varying between granodiorite and quartz monzonite. The potash feldspars are irregularly distributed. The Ävrö granite partially cuts through the Äspö diorite and therefore appears to be of younger age. Dating gives an age of 1.802 ± 4 billion years and is therefore almost the same age as the Äspö diorite with 1.804 ± 3 billion years.

The greenstones are fine-grained as well as medium to coarse-grained (diorite or gabbro). They differ from the granitoids by their grey to dark-grey colour. They occur as small intrusions and are themselves often penetrated by aplite granite veins.

The fine-grained granite is a brittle, red to light red-grey granite with a large proportion of quartz and potash feldspar. Unlike the Småland granite, its composition reflects that of a "true" granite. The fine-grained granite mostly occurs in veins in the Äspö diorite or the Småland granite. However, veins also cut the fine-grained granite. It has been dated at 1.794 billion years. The Äspö diorite is grading into the fine-grained granite. The typical chlorite banding of the fine-grained granite is clearly visible.

Table 2-1. Mineral composition of the Äspö diorite and the fine-grained granites /Wikmann, Kornfält, 1995/

Mineralogy:		Äspö Diorite	Fine-grained granite
	porosity (vol %)	0.5 (+/- 0.2)	0.3 (+/- 0.2)
	mineral comp. (vol %)		
	quartz	15	30
	K-feldspar	12	39
	Plagioclase	46	20
	Biotite	15	2
	Muscovite	0.5	3
	Epidote	6	2

2.3 Geological characterization of the test site

The aim of the geological characterization was to map all of the fractures around niche 2715 and the surrounding area, and to classify them according to their hydraulic importance. This was necessary because a hydraulically highly effective fracture with as few intersets and branches as possible was needed for the two-phase experiment.

For orientation and for location surveying, a net with a 1x1 metre grid was attached to the walls and the floor of the niche to facilitate the surface mapping. It was only possible to map parts of the roof because due to mining safety requirements the roof had been sprayed with shotcrete and hidden by tarpaulins to prevent water dropping. The mapping of the niche was carried out from November 1997 until February 1998.

Äspö diorite and fine-grained granite cropped out in the area of the niche. There are also some younger pegmatitic veins which cut through both of these rock types. Because the lithology is of no direct significance for the position of the fracture, and thus also for the position of the subsequent boreholes, no detailed description of the outcropping rocks was carried out.

The fractures were differentiated into vertical fractures which were often open, and horizontal fractures which were mostly sealed. Mapping included all fractures with an outcrop length of at least 50 cm. Fractures considered to be caused by excavation of the niche were not mapped. The origin of these fractures was indicated by the absence of any fracture filling or their immediate proximity to blast holes.

The following parameters were selected to describe the fractures (Table 2-2):

Table 2-2. Parameters for describing the fractures

Parameter	Description	Comments
Type	Fracture, fault, contact, mylonite	
Form	Smooth, undulating, straight, veined, bent	
Azimuth and dip	(degree)	
Length	(m)	
Fracture filling	Mineral name	
Transition to surrounding rock	Sharp, diffuse	
Alteration	None, weak, medium, strong, complete	
Aperture	(mm)	
Form of fracture surface	Smooth, rough	
Degree of separation	1	Fracture completely traceable and healed by fracture minerals, or fracture trace only visible as a line without morphological breaks
	2	Fracture trace partially broken up or not continuously traceable, some elements are correlatable
	3	Fracture largely separated and free of minerals, or only a few joins associated with mineralisation which in some case may themselves be separated
	4	Fracture completely separated and open. No healing by fracture minerals or these are themselves separated
Water bearing and/or description of the water flow	Dripping or flowing, wide spread or localised	

The migration paths for gases and liquids in crystalline rocks are primarily associated with fractures. Matrix permeabilities are only of secondary importance. Therefore, the description of the fractures was done in a way which allowed the subsequent hydraulic classification of the fractures. Hydraulic classification involved the parameters: fracture length, fracture aperture or degree of separation, surface and flow rate.

In the rock around the niche, a total of 15 horizontal fractures and 14 vertical fractures were mapped and are classified as follows:

Table 2-3. Orientation values and average fracture spacing of the fracture systems

Fracture system	Average fracture spacing
S1 (44/85)	approx. 2 m
S2 (224/86)	approx. 2 m
S3 (112/77)	approx. 4 m
L1 (299/10)	approx. 1 m

Because of the very steep dip of the S1 and S2 systems, it was assumed that they can be bundled within a single system. Therefore, in the following the systems S1 and S2 are jointly described as S1.

The mapped fractures have outcropping lengths between 0.1 and 12 m. Most fractures have an outcrop length of 1 to 3 m and therefore only have a minor impact on the hydraulic regime of the niche. The distribution of the outcropping length is shown in Figure 2-1. The average spacing of the fractures in any system is 1 to 4 m (Table 2-3).

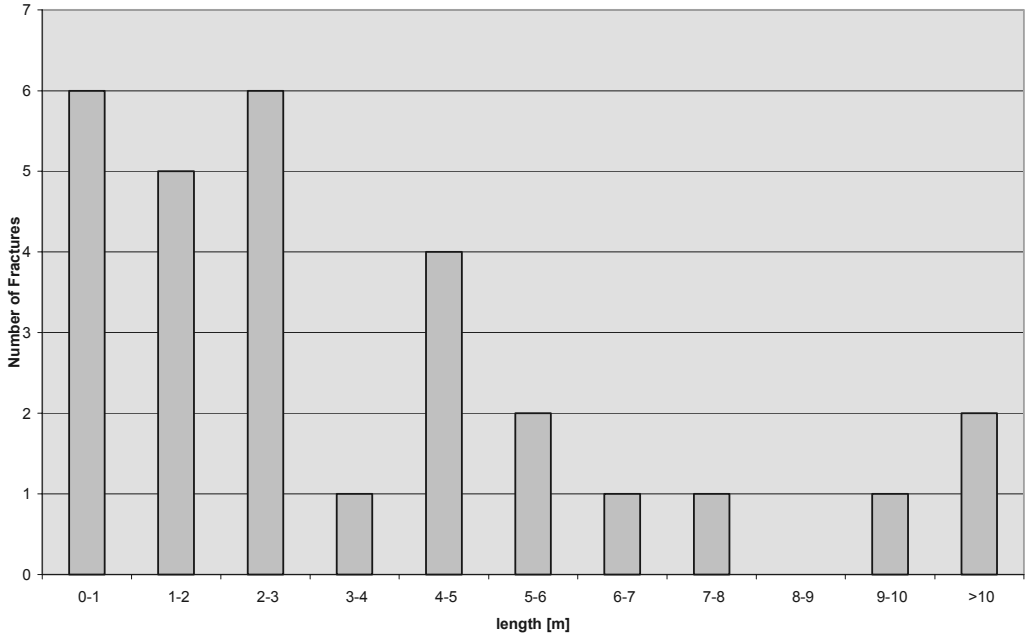

Figure 2-1. *Fracture length distribution diagram in the area around the niche*

In order to select the hydraulically most effective fracture, the fractures within and around the niche were classified (Table 2-4). In the weighting, particularly the level of separation and the fracture aperture were taken into account (Liedtke et al., 1999).

Table 2-4. Weight classes

W1	The aperture is smaller than 0.5 mm with a degree of separation of 1
W5	The aperture is 0.5 mm with a degree of separation larger than 1
W10	The aperture is 0.5 to 1 mm with a degree of separation larger than 1
W20	The aperture is > 1 mm with a degree of separation larger than 1

The diagram (Figure 2-2) only shows fractures with a weighting > W10. On account of its position, geometry and hydraulic effectiveness, vertical fracture V2 was considered to be optimal for the planned dipole for the two-phase experiment. This fracture was penetrated by some boreholes. The V2 fracture system consists of 1 to 4 separate fractures which are interconnected by branches and parallel fractures (steps and splays). The fractures have an azimuth of 30 to 50 ° or 210 to 230 ° degrees with dips of 84 to 90 ° and are assigned to the S1 system. The fracture filling consists of calcite and chlorite. The in situ aperture of separate fractures is 1 to 2 mm which was measured in the borehole by borehole scanning using the BIPS method.

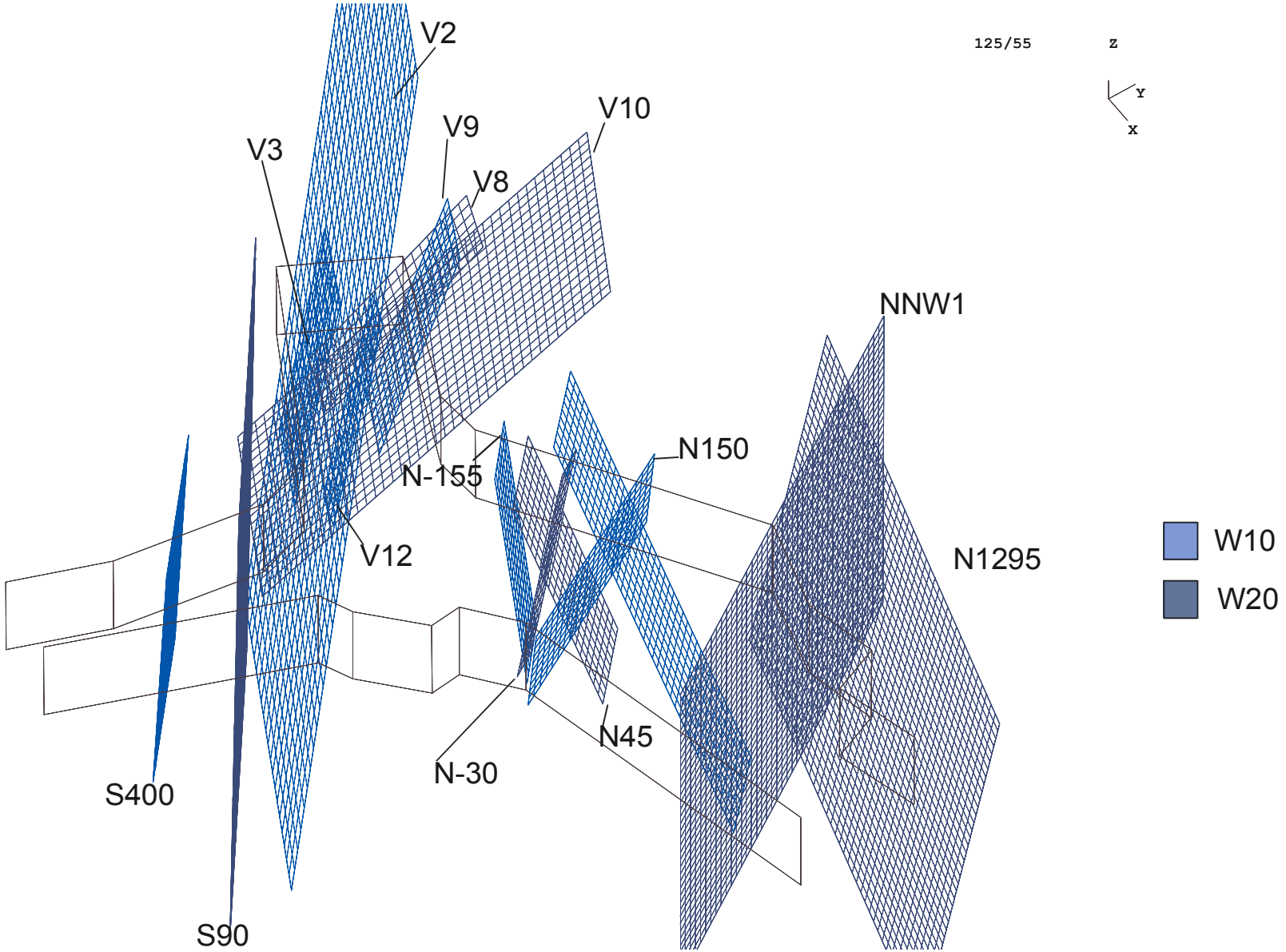

Figure 2-2. *Hydraulically most effective fractures at the test site*

The evaluation incorporated a total of 426 separate measurements from the mapping of the niche, the surrounding tunnel area, and from the boreholes. An overall evaluation of all the fractures only revealed the presence of the S1 and L1 systems. The S3 system only occurs in a very subordinate way in the overall evaluation. This system was only observed in the fractures which were penetrated by boreholes.

Four boreholes (KXP24BGR to KXP27BGR) were drilled in summer 1998 to access the V2 fracture system. The boreholes were drilled as pairs, two inclined upwards and two inclined downwards. One each of these pairs of boreholes penetrates the fracture close to the tunnel wall (approx. 3.5 m from the wall) whilst the other two boreholes penetrated the fracture in a distance of approx. 7 m from the tunnel wall. The borehole sections are shown in the appendix.

The pressure measurements in the older boreholes KXP04-07GRS, which penetrated the V2 fracture system and were separated with packers, showed clear drops in pressure during drilling of the new boreholes, thus confirming that all of the new boreholes had penetrated the V2 fracture system. After reaching the V2 fracture, the boreholes were lengthened by approximately 1.5 m.

Once the drilling had been completed, the boreholes were optically surveyed. The work was carried out by MILO Geoscience AB using the BIPS surveying system (Borehole Image Processing System) manufactured by Raax. This method uses a 360 ° frog-eye lens and provides an optical image of the borehole with a resolution down to 1 mm. The main advantage of this method is that it allows the direct in situ measurement of fractures, and unlike core analysis, allows reliable observations to be made on the apertures of the fractures.

The fracture photographs from the BIPS survey were used to analyse the fracture conditions only within the dipole because any influence caused by tunnelling on the fracture apertures could be completely excluded. A comparison of the predominant direction of the closed fractures and the open fractures shows that only vertical fractures can be considered as potential migration paths for liquids or gases because no open horizontal fractures were identified in the density diagram of open fractures. However, unlike the results of the mapping, this does reveal the possibility of intersections between the S3 system and the S1 system, which means that hydraulically effective lateral connections to the V2 fracture can be expected. The BIPS results clearly show that there are some parallel fractures to the V2 fracture and that intersection as a result of steps and splices cannot be excluded or is very likely. The apertures of the V2 fracture are 1 to 2 mm.

The BIPS scanning photographs show that the upward inclined boreholes differ tectonically from the downward inclined boreholes. This becomes particularly clear when considering the relationship between the open and the closed fractures.

Table 2-5. Ratio of open to closed fractures and fracture spacing in the boreholes

Borehole	Ratio between opened and closed fractures	Average fracture spacing of the open fractures, (m)
KXP24BGR (+dip)	0.9	0.57
KXP25BGR (-dip)	0.2	1.1
KXP26BGR (+dip)	0.8	0.48
KXP27BGR (-dip)	0.3	1.69

The ratios in boreholes KXP24BGR (0.9) and KXP26BGR (0.8) show that the ratio between open and closed fractures is virtually 1:1. In boreholes KXP25BGR and KXP27BGR, the ratio is 1:3 or 1:5. The different fracture frequencies in the boreholes is clear in the average fracture spacing of the open fractures.

Comparison of the borehole surveying methods

The borehole surveying methods (video, seismic and borehole scanning) and the core descriptions to identify open fractures enable a comparison of the results of the various methods.

As shown in Figure 2-3, the highest level of correlation is achieved between the borehole scanning results and the seismic results. The video survey only identified water bearing fractures. Video logging was only carried out in the upward inclined boreholes because the camera was not watertight. Because the core descriptions were based on extracted cores, no data could be gained on the aperture width of open fractures. This comparison also reveals that a large number of the open fractures in the core are attributable to fracturing during drilling or are resulting from core extraction.

The advantage of borehole scanning using the BIPS method compared to conventional core descriptions is that it enables to record data on thickness, aperture and fracture orientation. Some information can also be gained on the minerals filling the fractures.

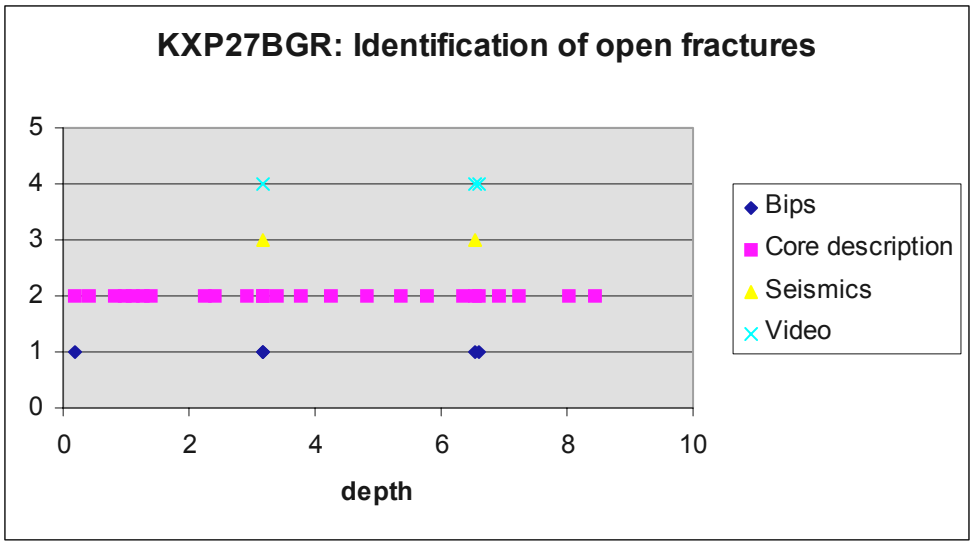

Figure 2-3. *Comparison of the methods used to identify open fractures*

2.4 Hydrological characterization of the test site

Electrical conductivity measurements were carried out in the downward inclined boreholes to gain an initial understanding of the inflow zones. The measurements involved flushing out the boreholes with mains water until no further decrease in the conductivity of the outflowing water was registered. Subsequently, a conductivity probe was run from the end of the borehole to the borehole opening. The conductivity log is shown in the diagram below (Figure 2-4).

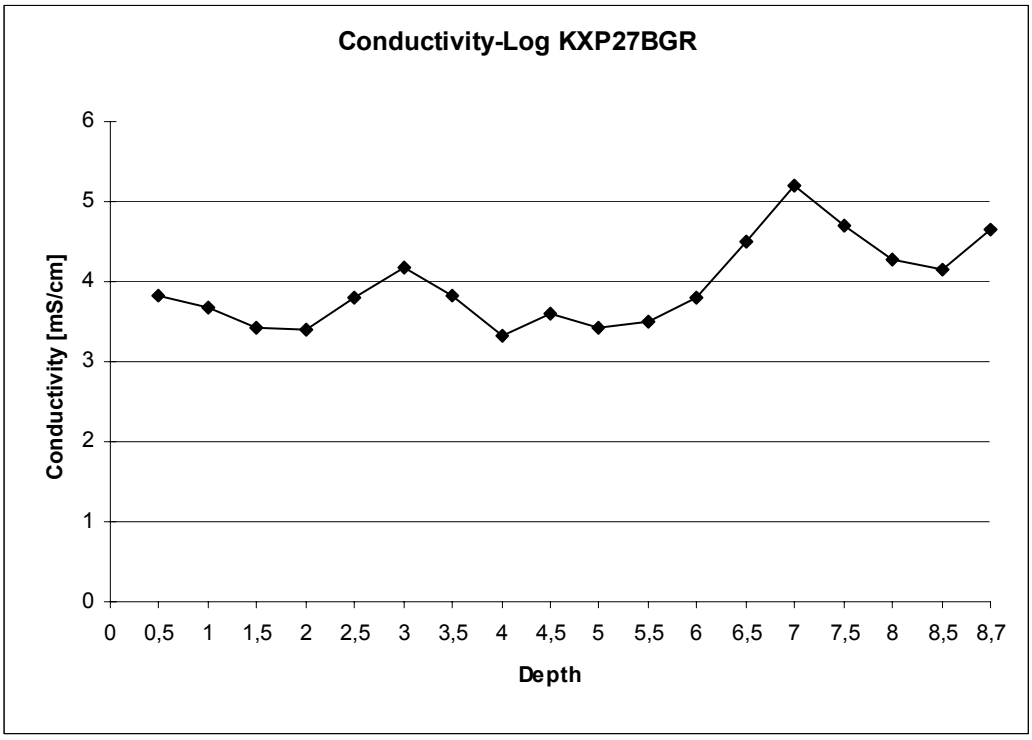

Figure 2-4. *Results of the liquid conductivity measurements KXP25BGR and KXP27BGR*

The results from borehole KXP25BGR can be well correlated with the results of the borehole scanning. A comparison of the conductivity log with the borehole scanning in borehole KXP27BGR reveals that the zones identified in the conductivity log are in each case 50 cm too deep. It is possible that the conductivity logging was carried out too slowly so that mixing of the formation water with the mains water had already taken place. The increase in conductivity recorded in each case at the base of the boreholes is attributable to the inadequate flushing of formation water and mains water.

From a hydrological point of view, the test site can be described as follows: The test site is at a depth of 354 to 360 m below sea level at tunnel metre 2175. The niche has a surface of approx. 40 m^2 and a volume of approx. 210 m^3. The average temperature is 13 °C with an air humidity of 98 %. The distance to the next experiment (TRUE) in the tunnel is about 150 m.

Many drip sites within the niche were drained for discharge measurements (Figure 2-5). The whole of the outflow from the niche was drained at measurement point MP6 to record the total flow from the niche. The measured electrical conductivity within the niche of approx. 33 mS/cm is very high, as expected for juvenile water. The total flow of 1.9 l/min was largely assigned to the V2 fracture system. No change in the overall flow was recorded during the hydraulic tests.

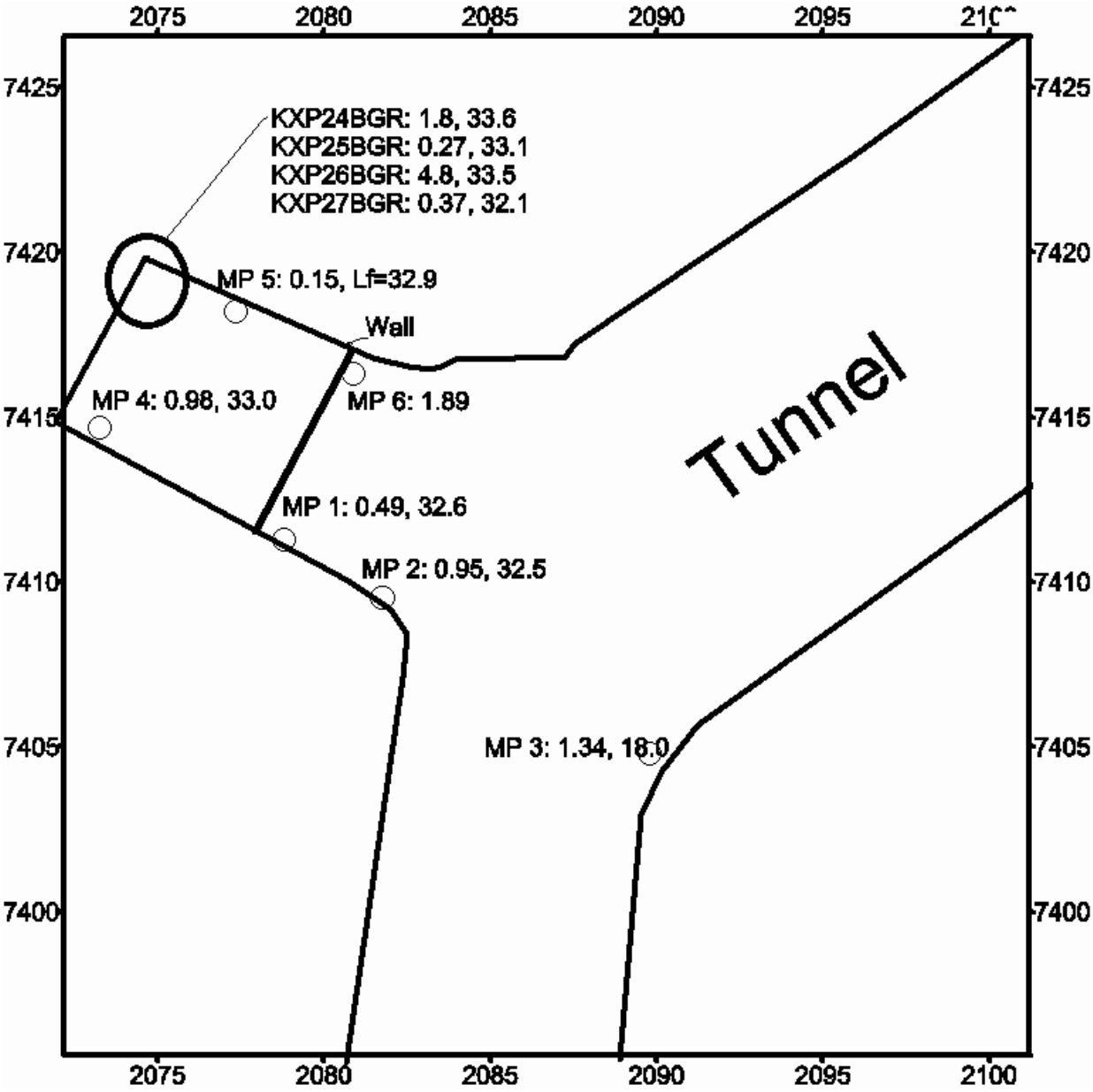

Figure 2-5. *Measurement point (MP) of the drip sites with measured outflow (l/min) and electrical conductivity (mS/cm), KXP24BGR: 1.8 (l/min), 33.6 (mS/cm)*

2.5 Seismic in situ measurements

2.5.1 Objectives and location

The knowledge of the petrophysical parameters of small scale fractures as well as their geometry is important for understanding and modelling gas and fluid transport phenomena within fracture systems. The detection was conducted using in situ seismic methods.

The measurements were performed in four boreholes (KXP24BGR, KXP25BGR, KXP26BGR and KXP27BGR) with diameters of 86 mm and inclinations between 15° and 17°. The length of the boreholes ranges from 4.4 m to 8.6 m (cf. Figure 2-6). The accessible depth of borehole KXP27BGR was reduced by several tens of centimetres as a result of water influx.

	Length [m]	Dip [°]
KXP24BGR	4.4	17.1
KXP25BGR	4.5	-15.6
KXP26BGR	8.35	17.6
KXP27BGR	8.61	-15.0

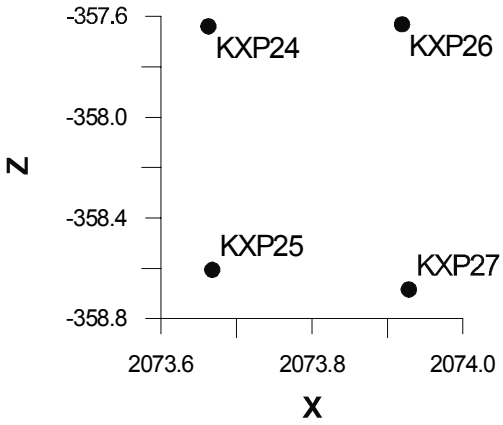

Figure 2-6. *Configuration of boreholes in niche 2715*

2.5.2 Methods

The seismic interval velocities were measured successively in steps of 10 cm along the borehole, with the exception of some zones where steps of 2 cm and 5 cm were chosen. A borehole probe with one source and three receivers was used. The measurements started at the borehole mouth or at the end of the borehole, depending on whether water influx was present or not. Then the probe was moved progressively in steps of 10 cm, 5 cm or 2 cm. The source and receiver were orientated upwards. This method reveals the seismic velocity as a function of distance from the tunnel wall. The advantage of this method is that the length of the ray path is independent of the measuring depth. Thus the signal to noise ratio and the frequency content of the signals neither depend on the depth nor on absorbing discontinuities outside the actual interval. Therefore, the measurements only reflect the conditions within the measuring interval. This is especially advantageous for the detection of fractures along the borehole.

In addition to the interval velocity measurements, cross hole measurements between some of the boreholes were also carried out. In this case the source is located in one borehole and the receivers in a different borehole. Both source and receivers are positioned at several depths. The quality of this type of data depends largely on the size of the collected data set. A seismic tomographic inversion can be carried out with densely spaced large data volumes, involving very time consuming data acquisition. In our case, the evaluation of the rather sparse data was used to support interpretations with respect to the connectivity of fractures between the investigated boreholes.

2.5.3 Results

With the BGR mini-sonic probe, a piezoelectric transducer is used as a seismic source. Three piezoelectric transducers at distances of 10, 20 and 30 cm to the source are used as receivers. The transducers were coupled to the borehole wall by pneumatic cylinders. This method showed strong and reproducible force coupling without using any coupling paste.

Different pressures for the force coupling of the source and receivers were tested. Good results were achieved with a pressure of 8 bar. This pressure was used for all the measurements discussed here. The quality of the received signals are strongly site-dependent, this includes of course the rock itself but also environmental conditions (humidity, noise).

Figure 2-7 presents the results. Fractures found by seismic interval velocity measurements are indicated with rectangles whereas anomalous zones are indicated by bold lines. Only the x-coordinate is relevant for this data. Additionally, results from the application of Borehole Image Processing System (BIPS) scans are plotted (diamonds and crosses). Crosses are related to the right y-axis. Zero values correspond to closed fractures, and a value of one represents open fractures. The width of the fractures (diamonds) varies between 1 and 8 mm and can be read on the left y-axis.

The 8 mm wide fracture detected by BIPS measurements in borehole KXP27BGR will be highlighted as an example to stress the depth determination problem. The midpoint of this fracture is plotted at 5.69 m. According to the video scan, this fracture intersects the borehole at a shallow angle. The seismic sensors which were directed upwards therefore detected this fracture at a greater depth, most probably at 6.2 m, as the beginning of the indicated anomalous zone. Additionally, the previously discussed uncertainty of ± 5 cm due to the source-receiver spacing of 10 cm has to be considered.

The above mentioned uncertainties in depth determination have to be taken into account for a comparison of both data sets (BIPS and seismic). In general, a good correlation can be seen, especially when we focus on open fractures and closed fractures with a width greater than 2 mm.

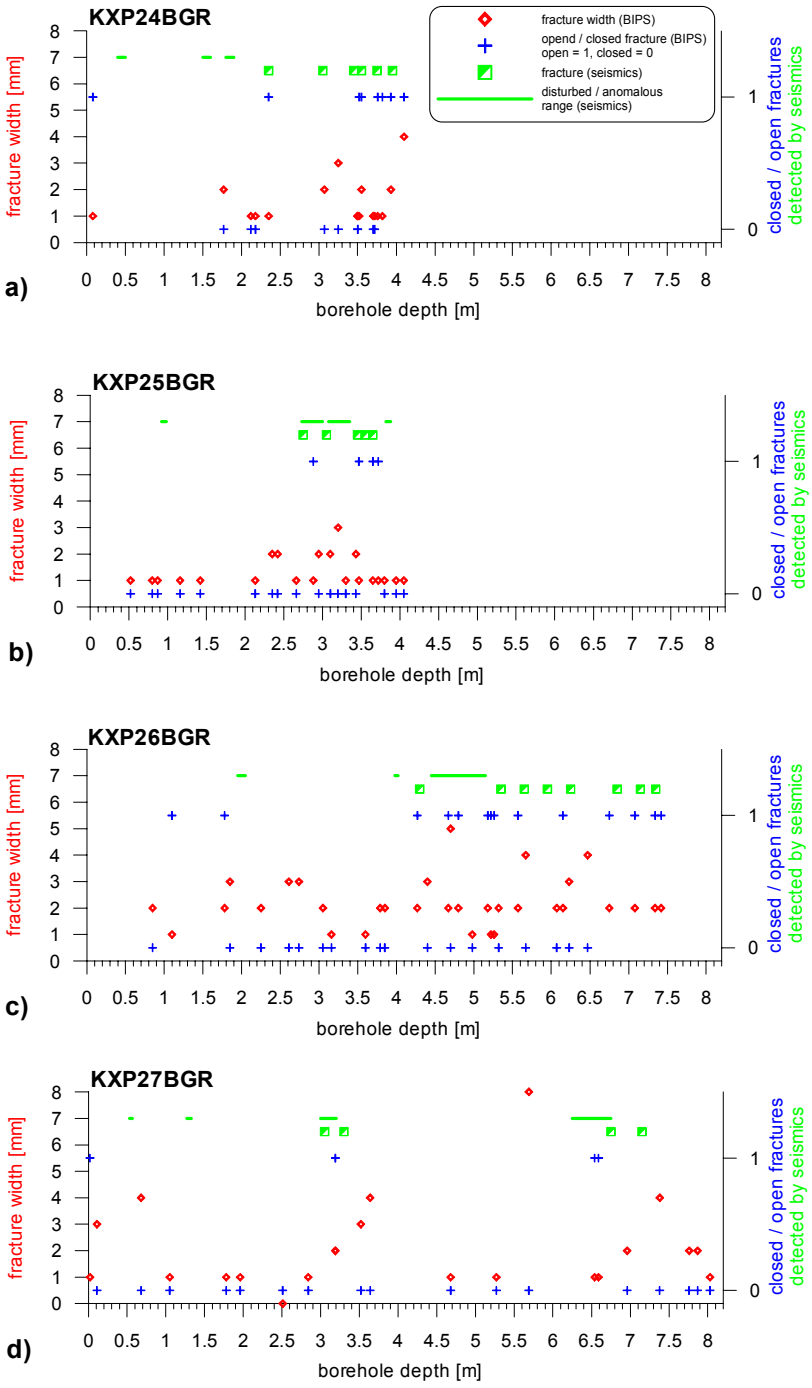

Figure 2-7. *Results of the seismic in situ measurements*

2.6 Single-phase flow parameters and gas entry pressure

The hydraulic pressure distribution, the effective hydraulic gradient and the fracture transmissivity/permeability were measured in the near-field. Extensive gas threshold pressure tests were carried out to measure the gas entry pressure and to determine the best configuration for the gas tracer tests on a dipole test.

2.6.1 Initial pressure distribution

The initial pressure distribution is determined from long-term pressure measurements in the fractures and the rock matrix. Considering the overburden, a maximum pressure of 3.5 MPa was expected.

The monitoring data indicate a steady-state pressure distribution lower than expected. Directly behind the front face a pressure of about 500 kPa was measured indicating an influence by the excavation (Figure 2-8). Beyond the excavation damaged zone the pressure increases steeply to 1,800 kPa within a few decimetres and then increases only slightly to 1,900 kPa at about 4 m depth.

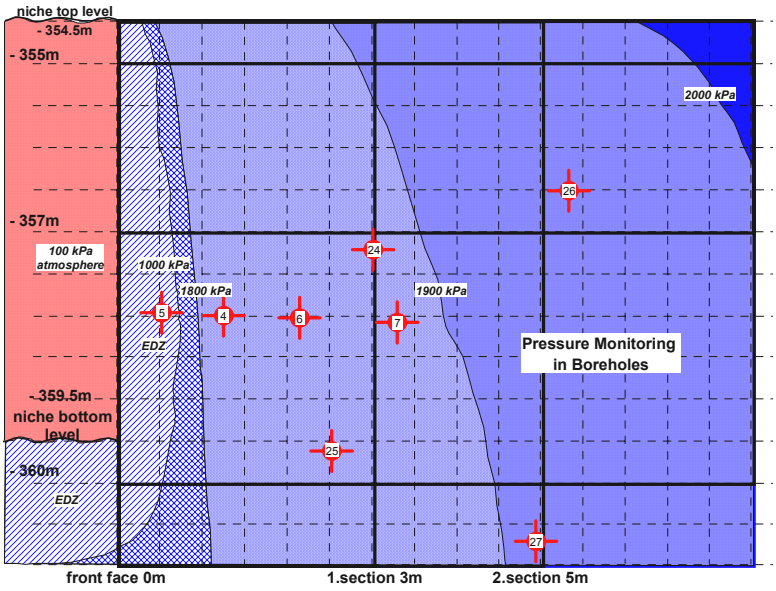

Figure 2-8. *The initial pressure distribution in a vertical section of the V2 fracture*

A possible explanation for the pressure drop within the excavation damaged zone is the decrease of fracture permeability caused by a post closure of the fracture itself.

2.6.2 Fracture transmissivity, aperture, permeability

The transmissivity was estimated from flow tests which were evaluated assuming validity of Darcy's law in the complex V2-fracture network. For empirical calculations laminar viscous flow conditions within the fracture were assumed. The flow field was considered to be a homogeneous isotropic confined aquifer. The calculated transmissivity values T were in the range from 10^{-9} to 10^{-6} m^2 s^{-1} (after Thiem, 1906). The relatively wide range of the values determined for the hydraulic V2-structure leads to the statements that:

- the natural variation of transmissivities in the single fault systems vary by orders of magnitudes,
- favoured flow paths are obviously within the fracture,
- anisotropy of the effective aperture of the fracture influences the water flow.

In approximation to the "cubic law" (Witherspoon et al., 1980), taken to describe the transmissivity of the fracture between two plates and the hydraulic conductivity K, the apparent aperture b values were derived. They range between 0.00002 m and 0.0005 m and the corresponding hydraulic conductivities range between 10^{-4} and 10^{-6} m s^{-1}.

To estimate the permeability k of the V2-fracture, complementary numerical simulations of the flow tests were performed (Weltest, 1997). Assuming homogeneous flow conditions, the simulations of the flow and the following pressure recovery period were performed. The evaluation of the simulation results of borehole KXP07 revealed a permeability of the V2-fracture of approximately 10^{-14} m².

2.6.3 Gas entry pressure

Gas injection testing in packered boreholes was used to determine the Gas Threshold Pressure (GTHP) and gas mobility in fractured and homogeneous tight rock (Figure 2-9).

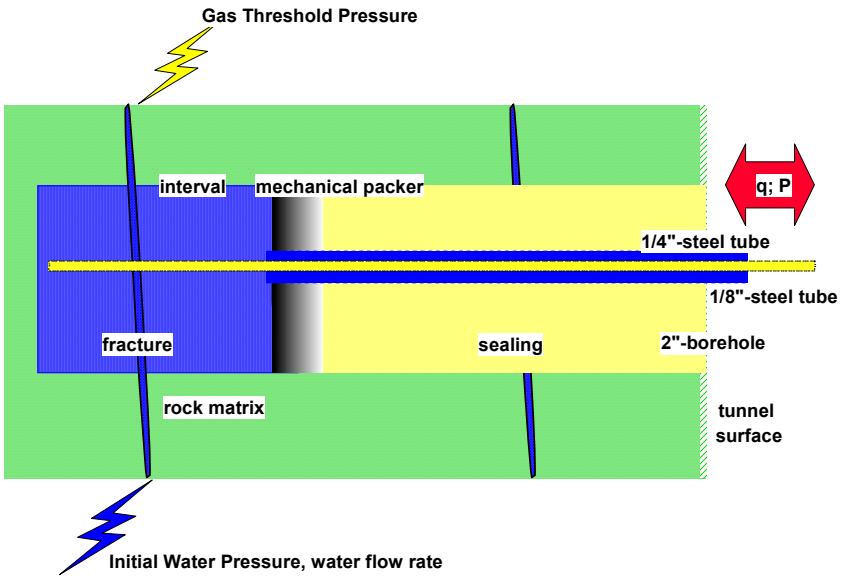

Figure 2-9. *Scheme of gas threshold pressure tests*

GTHP is one of the relevant parameters controlling gas and water flow in fractured crystalline rock. By definition, GTHP (or gas entry pressure) describes the pressure which is necessary to replace the wetting phase (e. g. water) by the non-wetting phase (e. g. gas) in a fully water saturated pore volume. Due to the surface tension and the size of pore spaces, GTHP can be orders of magnitudes higher than the initial hydraulic water pressure. Fractures with an aperture (width) in the range of millimetres normally have a negligible GTHP. To generate an advective gas flow in the interacting matrix the gas pressure must be much higher.

Results of gas threshold pressure measurements indicate no restrictions for gas entry into the water bearing V2 fracture (Figure 2-10). In matrix intervals gas was injected up to 5.0 MPa, being the limit of the test equipment. From the very low pressure decrease after shut-in it was concluded that the GTHP must be much higher than 5 MPa.

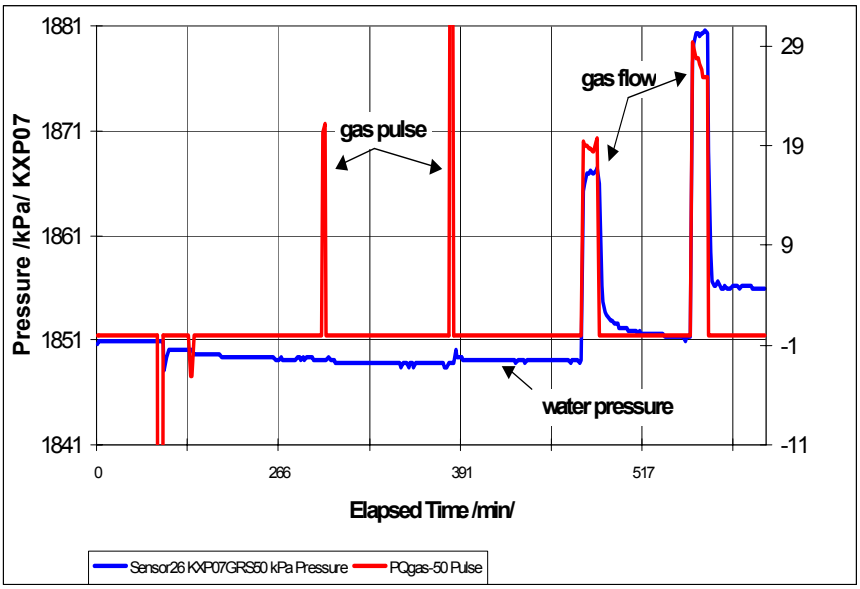

Figure 2-10. *Results of gas injection in the V2 Fracture*

2.7 Two-phase flow experiments

2.7.1 Equipment

Hydraulic tests with gas and water were carried out in order to measure the interval pressures and flow rates of gas/water. In these tests, the marker had to be injected in a controlled way and detected in the flowing medium. In addition, the extracted gas/liquid mixture was to be separated again after gas injection into the water-filled fracture. Because of the high air humidity and the electrical conductivity (> 30 mS/cm) all of the metal parts were made out of stainless steel or protected by a spray-water resistant coating.

The injection gases helium (100 %) and nitrogen (100 %) were made available in gas bottles. Helium and nitrogen were injected via separate flow controllers (Bronkhorst) which enabled volume controlled as well as pressure controlled injections. The flow controller is designed for an injection rate of 0 to 20 ln/min and is accurate to ± 0.9 % (N) or ± 0.7 %, respectively. The equipment is controlled by two separate control elements (Bronkhorst E-7000 type D).

As the fluid injection medium, mains water present in the tunnel with an electrical conductivity of approximately 355 µS/cm was used. Injection was performed using a three piston eccentric pump (Speck) with a maximum flow rate of 12 l/min and a maximum pressure of 60 bar. The three pistons ensure virtually pressure-pulse free injection. The volume is controlled via a pressure control in the pump. The volumes injected were initially recorded using a water meter. However, because this did not provide reliable readings during the injection phase, but only showed the injected total amount at the end of the test, a flowmeter was installed in the injection pipe for the gas/water tracer test. Information on the precise injection rate allowed to apply optimal injection pressures for gas and water during the two-phase tests.

Both injection media were injected via a common pipe. The extraction of both phases was done via a common pipe equipped with a valve to control pressures and/or volumes of the extracted fluids. The two phases were separated in a separator.

A dome pressure reducer was installed upstream of the venting valve to control the volumes of fluid flowing out. It consists of a membrane which is pre-pressurised to 20 bar via a nitrogen bottle. This membrane acts as a buffer to prevent pressure shocks in the pipe and thus the accumulation of gas in front of the valve in the extraction pipe, (Figures 2-11 to 2-13).

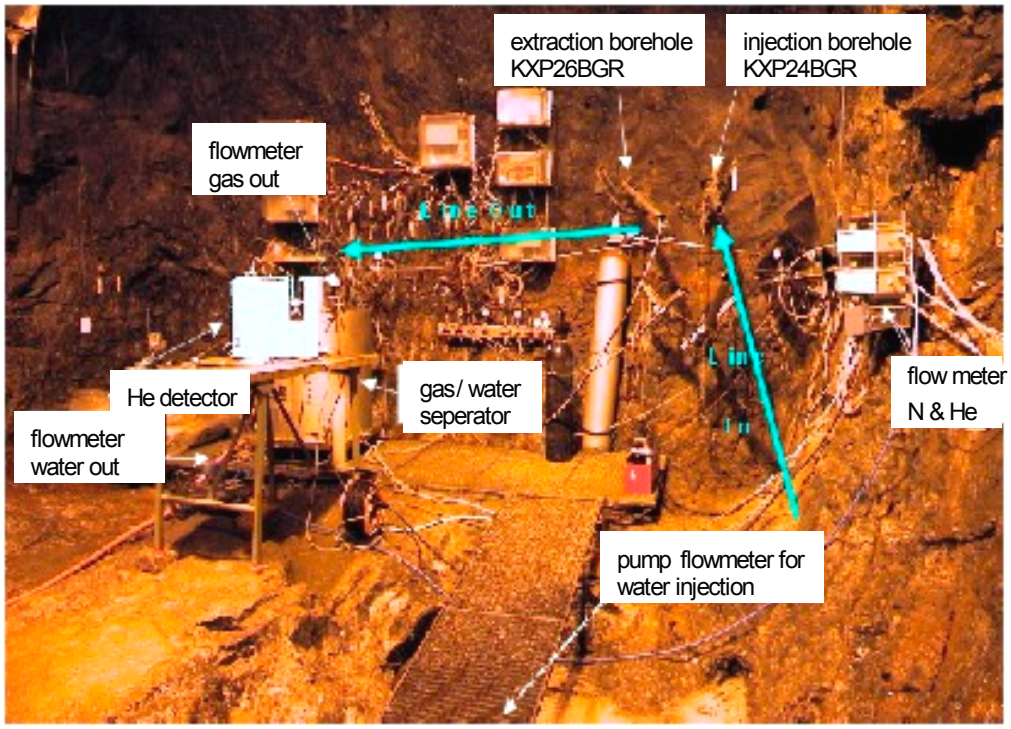

Figure 2-11. *View of the test apparatus in niche 2715*

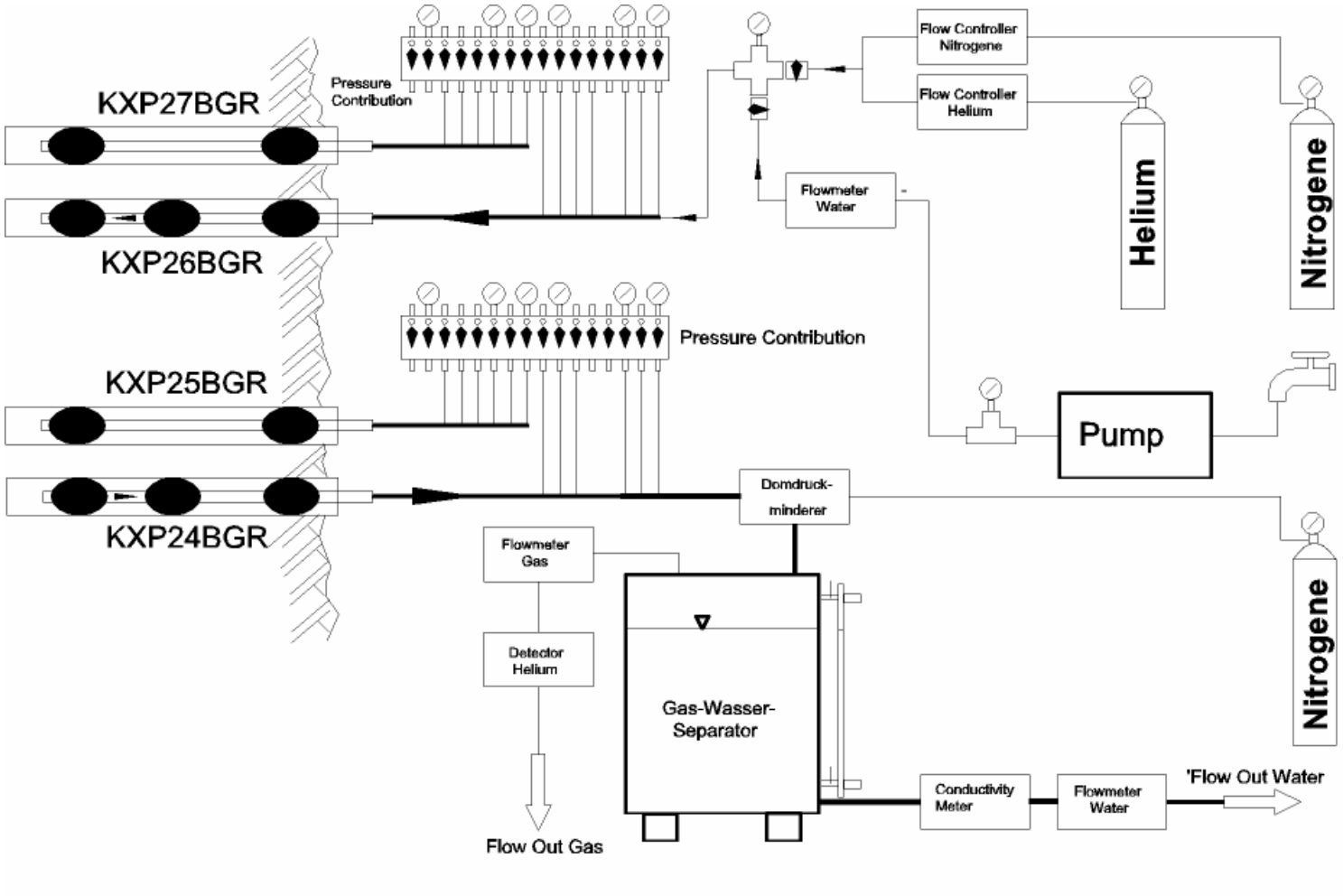

Figure 2-12. *Test apparatus diagram*

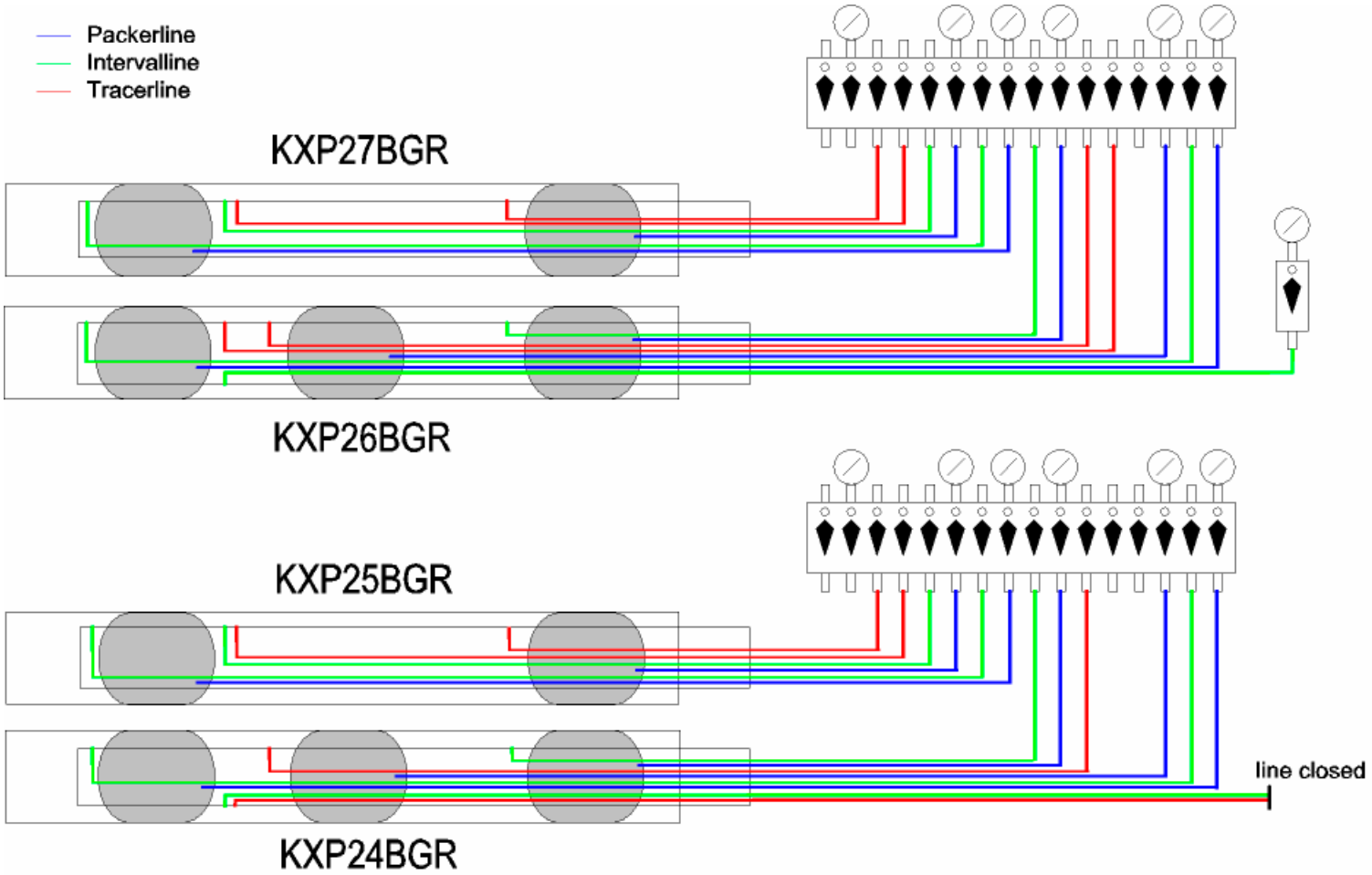

Figure 2-13. *Test apparatus, pipes*

The separator consists of a 200 l stainless steel tank with one input and two outputs. The extraction mixture is fed from the top into the tank so that the gas and water can separate under sealed conditions as a result of pressure release. Internal packing materials ensure that the water jet is vaporised into small drops. This increases the surface to volume ratio to improve degasification of the gas dissolved in the water.

The gas phase was piped out of the separator top. The probe of the helium detector installed in the outlet pipe creates a slight underpressure to ensure that the gas phase is completely withdrawn from the container without any long dwell times. The extraction pipe for the gas phase leads out of the upper part of the separator. In the pipe the flowmeter and a helium probe were installed. The measuring range of the flowmeter was 0 to 20 ln/min at a resolution of 0.1 % and the accuracy was ± 0.7 %. The temperature influence was max. ± 0.02 %. The water phase was drained at the base of the container. A U-tube at the water outlet pipe ensured that the gas phase could not uncontrolled escape from the container.

To minimise the dead space and the delay in the arrival of the helium, during the gas tests the water level in the separator was maintained at a high level. However, since due to this large water volume measurement of the water tracer was difficult, the water volume was maintained at a low level during the water and/or the gas/water tests. This measure seems to have no effect on the arrival time of the helium.

2.7.2 Helium measurements

The helium detector, (Leybold UL 200), was directly installed in the gas extraction pipe. The measurement range is $5*10^{-11}$ to $1*10^{-10}$ mbar*l/s and the resolution is 0.01 % with an accuracy of 0.5 %/°C and a line loss of < 0.8 %. The device creates a slight underpressure in the probe and ensures that changes in the helium concentration are rapidly detected and measured. Because it was originally developed as a leak detection device and measures in leak rate units of mbar*l/s, the results had to be converted to volume-%. This was achieved by creating a nitrogen/helium mixture in the laboratory with a fixed concentration. The concentrations were subsequently measured and the results (volume-%/mbar*l/s) recorded on a plot. The linear equation determined from the gradient of the straight line was utilised for all of the other measurement conversions.

The pressure dependence of the helium leak detection device created problems during the tests, because the pressure pulses, in particular those of the partially pulsing gas phase, had an impact on the measurements. This problem was considerably reduced after the dome pressure reducer had been installed. Additional pressure sensors were installed in the gas filled and water filled sections of the separator to record any pressure shocks that might occur. However, the registered pressure shocks were so small or of such a short duration that their effect on the helium measurements could be neglected.

An outlet for the liquid phase with an intermediate flowmeter was installed at the base of the separator. Flowmeters made by Mircomotion and Promag were used. Manual measurements with a measuring beaker had to be carried out because the flow rates were in some cases larger than the capacity allowed by the pipe cross sections of the flowmeters. Blocking the flow of the extracted water would have caused a rise in water level in the separator and thus an increased degasification which in turn would have resulted in an unrealistic gas flow and higher helium measurements associated with the pressure. The extracted water phase was passed from the outflow into a graduated beaker which contained a conductivity probe.

2.7.3 Index tests

These tests were aimed at characterising the hydraulic connection between each of the boreholes and establishing a dipole interval for the two-phase experiments.

Interference tests between the four boreholes KXP24BGR, KXP25BGR, KXP26BGR and KXP27BGR served to characterise the hydraulic connections between the boreholes which then were weighted as "very good" to "relatively poor". For the tests the openings of all the boreholes were closed with packers. First, one of the four boreholes was opened and then the other three boreholes were opened simultaneously to measure water outflow and pressure reduction. The hydraulic connections were characterised in line with this pressure feedback. A large pressure reduction indicated good hydraulic connections, a slight pressure reduction indicates minor hydraulic connection.

Measurements were conducted at 117 micro-fractures and 17 injection intervals. The classification of the intervals is shown in Table 2-6. The location of the intervals, the water flow rates and the fracture apertures were derived from the BIPS measurements and the core analysis. The intervals were packered so that gas could be injected into a specific interval in each test, and the pressure build-up was measured in parallel in the other intervals. This involved closing the packers in the observation boreholes.

Table 2-6. Pressure behaviour of the boreholes

Extraction boreho	P	KXP24BGR	KXP25BGR	KXP26BGR	KXP27BGR	Reaction
KXP24BGR	Pmin	1,04	9,67	16,95	9,41	26<25<27
	Pmax	18,44	18,24	19,34	18,02	
	Pdiff	17,40	8,56	2,38	8,61	
KXP25BGR	Pmin	17,35	0,99	19,12	15,81	26<24<27
	Pmax	18,49	18,18	19,39	17,98	
	Pdiff	1,15	17,19	0,26	2,17	
KXP26BGR	Pmin	10,52	12,77	0,89	12,55	25<27<24
	Pmax	18,46	18,36	19,29	18,13	
	Pdiff	7,94	5,59	18,40	5,59	
KXP27BGR	Pmin	17,02	15,95	18,82	0,90	26<24<25
	Pmax	18,41	18,32	19,20	18,07	
	Pdiff	1,39	2,37	0,38	17,17	

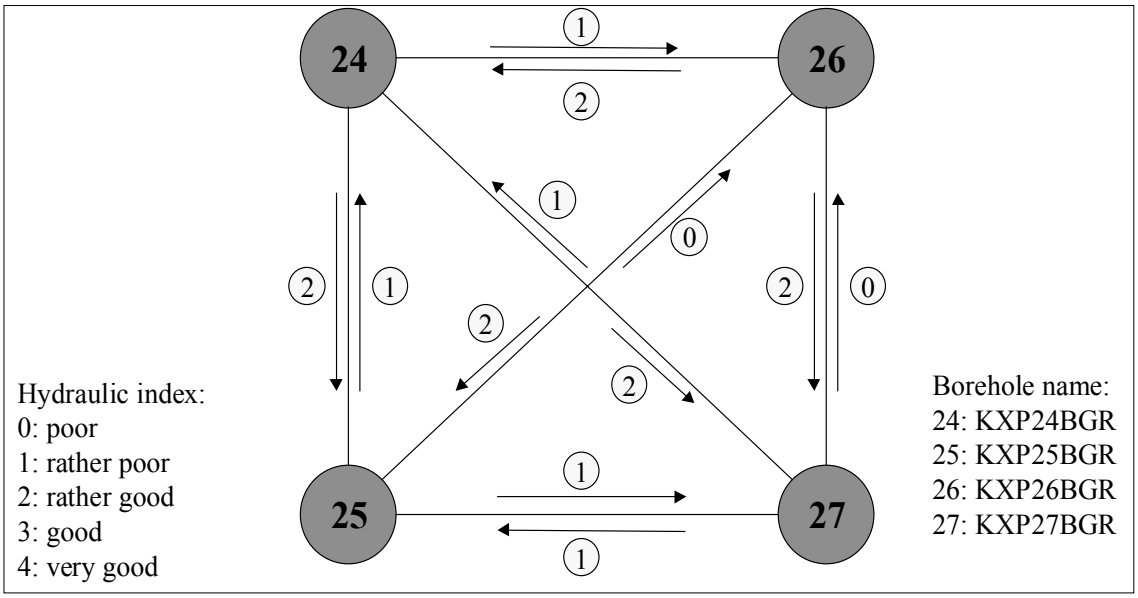

Figure 2-14. *Evaluation of the hydraulic reaction between the boreholes*

Typical test results are shown for a connection with a low permeability in Figures 2-15 and 2-16 and for high permeabilities in Figures 2-17 and 2-18. In tests with low permeabilities, boreholes KXP24BGR, KXP25BGR and KXP27BGR were specifically packered to close the mutually associated micro-fractures (cf. Figure 2-15). No significant pressure reaction was recorded in any of the measuring intervals (cf. Figure 2-16). It was therefore assumed that the micro-fractures in this interval only have insignificant hydraulic connections to the V2 fracture system.

Table 2-7. Hydraulic parameters of the micro-fractures

Tests	Borehole	Test interval [m]	Fracture(s) in depth (m)	Width [mm]	Con-nection	Permeability [m²]
TE001	KXP26BGR	7.18-7.68	7.42 (V2)	2	Yes	1.4e-12
TE002	KXP27BGR	6.15-6.65	6.54/6.59 (V2)	1/1	Yes	7e-13
TE003	KXP27BGR	7.15-8.61	7.2	#	No	2e-13
TE004	KXP26BGR	6.15-6.65	6.15	2?	No	5.5e-13
TE005	KXP26BGR	6.10-6.60	6.15	2	No	1.5e-13
TE006	KXP26BGR	5.10-5.60	5.18/5.26/5.57	2/1/2	Yes	2e-13
TE007	KXP26BGR	4.40-4.90	4.67/4.8	2/2	Yes	2e-12
TE008	KXP26BGR	4.00-4.50	4.27	2	No	5e-14
TE009	KXP27BGR	1.45-5.65	3.19/5.5	2/#	No	1.5e-13
TE010	KXP25BGR	3.80-4.30	3.95/4.05	1/1	No	2e-13
TE011	KXP25BGR	2.80-3.30	2.88	1	Yes	3.5e-12
TE012	KXP25BGR	3.23-3.73	3.47/3.65/3.72 (V2)	1/1/1	Yes	1.5e-11
TE013	KXP24BGR	3.90-4.40	3.93	2	No	1e-11
TE014	KXP24BGR	2.90-3.40	3.2	3?	Yes	1.5e-12
TE015	KXP24BGR	3.60-4.40	3.76/3.82/3.93	1/1/2	Yes	2e-13
TE016	KXP24BGR	3.15-3.65	3.52/3.55 (V2)	1/2	Yes	1.4e-12
TE017	KXP24BGR	2.10-2.60	2.35	1	No	8e-14
TE019	KXP26BGR	5.20-5.70	5.26/5.57	1/2	Yes	2e-12

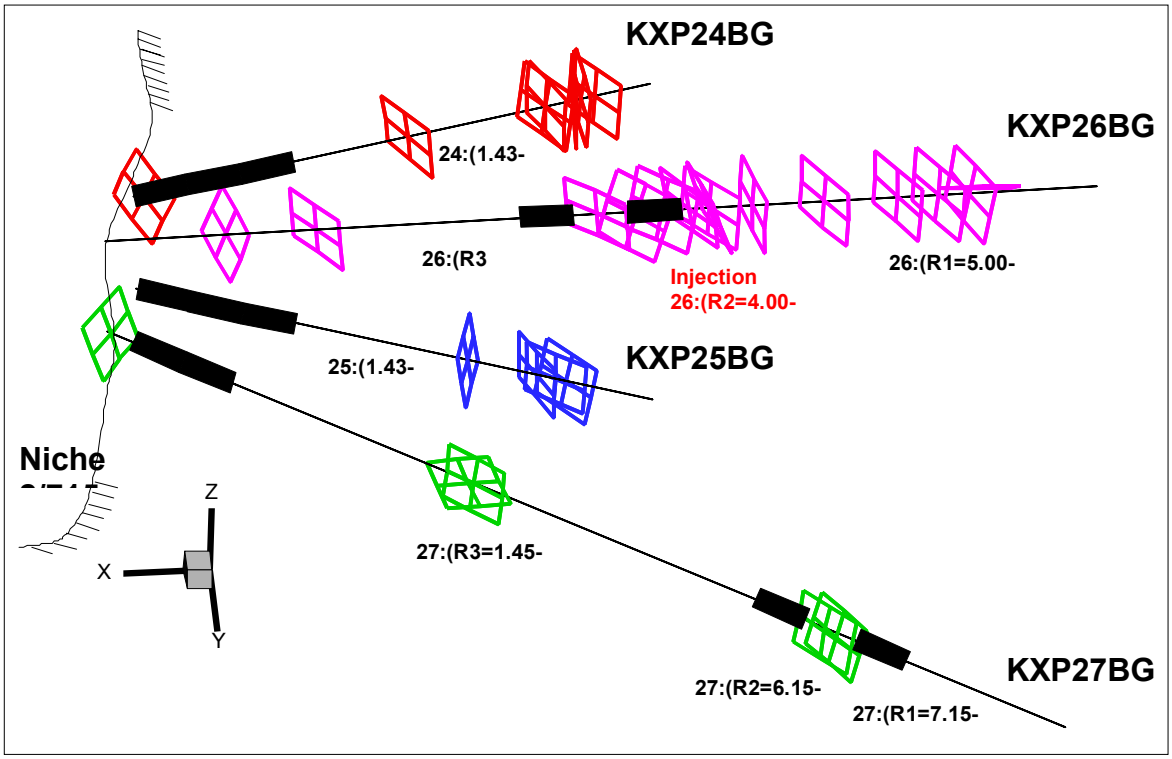

Figure 2-15. *Packer positions for low-permeability tests*

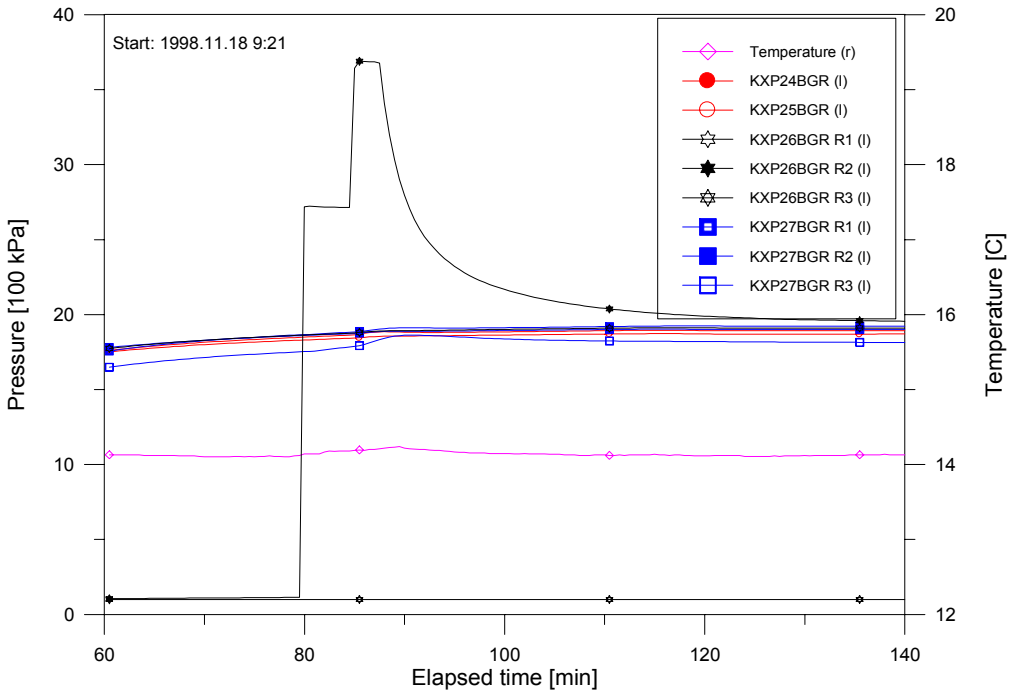

Figure 2-16. *Pressure reaction at the boreholes for hydraulically poor connections*

In the second test in borehole KXP26BGR, an injection interval from 5.10 m to 5.60 m was packered (Figure 2-17). A clear response in all of the boreholes was shown in this experiment. The borehole KXP24BGR showed a particularly marked reaction to gas injection (Figure 2-18). A connection with a high permeability was therefore confirmed between the 5.10 m to 5.60 m interval in borehole KXP26BGR and the 1.43 m to 4.44 m interval in borehole KXP24BGR. Similar tests were carried out for all 17 intervals and allowed conclusions to be drawn on connections between the discontinuities in the V2-fracture system. The results are shown in Table 2-7 in the column "connection".

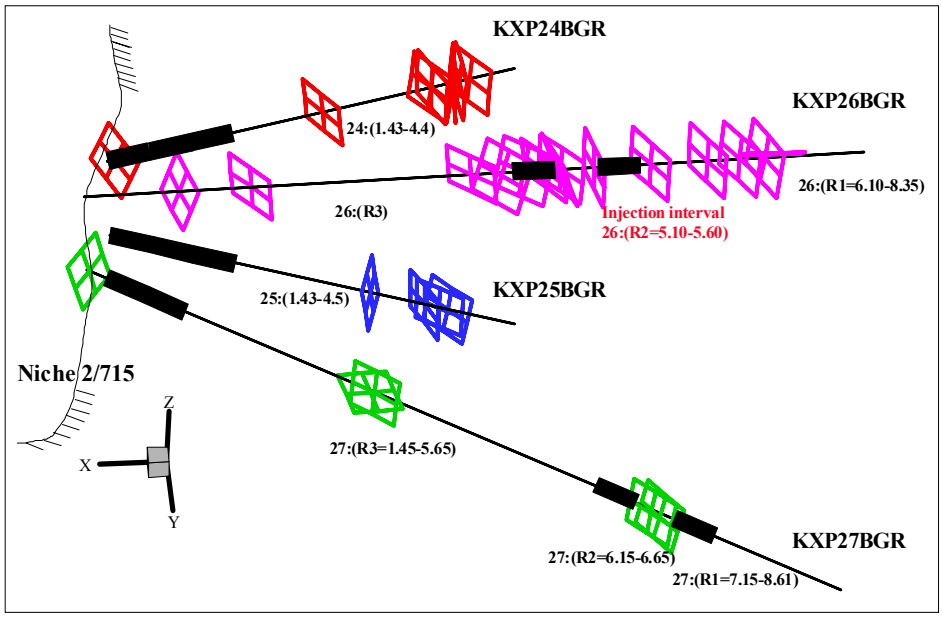

Figure. 2-17. *Packer positions for high-permeability tests*

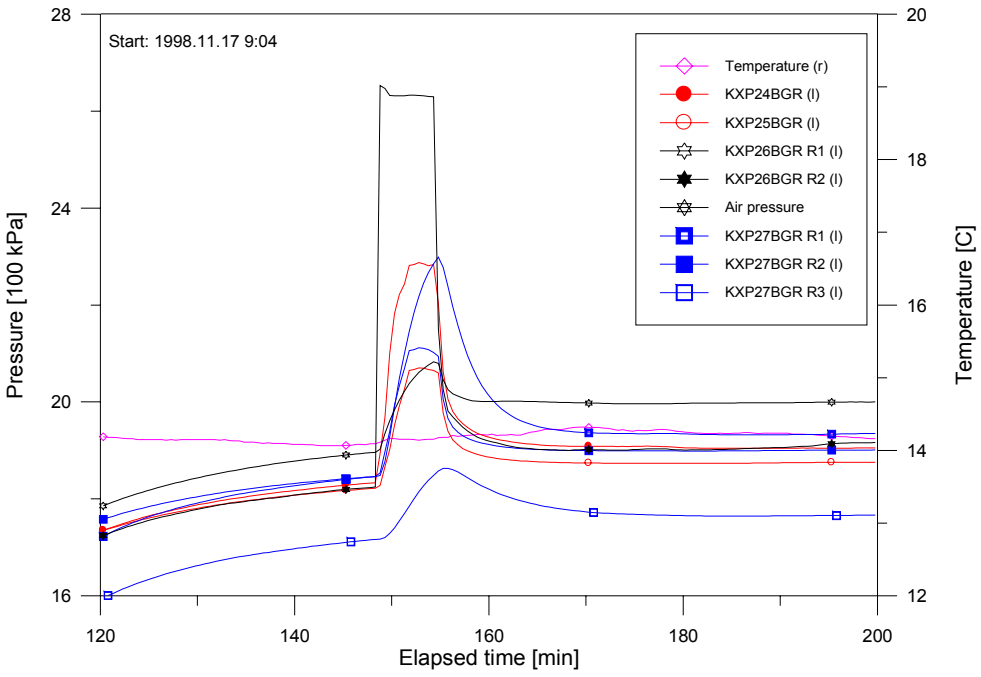

Figure 2-18. *Pressure reaction for a hydraulically good connection*

2.7.4 Evaluation of the measurement results

Fracture permeability and pressure reaction to gas injection in the water saturated system are directly related. The dimensionless pressure-time index is calculated to determine the fracture permeability. This index is defined by:

$$I = (\Delta p_{rec}/p_{ini})*(t_{inj}/\Delta t_{rec}) \; [-]$$

where I = pressure index [-]
Δp_{rec} = difference between injection pressure and pressure at the end of the experiment [bar].
p_{ini} = initial pressure [bar]
t_{inj} = injection duration [s]
Δt_{rec} = breakthrough time [s]

This reflects the relationship between initial pressure and injection time as well as response pressure and breakthrough time. An index > 1 characterises a large pressure interval or a short breakthrough time and thus a higher permeability. Table 2-8 shows each step in calculating the pressure-time indices.

Table 2-8. Calculation of the pressure-time index

Tests	(1) t_{inj} (s)	(2) t_{rec}	(3) Δt_{rec} (s)	(4) p_{ini} (bar)	(5) p_b (bar)	(6) p_e (bar)	(7)=6-5 Δp_{rec}(bar)	$\Delta p_{rec}/p_{ini}$* $t_{inj}/\Delta t_{rec}$
TE002	90	194	600	18.50	38.80	20.90	17.90	0.145
TE003	360	284	1800	19.60	28.30	19.03	9.27	0.094
TE004	780	331	630	20.00	26.96	19.82	7.14	0.442
TE005	240	973	1050	19.29	26.65	19.82	6.83	0.081
TE006	330	140	450	18.25	26.35	19.10	7.25	0.291
TE007	570	585	120	18.82	26.91	19.40	7.51	1.90
TE008	450	301	3720	19.40	30.78	19.50	11.28	0.07
TE009	600	727	3930	17.59	26.73	17.30	9.43	0.082
TE010	630	269	2700	20.74	34.10	19.91	14.19	0.116
TE011	630	637	120	21.60	30.02	21.23	8.78	2.14
TE012	660	249	1350	19.02	31.70	19.52	12.18	5.95
TE013	510	722	1440	19.60	30.05	19.62	10.43	3.70
TE014	750	124	1200	19.45	26.46	20.03	6.43	0.21
TE015	1110	323	2190	19.65	26.89	19.634	7.25	0.187
TE016	900	375	1650	19.55	26.70	19.99	6.71	0.187
TE017	870	262	3690	19.11	27.34	19.62	7.72	0.095

In ROCKFLOW (MM) the pressure-index permeability type curve can be calculated for different saturation levels and fracture apertures. These type curves are based on a rectangular grid measuring 4 x 4 m and a variable fracture. The pressure index determined for the 17 gas injection tests is shown in Table 2-8. The pressure indices are entered in the type curves simulated by ROCKFLOW and a permeability can be derived dependent on fracture aperture for each injection interval. The fracture permeabilities vary between $1x10^{-10}$ m^2 and $1x10^{-14}$ m^2. The permeabilities determined in this way are shown in Table 2-7.

2.7.5 Determining the dipole

The intervals that could be used as test intervals were determined on the basis of the "connection" and "permeability" properties. The test intervals need high permeabilities, must cut the V2-fracture system, and have high water flow rates.

The following intervals cut the V2-fracture system and are hydraulically dominant:

KXP24BGR: 3.13 - 3.65 m
KXP25BGR: 3.23 - 3.73 m
KXP26BGR: 7.18 - 7.68 m
KXP27BGR: 6.15 - 6.65 m

For the dipole experiments, the suitable dipole configuration was selected from these four intervals taking into account the following criteria:

- Hydraulic index
- Permeability
- Water flow rate
- EDZ influence

Table 2-9. Criteria for selecting the suitable dipole configuration

Good hydraulic onductivity	Permeability [m^2]	Water flow rate [l/min]	EDZ influence
24: → 25, 27 25: → - 26: → 24 25: → -	24: 1.4 x 10^{-12} 25: 1.5 x 10^{-11} 26: 1.4 x 10^{-12} 27: 7.0 x 10^{-13}	24: 1.8 25: 0.27 26: 4.8 27: 0.37	24: large 25: large 26: small 27: small

Because of the low permeability and the minimum water flow rates, borehole KXP27BGR is unsuitable as a dipole. Although borehole KXP25BGR has a high permeability, it lay in the area influenced by the EDZ and has the lowest water flow rate compared to the other boreholes.

Boreholes KXP24BGR and KXP26BGR were therefore selected as the dipoles.

2.7.6 Optimising the dipole

The first step consisted of gas injection in the 3.2 m to 3.7 m interval in borehole KXP24BGR. Although borehole KXP26BGR showed a pressure drop, also a simultaneous pressure reduction in the direction to the niche and thus towards the tunnel wall was observed (cf. Figure 2-19). In this test a gas outflow on the tunnel walls was clearly determined. Gas injection in borehole KXP24BGR was therefore associated with a pressure reduction in the direction to the niche and therefore with a mass loss of the injection mass solely attributable to the pressure conditions.

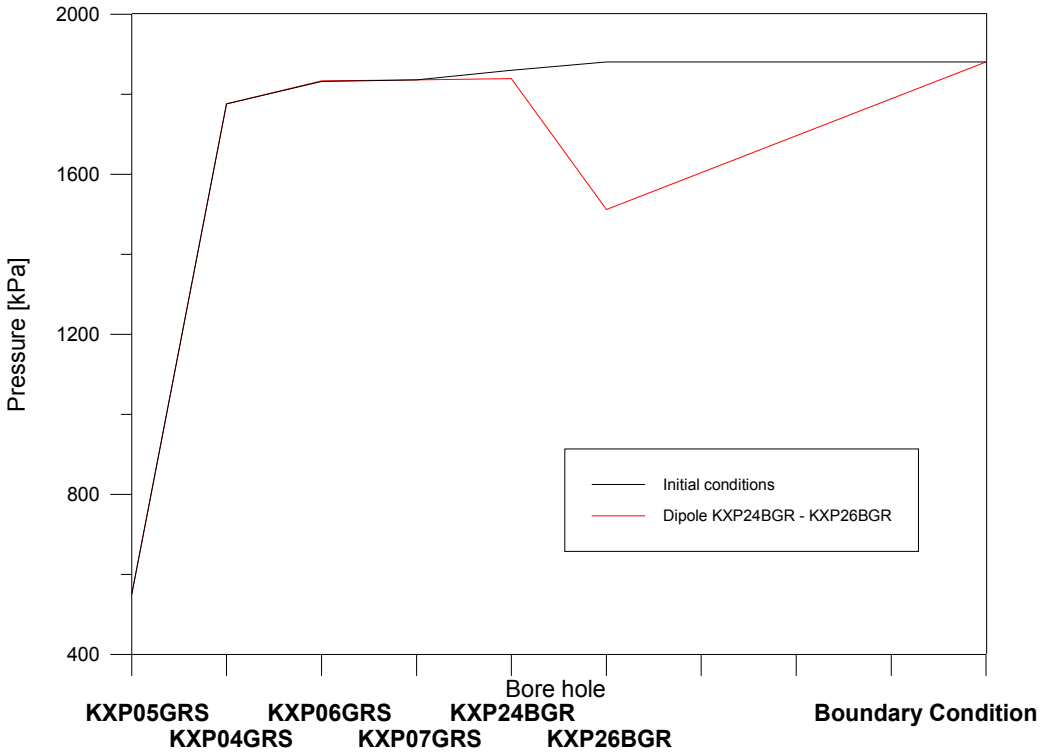

Figure 2-19. *Dipole configuration: KXP24BGR→KXP26BGR*

Gas injection in interval 5.2 - 5.7 in borehole KXP26BGR resulted in a pressure increase in the direction to the niche. This indicated that the injected gas did not move towards the tunnel wall but rather directly to borehole KXP24BGR. Mass loss was very low in this experiment. Figure 2-20 shows the pressure development of the injection and extraction boreholes for this dipole configuration.

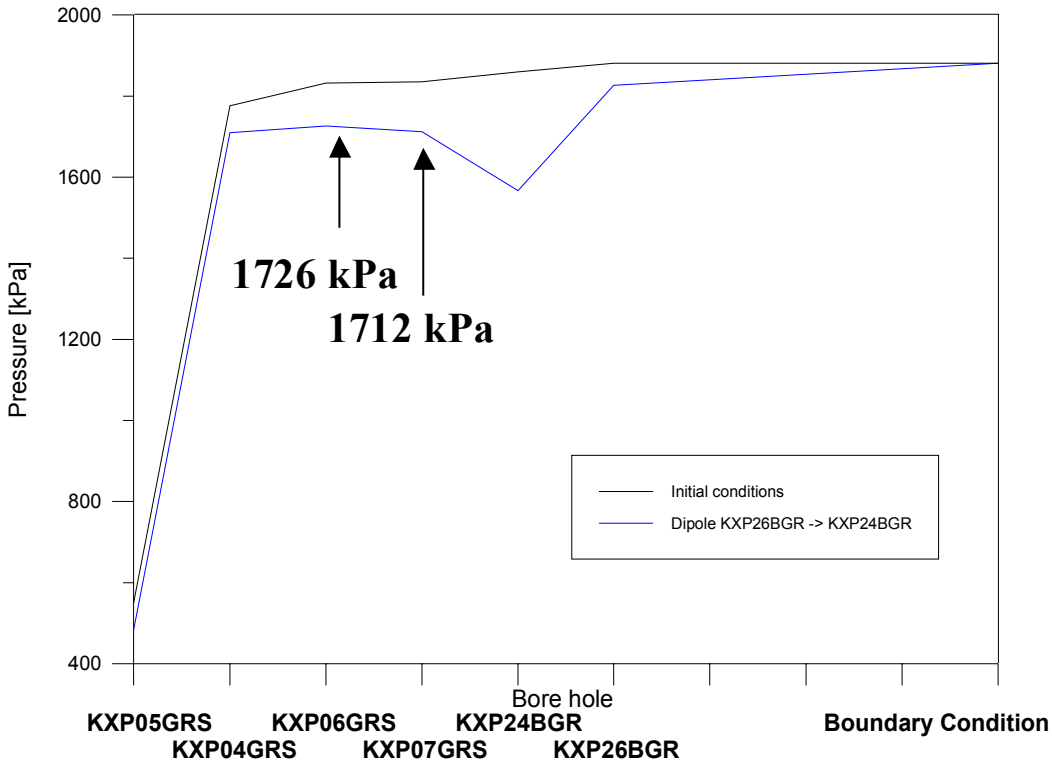

Figure 2-20. *Dipole configuration: KXP26BGR→KXP24BGR*

2.7.7 Selection of the test intervals

The following intervals were available as test intervals because of their high hydraulic conductivity and their connection to the V2-fracture system.

Borehole KXP24BGR: 3.20 - 3.70 / 3.90 - 4.40
Borehole KXP26BGR: 5.20 - 5.7 / 6.65 - 7.08 / 7.0 - 7.5

The 3.90 to 4.40 m test interval could not be isolated with a double packer system.

Table 2-10 shows each of the mutually communicating intervals. For instance, if interval 3.2 - 3.7 in borehole KXP24BGR is opened, the pressure in this borehole drops from 19 bar to 2.1 bar and there is a measured water outflow 1.5 l/min. In borehole KXP26BGR, a pressure reduction of 19 bar to 18.42 bar is measured in the 7.0 - 7.5 interval whilst the reduction in the 5.2 - 5.7 interval drops as low as 10.06 bar. Subsequently, the three intervals in KXP26BGR are successively opened. In this test, the maximum pressure reduction between interval 5.2 - 5.7 in KXP26BGR and 3.2 - 3.7 in KXP24BGR was confirmed. The pressure in borehole KXP26BGR over interval 5.2 - 5.7 drops to 1.25 bar with a measured water outflow of 0.9 l/min. In borehole KXP24BGR (3.2 - 3.7 m) the pressure then decreases to 13.85 bar. When opening the other intervals in borehole KXP26BGR, the pressure in borehole KXP24BGR decreases to 17 bar.

Table 2-10. Selecting the suitable dipole interval

Open ⇒ / State ⇓	KXP24BGR [3.20-3.70] Pressure[bar]/ Flow[Lt/min]	KXP26BGR [7.0-7.5] Pressure[bar]/ Flow[Lt/min]	KXP26BGR [6.65-7.15] Pressure[bar]/ Flow[Lt/min]	KXP26BGR [5.2-5.7] Pressure[bar]/ Flow [Lt/min]
KXP24BGR (3.52/3.55) [3.20-3.70]	2.10-2.09-2.06/ 1.5-1.5-1.46	17.27	17.71	13.85
KXP26BGR (7.42) [7.0-7.5]	18.42	2.4/2.1	-	-
KXP26BGR (6.75/7.08) [6.65-7.15]	18.52	-	1.53/1.25	-
KXP26BG (5.26/5.57) [5.2-5.7]	10.06	-	-	1.25/0.9

The dipole for the two-phase experiment was therefore selected as follows:

Injection: KXP26BGR: 5.2 - 5.7
Extraction: KXP24BGR: 3.2 - 3.7

2.7.8 Determining the injection mode

Figure 2-21 shows that when injecting gas under constant pressure in the injection and extraction boreholes, the injection rate has to be steadily increased to maintain the pressure. Generating a stationary flow field would therefore not be possible without process control. This procedure is therefore not applicable.

When maintaining a constant injection of 1.6 l/min, a constant gas/water outflow was measured in the extraction borehole after less then 1 hour. Moreover, Figure 2-22 shows that the pressure dipole reaches a quasi-stationary state after approx. 5 hours. Injection with a constant injection mass was therefore selected as the suitable method for the two-phase experiments.

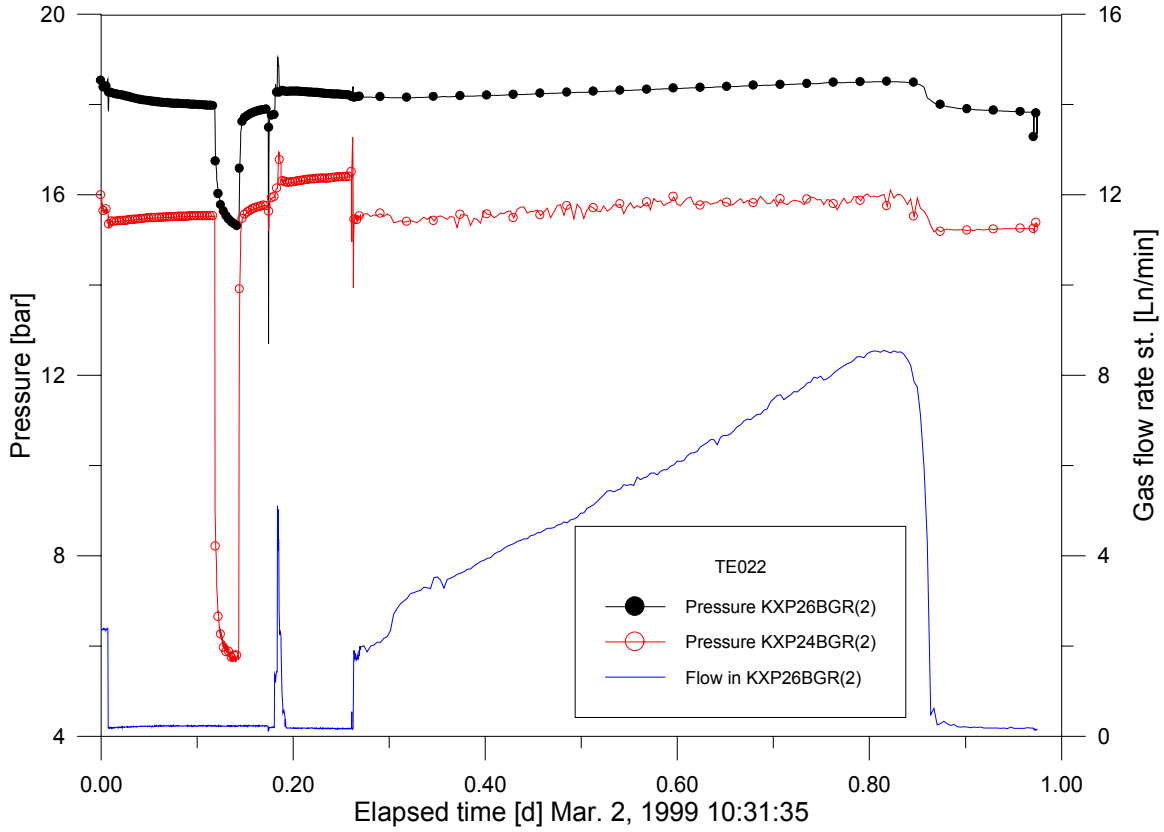

Figure 2-21. *Injection at constant pressure*

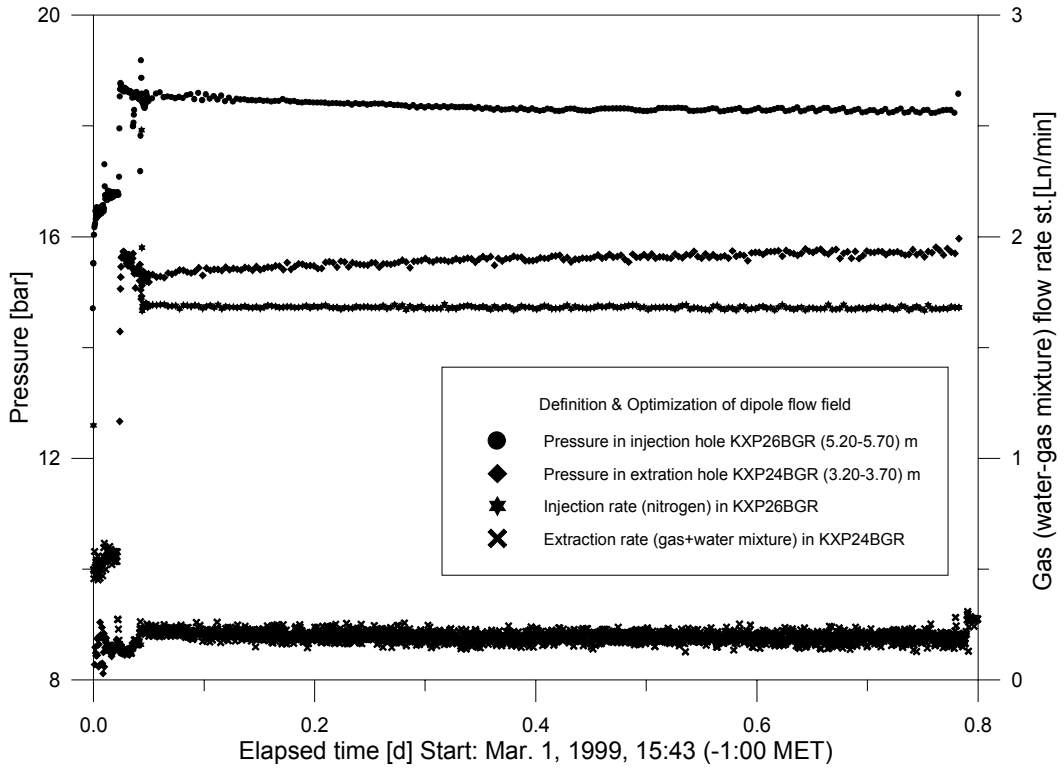

Figure 2-22. *Injection with a constant injection mass*

2.7.9 Tracer tests

All of the tracer tests were carried out between boreholes KXP26BGR and KXP24BGR. This required the use of three-fold packers in boreholes KXP24BGR, KXP26BGR and two-fold packers in boreholes KXP25BGR and KXP27BGR. The front packers with an installed length of 1 m were required to isolate the borehole interval from the EDZ or the tunnel. The middle and rear packers with an installation length of 0.5 m in boreholes KXP24BGR and KXP26BGR were installed to isolate the test interval from other open fractures in the boreholes. The rear packers in boreholes KXP25BGR and KXP27BGR sealed the V2 fracture at those points to prevent the escape of tracer injected into these wells (Figure 2-23).

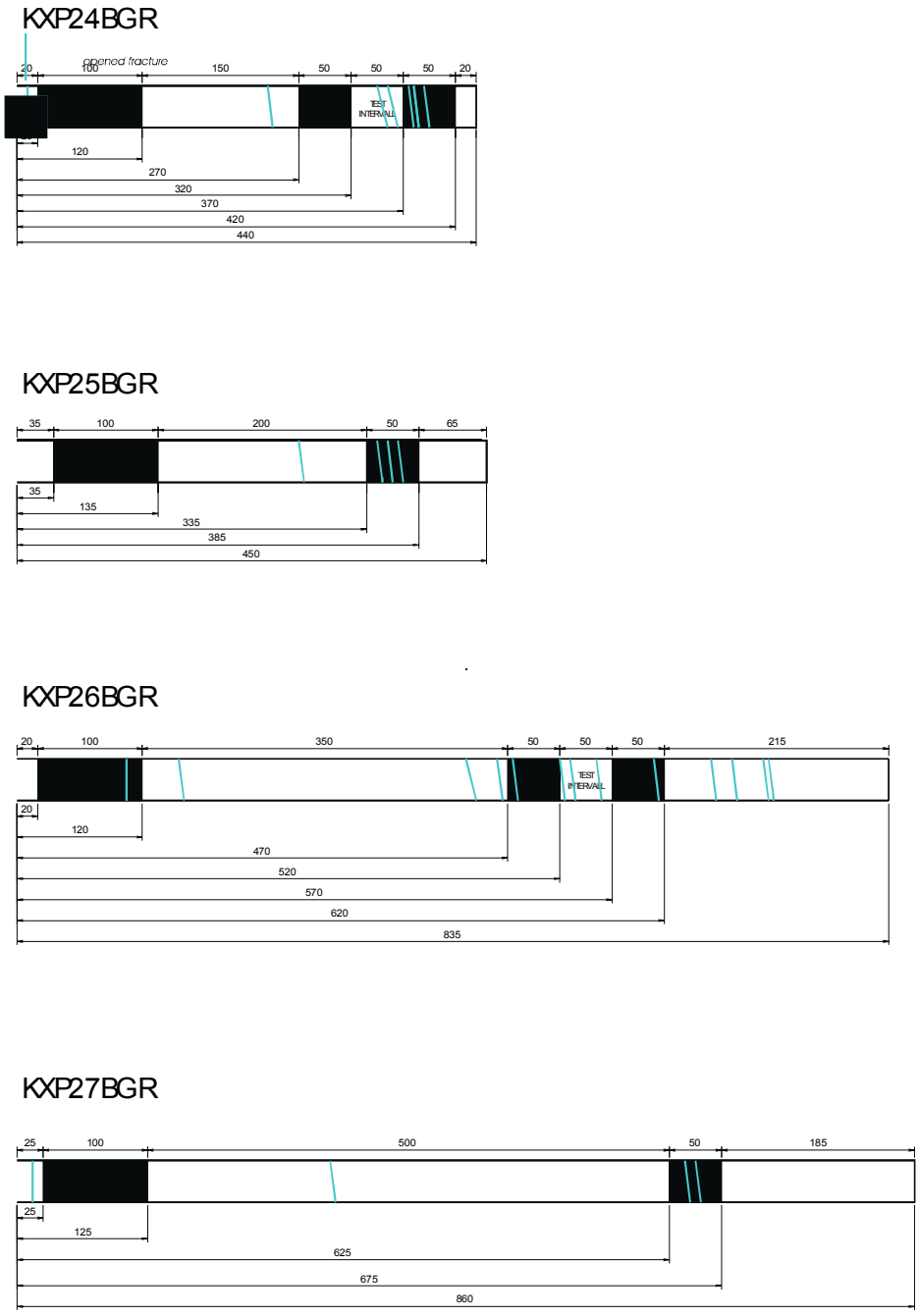

Figure 2-23. *Position of the packer, test intervals and open fractures in boreholes KXP24BGR and KXP26BGR*

In total, 16 tests were carried out: five gas tracer tests, four water tracer tests and seven gas/water tracer tests. Some of the tests could not be used for the subsequent evaluation because of problems arising during the tests. Moreover, as the tests were being carried out it became evident that the measurements could be improved by further optimising the measuring apparatus or the testing procedure. Successful tests were repeated at least once in order to provide representative data. The following section describes a typical test to highlight the test procedure and the results.

Gas tracer test GTR1

Gas tracer tests were carried out to determine the flow and transport conditions for gases in a water-saturated fracture. In test GTR1, by opening borehole KXP24BGR (3.2 - 3.7), a constant pressure of 18.2 bar was achieved at the extraction interval. Nitrogen at a pressure of 19.4 bar was constantly injected at a rate of 4.8 ln/min into the injection interval 5.2 - 5.7 of borehole KXP26BGR,. The nitrogen flow was mixed with a total of 1.7 ln helium as a tracer gas for a period of one minute. Helium reached the extraction interval within 300 seconds. The maximum concentration was measured after 440 seconds and the volume half-life was determined to be 1578 seconds. The initial helium concentration was reached after 4872 seconds.

Evaluation of the GTR1 test revealed a special problem with the natural helium level of the rock. Detailed analysis showed (Figure 2-24) that the helium level prior to and after injection of the helium was still decreasing. A further decrease was observed even after returning to the initial value. This was attributed to the naturally high helium concentration in the rock and to dilution as a result of nitrogen injection. The mass balance between the injected and extracted volumes supports this explanation. A total of 398 ln nitrogen were injected during the test. The extracted volume of 374 ln represents a recovery factor of approx. 94 %. In comparison, 2.35 ln of helium were extracted, although only 1.7 ln were injected which corresponds to a recovery of 140 %. The excess helium is attributable to the extraction of natural helium. It was not possible to calculate the production rate of natural helium because no constant minimum level could be achieved during the whole period of the test. Moreover, the injection of 1.7 ln helium appeared too low. In the following tests, a higher helium injection volume was therefore used because the contamination of the rock with injected helium could be removed within a few hours by flushing with nitrogen.

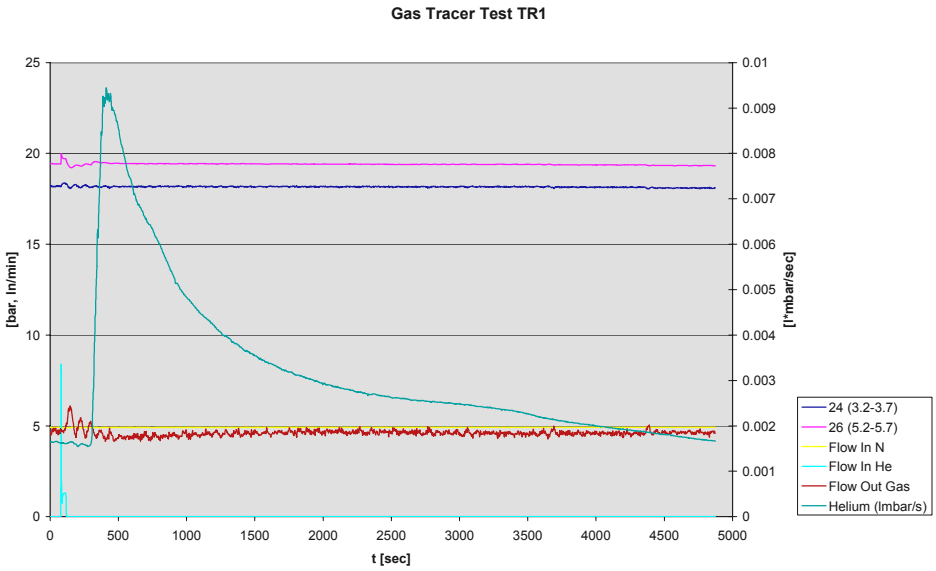

Figure 2-24. *GTR1 gas tracer test curve*

Gas tracer test GTR5

Experience from the previous tests showed that the helium level had to be reduced to a constant minimum by injecting nitrogen prior to injecting the helium tracer.

After reaching the minimum helium concentration, 2.6 ln helium were injected within 14 seconds (Figure 2-25). The injection caused a slight increase in pressure. Of note is the rapid gas breakthrough about 60 seconds after injecting the helium. The test parameters can be derived from the test data of the GTR5 gas tracer test in Table 2-11. The test was carried out until reaching the initial helium concentration. Nitrogen was injected for another 3 hours to measure the helium concentration or helium extraction during this phase. At constant helium levels, 0.4 ln helium (0.14 ln/h) were measured in the gas volume flow during these 3 hours. According to these levels, the background value for natural helium was 0.82 ln during the actual test phase.

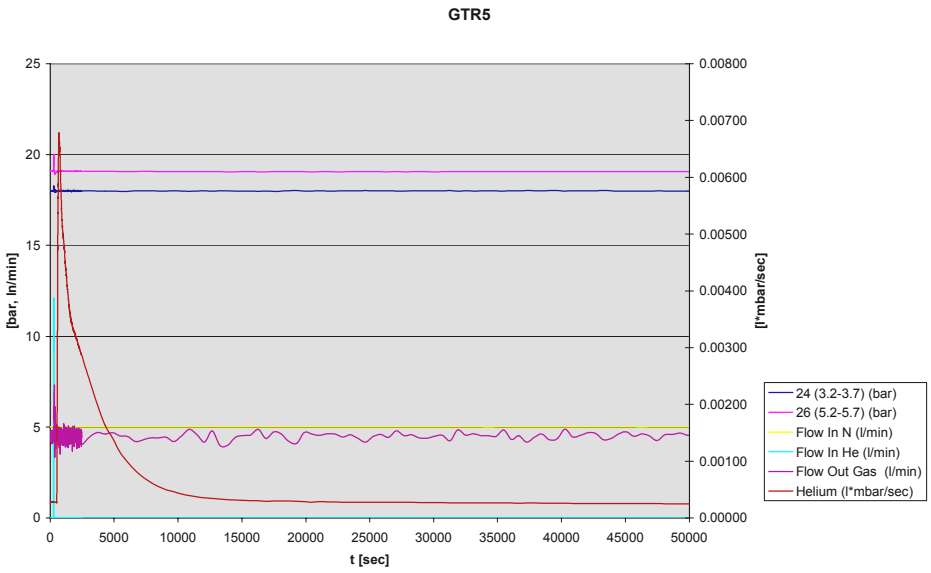

Figure 2-25. *Gas tracer test GTR5 over the whole test period*

Table 2-11. Test data for the GTR5 gas tracer test

Pressure extraction interval prior to tracer injection	18.0 bar
Pressure injection interval prior to tracer injection	19.01 bar
Pressure extraction interval during tracer injection	18.14 bar
Pressure injection interval during tracer injection	19.8 bar
Nitrogen injection volume	5 ln/min
Helium injection volume	2.3 ln/min
Nitrogen recovery	89.7 %
Helium recovery	86.8 %
Fastest interval velocity Vamax	$1.0 * 10^{-02}$ m/s
Dominant interval velocity Vadom	$5.8 * 10^{-03}$ m/s
Average interval velocity Vamit	$7.6 * 10^{-04}$ m/s

3.14 ln helium were extracted from the flow during the test.

$$He_{extracted} + He_{noise} = He_{total}$$
$$3.14 \quad - 0.824 \quad = 2.32 \text{ ln}$$

The almost identical recovery factors for nitrogen (89.7 %) and helium (86.8 %) underline the representative nature of the measured values.

Water tracer tests

Water tracer tests were carried out to estimate the flow and transport properties of liquids within the V2 fracture before carrying out subsequent two-phase tests. Because on account of the high conductivity of the formation water it was not possible to use easily detectable saline water as a tracer, another suitable tracer substance had to be found. The injection medium chosen was the mains water available in the tunnel with an electrical conductivity of 350 µS/cm. In contrast to the use of salt tracer, this method did not result in an increase in concentration, but in a decrease.

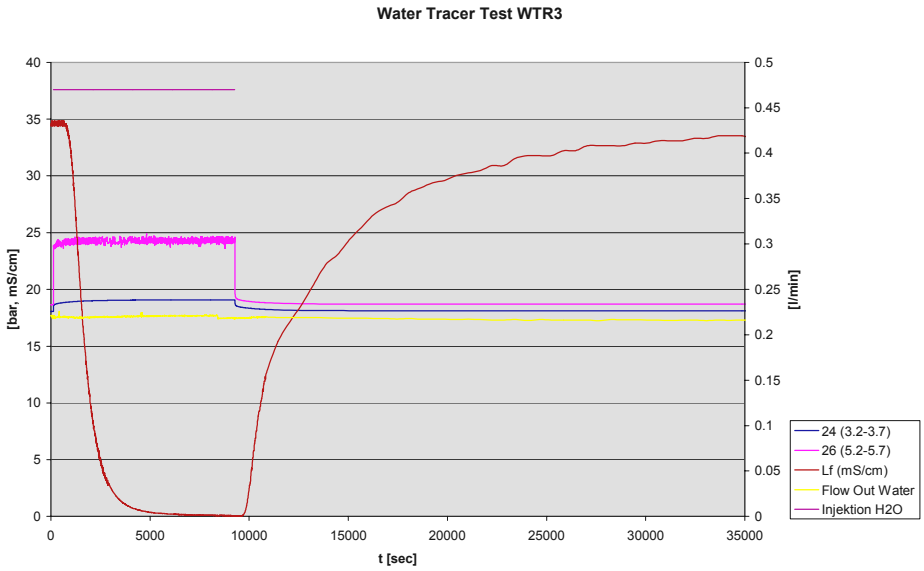

Figure 2-26. *WTR3 water tracer test curve*

The pressure in interval 3.2 - 3.7 of borehole KXP24BGR was lowered to 18 bar by opening the packer prior to injecting the mains water. Mains water was then injected at a rate of 0.47 l/min (Figure 2-26) into the interval KXP26BGR, 5.2 - 5.7. The extraction rate prior to the test was 0.21 l/min and approx. 0.22 l/min during the injection phase. A spontaneous pressure increase was observed in both intervals. The first recording of the arrival of the tracer or reduction in conductivity of the extracted water came 640 seconds after injection. This corresponds to the fastest spacing velocity (Vamax) of 3.8 10^{-03} m/s. Injection was carried out until a constant conductivity of the extraction water was reached. The minimum conductivity of 395 µS/cm, or the tracer maximum, was reached after 9040 seconds. Because natural formation water was not available for further injection, injection had to be shut down completely. The reduction in the tracer construction therefore subsequently took place under hydraulic conditions different to those during the injection phase.

Table 2-12. Test data on the WTR3 water tracer test

Pressure extraction interval prior to tracer injection	18.0 bar
Pressure injection interval prior to tracer injection	18.6 bar
Pressure extraction interval during tracer injection	19.0 bar
Pressure injection interval during tracer injection	24.4 bar
Initial conductivity	34600 µS/cm
Volume of injected water	0.47 ln/min
Conductivity of the mains water	355 µS/cm
Fastest interval velocity Vamax	3.8 * 10^{-03} m/s
Dominant interval velocity Vadom	2.7 * 10^{-04} m/s

Gas/water tracer tests

Gas/water tracer tests were carried out to determine the flow and transport properties of gases and liquids under two-phase conditions. The test procedure was the same as that during the previous gas and water tests. At the start of the test, the extraction interval 3.2 - 3.7 in borehole KXP24BGR was slightly opened and nitrogen injected into the injection interval KXP26BGR, 5.2 - 5.7. This was carried out to establish a flow of carrier gas. Nitrogen was injected until a constant helium level was reached. Then also water was injected. In this test also mains water available in the tunnel was used having a conductivity of 355 µS/cm. In order to create a peak, helium was additionally injected after the nitrogen/water phase. In total, seven gas/water tracer tests were carried out.

Gas/water tracer test GWTR2

The change in helium level and conductivity clearly shows that helium as a gas tracer and mains water as the fluid tracer were injected and reextracted. The change in conductivity was much lower compared to the water tracer tests. The change in helium level was also lower than during the gas tests. The helium recovery factor of 37 % during the whole test was much lower than the recovery factor from nitrogen (92 % for the whole period of the test) and the figure of approx. 90 % achieved during the gas tests. When water injection started, the flow rate of the extracted gas dropped from 5.1 to 0.4 l/min. The flow rate increased slightly to 1.4 l/min after helium injection. The recovery factor for nitrogen during the water injection phase was therefore approx. 30 % and roughly corresponded to the helium recovery factor (37 %). The volume of extracted water rose for a short period after helium injection from 0.78 to 0.98 l/min.

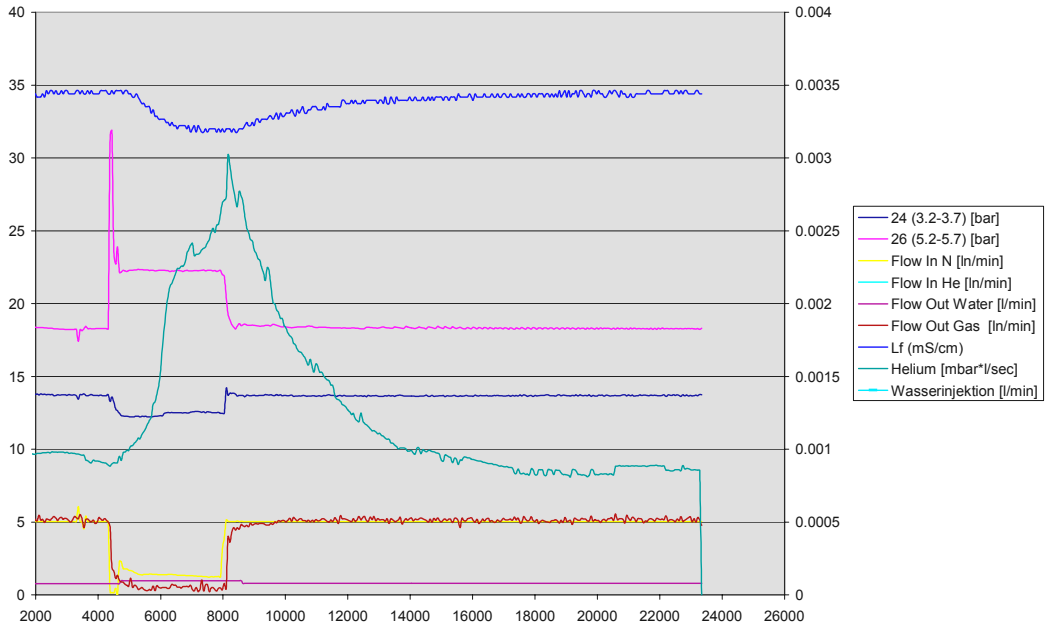

Figure 2-27. *GWTR2 gas/water tracer test curve*

Table 2-13. Test data on the GWTR2 gas/water tracer test

Injection pressure prior to water injection	18.3 bar
Extraction pressure prior to water injection	13.7 bar
Injection pressure during water injection	22.3 bar
Extraction pressure during water injection	12.4 bar
N or H_2O injection rate	4 ln/min 0.3 l/min
He injection rate	11.3 ln/min
Nitrogen recovery	92 %
Helium recovery	37 %
Fastest (Vamax) water	$2.60 * 10^{-03}$ m/s
Dominant (Vadom1) water	$8.20 * 10^{-04}$ m/s
Fastest (Vamax) gas	$1.40 * 10^{-02}$ m/s
Dominant (Vadom1) gas	$6.80 * 10^{-04}$ m/s
Average (Vadom1) gas	$4.00 * 10^{-04}$ m/s

Gas/water tracer test GWTR6

The difficulties associated with simultaneous injection of two phases is attributable to the difference in threshold pressures for gas and liquids. It was therefore necessary to adjust the test conditions so that it was possible for both phases to be injected simultaneously or alternately. Special attention was therefore given to the injection rates during injection.

Table 2-14. Test data for GWTR6 gas/water tracer test

Injection pressure prior to water injection	18.2 bar
Extraction pressure prior to water injection	13.6 bar
Injection pressure during water injection	22.7 bar
Extraction pressure during water injection	13.1 bar
N injection rate	2.9 ln/min
H2O injection rate	0.05 l/min
He injection rate	10.5 ln/min
N recovery	26 %
He recovery	7.5 %
Fastest (Vamax) water	$1.50 * 10^{-03}$ m/s
Dominant (Vadom1) water	$3.90 * 10^{-04}$ m/s
Fastest (Vamax) gas	$4.90 * 10^{-03}$ m/s
Dominant (Vadom1) gas	$2.10 * 10^{-03}$ m/s
Average (Vadom1) gas	$1.40 * 10^{-04}$ m/s

Prior to the GWTR6 test, nitrogen was injected at a rate of 2.9 ln/min until a constant minimum value for helium had been reached. Subsequently, water was also injected at a rate of 0.05 l/min (Figure 2-18). As also observed in the preceding tests, there was a reduction in the gas flow in the extraction borehole and thus also an increase in the helium level.

Two-phase injection was maintained by minor adjustment of the injection pressures. After re-reaching the constant helium level, 101.5 l of helium were injected into the carrier gas in one minute. Water injection stopped completely for a short period but this could be re-established by slightly adjusting the injection pressures. However, an upswing in the system was observed after injecting the helium. Improvement in the constant flow of water injection could be established by slightly reducing the injection pressure for nitrogen. A stronger reduction would probably haved caused a complete breakdown in gas flow, and was not carried out for this reason.

The increase in helium level after approx. 80,000 seconds (Figure 2-28) is attributable to a breakdown in nitrogen injection. However, because the initial helium level prior to injection had already been reached after approx. 53,000 seconds this had no impact on the test. As in test GWTR2, a pressure reduction was observed in the extraction interval and in other intervals.

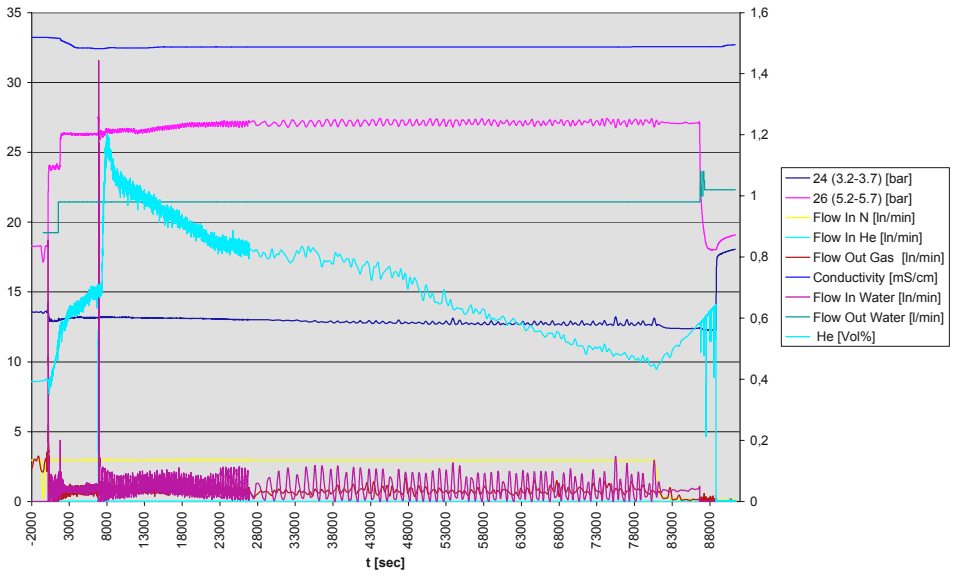

Figure 2-28. *Test curve, Gas /Water tracer GWTR6*

3 Modelling

3.1 Objectives and introduction

The primary goal of the two-phase flow experiments was to establish numerical models for two-phase flow - especially gas propagation - and transport phenomena in fractured rock. After collecting data from the field additional information had to be gained by the interpretation of the in situ tests using numerical models. Of particular interest were the constitutive relationships between saturation on one hand and relative permeability and capillary pressure on the other hand. But before two-phase flow models could be utilised, the basic hydraulic parameters and boundary conditions for the undisturbed single-phase flow had to be identified.

From the modelling point of view, three development stages of the project can be distinguished. At the beginning of the project, only a general understanding of the regional scale flow existed. Little was known about the particular hydraulic properties in the vicinity of the niche. In the first stage it was therefore necessary to establish a regional scale single-phase model for the undisturbed flow into the test niche. This work comprised the tasks of finding an appropriate flow domain, of identifying the relevant flow processes and of calibrating an averaged permeability on the regional scale.

The second stage was marked by the completion of test boreholes around the niche. Measurements of the hydraulic pressure in these boreholes showed clearly that the pressure field was not consistent with a homogeneous permeability. Additional work was necessary to incorporate the knowledge which was gained by these tests into the single-phase model.

In the third and final phase the actual two-phase flow experiments were performed. Predictions of the two-phase flow as well as interpretation of the measurements were necessary in order to design the experiments and to calibrate the required saturation dependent constitutive equations. The models developed during the three stages as well as the results and conclusions are presented in Chapters 3.2 and 3.3. A comparison of the models used is given in Chapter 3.5. Conclusions from the modelling exercise are drawn in Chapter 3.6.

Parallel to the in situ experiments theoretical work was started to gain the constitutive equations from geostatistical data. Additionally, an existing code was advanced to simulate two-phase two-component flow in three-dimensional discrete fracture-matrix systems. The concerning results can be found in Chapter 3.4.

A final remark concerning the use of the term ‘model’ appears to be necessary. This expression is extensively used in the literature but not always with the same meaning. In Chapter 3 the term ‘model’ is defined as an entity consisting of

- the conceptual model of groundwater flow,
- the physical processes involved,
- their mathematical description,
- a numerical simulation code,
- the description of the modelled domain including the parameters to quantify the processes, and
- the results.

If several models are to be distinguished or to be grouped together this is done according to certain aspects like size, physical processes or the originator of a model. As a general rule, the term ‘model’ is then supplemented by a specifying expression like ‘regional model’ or ‘two-phase flow model’.

3.2 Modelling of the two-phase flow experiments (BGR)

Compared with single-phase groundwater models, in a two-phase model the number of needed model parameters increases. For example, multi-phase flow processes are dependent on fracture surfaces as well as on the structure of the fracture system within the overall flow system. In addition, the interactions between the following physical values has to be considered: capillary pressure, relative permeability and degree of saturation. With the aim of improving the understanding of the two-phase flow processes, a numerical model was developed on the basis of hydraulic in situ experiments carried out in the HRL Äspö. The TOUGH2 computer program (TOUGH: Transport Of Unsaturated Groundwater and Heat) was used with the EOS modules 1 and 3 (Equation-Of-State modules). The code ROCKFLOW_MMTM (MehrphasenModul and TransportModul) is a development of the University of Hanover.

3.2.1 Models used

The results of the hydraulic tests carried out in the rock surrounding niche 2175 indicate the presence of a narrow branched fracture system. It is dominated by three hydraulically linked discontinuities. The injection and extraction boreholes cut through this fracture system. In the numerical model, the fracture system is simplified to isotropic, homogenous, isothermal, plane-parallel plates which can be formulated according to the cubic law. The spatial location of the model compared to the fracture is shown in Figure 3-1.

Model geometry

The two-dimensional fracture model has an azimuth of 233° and a dip of 90°, and therefore dips north-east. The spatial co-ordinates of the model are projected on the x-z-plane. The z-axis corresponds to depth and the y-axis to fracture aperture. The permeability and porosity are assumed to be isotropic and the rock is assumed to be homogenous. The injection and extraction borehole cut the model and are taken into consideration as source and sink. The spatial location of the model fracture is shown in Figure 3-2. The horizontal separation between the injection borehole and the extraction borehole is 2.35 m, and the vertical separation is 0.64 m. The finite-difference grid was generated using the MESHMAKER module which is contained in TOUGH2 as the grid generator.

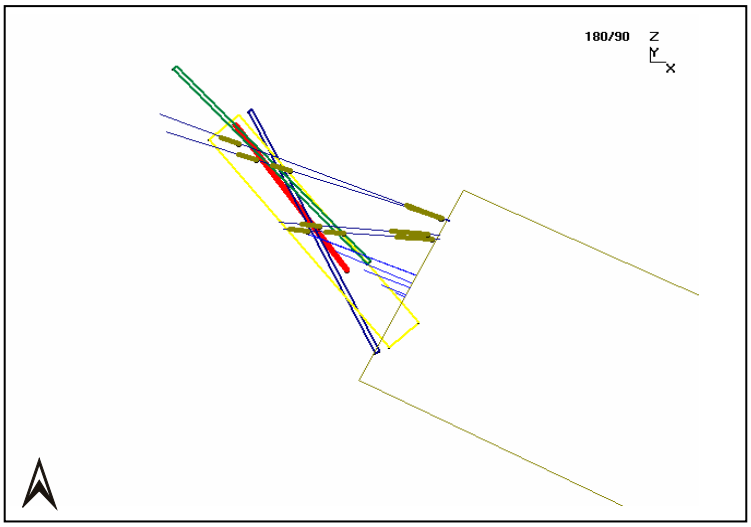

Figure 3-1. *Spatial location of the model fracture (red) and the three fractures of the V2-fracture system (blue, green and yellow)*

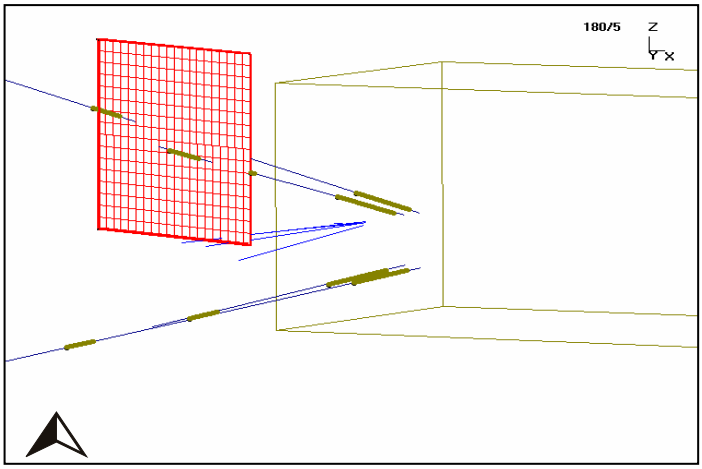

Figure 3-2. *Geometry of the fracture model*

Initial conditions and boundary conditions

In the single-phase flow model, a constant temperature of 13 °C and a stationary pressure field of 18.5 bar was assumed for initial conditions. The Neumann type boundary condition was used for the boundary conditions: a constant water inflow of 0.03 kg/s (1.9 l/min) is distributed uniformly over the whole volume of the model margin at the western edge of the model. At the eastern edge of the model a water outflow of –0.03 kg/s (-1.9 l/min) was assigned to the model.

In the two-phase flow model, the pressure distribution calculated from the single-phase model was used. This involved the pressure calculated for each element being used as the initial conditions in the two-phase model. A temperature of 13 °C and a geogenic gas content of 4 % were defined for the initial conditions. The boundary conditions in the two-phase model were of Neumann as well as of Dirichlet type. A constant pressure of 18.25 bar was used for the extraction borehole. The injection borehole was considered to be a source and the associated elements were assigned a constant gas inflow of 0.082 L_n/s (= 1.862 x 10^{-3} kg/s) (L_n = standard litre).

3.2.2 Performance

Conceptual procedure

In the first stage, a single-phase model was developed. This model estimates the main parameters involved in the hydraulic flow regime. The permeability and porosity parameters can be simulated in this first step on the basis of the hydraulic pressure gradients in the water-saturated system.

These parameters were then incorporated in the two-phase model. The new parameters involved at this stage were the residual gas and water saturation as well as the selection of a suitable relative permeability saturation equation. The model was calibrated using the mass outflow of water and gas. The hydraulic parameters permeability and porosity can only be considered to be reliable after successful calibration. Normally, calibration requires an iterative process until the simulation is in agreement with the data measured in the field. The procedure for calculating the hydraulic parameters is shown in Figure 3-3.

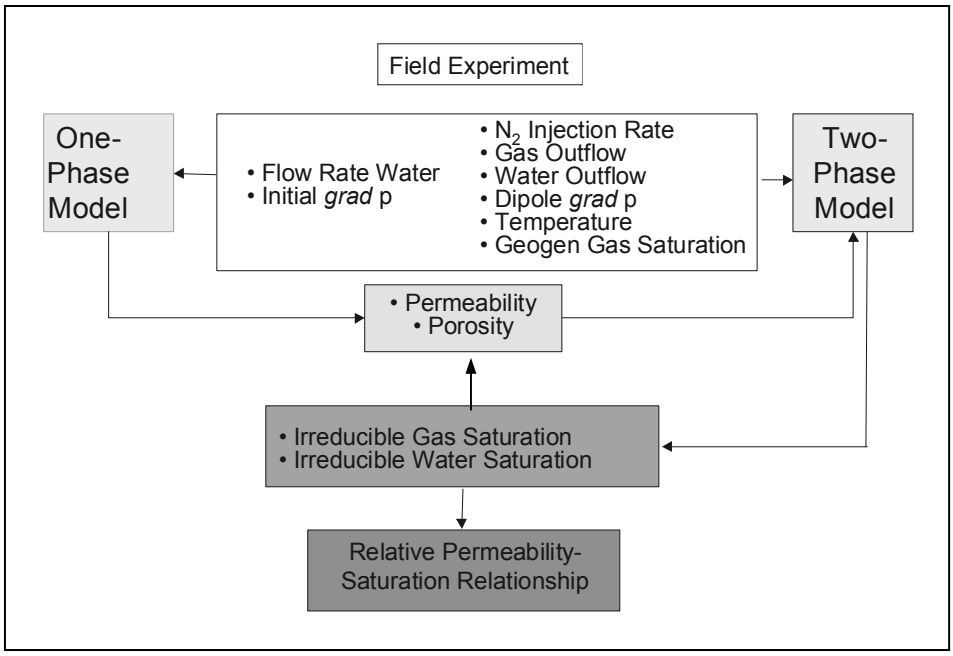

Figure 3-3. *Conceptual flow diagram to establish a two-phase simulation*

Simulation of the GWTR6 gas water tracer test using the "Multi-phase flow and transport model (MMTM)" computer program.

The GWTR6 dipole test which was carried out and described in chapter 2.3 was used to verify the developed finite-element program. The test involved was a tracer test with simultaneous injection of gas and water. The salt concentration of the injected fresh water was about 100 times lower than that of the formation water.

Three different element meshes were used in the numerical modelling (Figure 3-4).

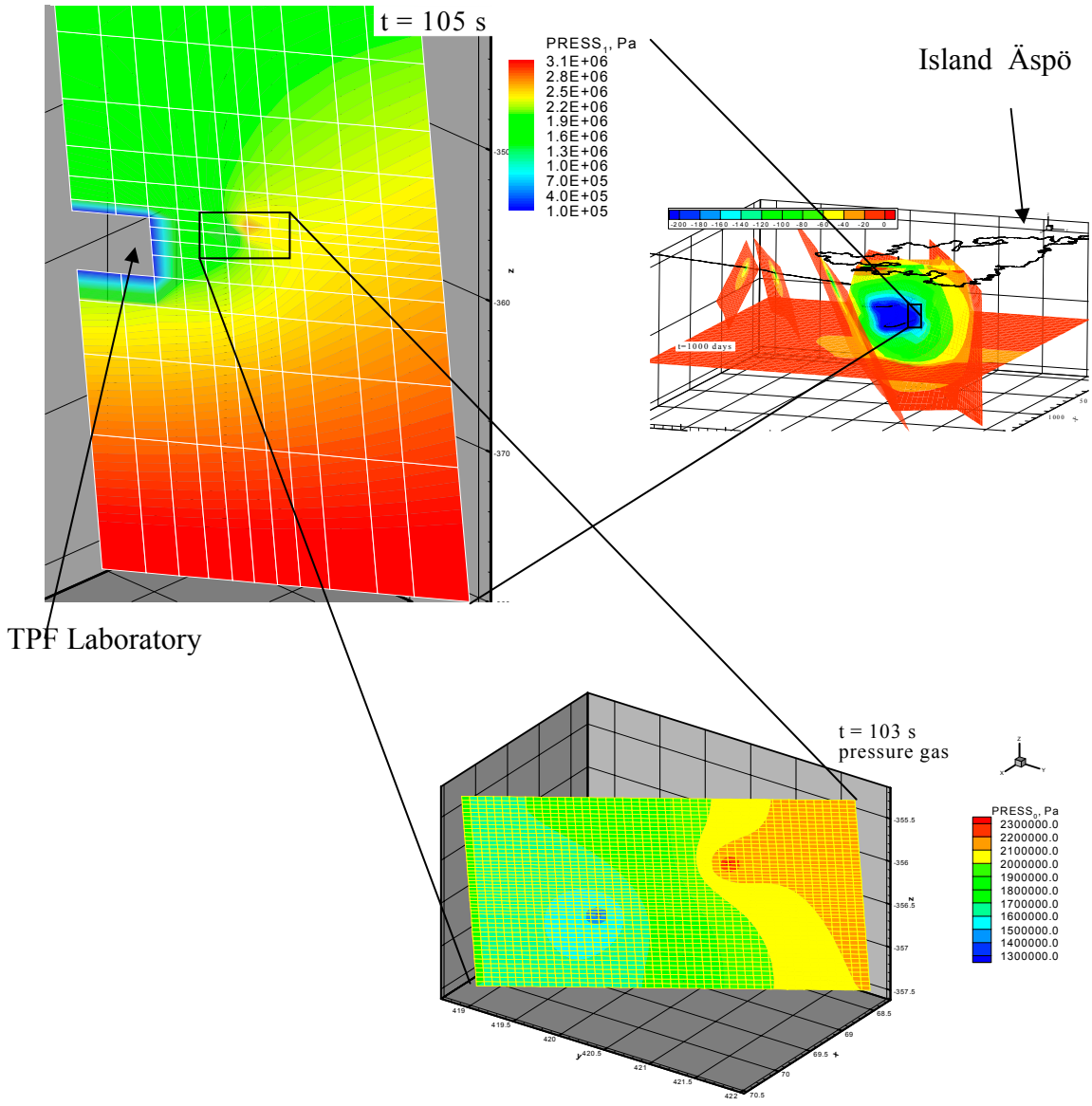

Figure 3-4. *Model mesh of the regional model, the larger local model, the local model and water pressure distribution*

The “Regional 2,5D model” with dimensions of 2000 x 2000 x 1000 m (> 10000 elements) provided the framework for the “Larger local model”. This 2D model, 40 x 20 m (approx. 150 elements) was used to estimate the influence of the excavation disturbed zone (EDZ) and the measured large drop in pressure of 10 bar within a one-metre zone in the rock adjacent to the tunnel. The results of the “Regional 2.5D model” and the “Larger local model” were used to calculate the boundary conditions for the “Smaller local model” measuring 1.5 x 2 x 3 m (2304 elements). All three models were calculated with transformed location co-ordinates.

The finite element program ROCKFLOW was used in the numerical simulation of the “Regional 2.5D model” and the “Larger local model”. Both models simulate the hydraulic behaviour of the rock incorporating the influence of the access tunnel.

The following parameters were used for the “Smaller local model” (1.5 x 2 x 3 m):

Fracture V2:

- dip f_w = 88.3°
- strike a_z = 235.3°
- fracture widths w = 1 to 6 mm

Co-ordinates:

Penetration point of the injection borehole

x	=	2070.37 m	(70.37 m)
y	=	7418.88 m	(418.88 m)
z	=	-356.63 m	

Penetration point of the outflow borehole

x	=	2069.09 m	(69.09 m)
y	=	7419.84 m	(419.84 m)
z	=	-356.06 m	

Uniform initial conditions

Gas saturation	S_0	=	0.05
Water saturation	S_1	=	0.95
Tracer concentration	C_0	=	0.00

Boundary conditions:

Proximal tunnel top edge

pressure	p	=	1700000 Pa
free outflow			

Lower edge

gas saturation	S_0	=	0.0
water saturation	S_1	=	1.0

Distal tunnel edge

pressure	p	=	2100000 Pa
water saturation	S_1	=	1.00

Upper edge

gas saturation	S_0	=	0.05
water saturation	S_1	=	0.95

Outflow borehole pressure p = 1300000 Pa

Free outflow from the outflow borehole

The upper and lower edges are impermeable

Time-dependent mass flow in the injection borehole

Water	q_1	=	0.051 l/min
Gas	q_0	=	2.91 l_n/min

porosity	n	=	1.0
tortuosity	τ	=	1.0
storativity	s	=	0.0 to 0.0001 ms^2/kg
permeability	k	=	$5*10^{-13}$ m^2
dispersion length	$\alpha_{l/t}$	=	1.0 m /0.5 m
diffusivity	D	=	10^{-6} m^2/s

The constitutive law for pressure dependent density variation of the non-wetting fluid phase is approximated by a linear term $\rho_1 = \rho_0 + \rho * \Delta\rho/\Delta p$

density	ρ_0	=	0.0 kg/m^3
$\Delta\rho/\Delta p$		=	$1.225*10^{-5}$
viscosity (gas)	ν_0	=	$1.7*10^{-5}$ kg/(m*s)
viscosity (water)	ν_1	=	10^{-3} kg/(m*s)

no capillary pressure – saturation relation
rel. permeability –saturation relation

$$k_{rel\ g} = \left(\frac{(S - A_1)}{(A_2 - A_1)} \right)^{A_3} \qquad k_{rel\ w} = \left(\frac{(S - A_4)}{(A_5 - A_4)} \right)^{A_6}$$

A_1	A_2	A_3	A_4	A_5	A_6
0.05	0.9	4.0	0.05	0.9	4.0

In the model, the time-dependent boundary conditions, such as injection of the gas (nitrogen), the water, and the gas tracer (helium), have a chronological order corresponding to the GWTR6 test. The injected water had a salt concentration of approximately 0.2 g/l. The calculation was begun at time $t_0 = 0$ and carried out in part until $t_e = 3000$ s. The time steps were varied according to the automatic time step calculation. They began with approximately 1/100 s, increased shortly before injection to around 10 s, reduced after fluid injection to approximately 5 s and reduced further with injection of the gas tracer to approximately 2 s. A slight further reduction was observed after the gas phase had reached the outflow borehole. A lead time of 95 s was required to stabilise the pressure oscillations. The injection periods for the gas, the fresh water, the tracer and the time for the pressure to drop to p = 100 kPa by opening borehole 24 are summarised in Table 3-1.

Table 3-1. Action times of the parameters in the GWT6 test simulation

Medium	parameter	start t_i (s)	end t_e (s)
water in Bo 26	q_i (l/min)	95	3000
water out Bo 24	p (Pa)	95	3000
Gas	q_i (l_n/min)	100	3000
Tracer	C (-)	210	270

3.2.3 Results

The single-phase model was used to determine the porosity and permeability parameters. In the selected test the hydraulic original state of 19.2 bar and 18.7 bar was measured for the injection borehole and for the extraction borehole, respectively. The results show that the measured pressure difference of 0.5 bar is optimally simulated by using a permeability of $5x10^{-10}$ m^2.

Hydraulic pressure dipole

In simulating a hydraulic pressure dipole (Figure 3-5), the measured pressure gradient was calculated by selecting a permeability of $5x10^{-10}$ m^2 and using an injected nitrogen mass of $1.86x10^{-3}$ kg/s for the specific test. A difference of 0.58 bar was determined for this test, the simulation gives a dipole pressure difference of 1.35 bar.

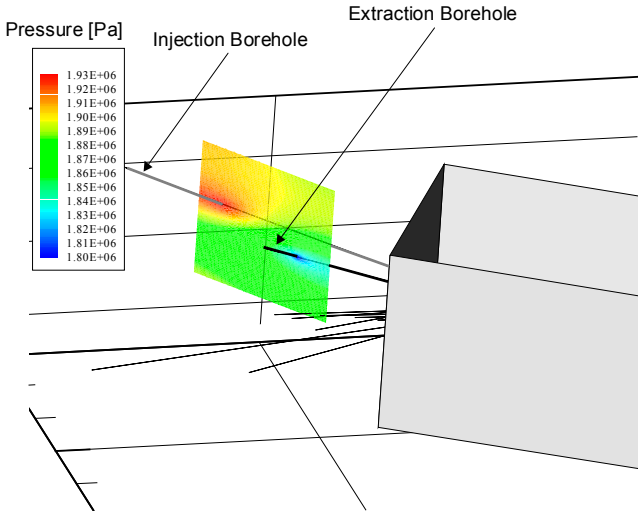

Figure 3-5. *Hydraulic pressure dipole after nitrogen injection*

The most suitable correlation for describing the two-phase processes in the V2-fracture system in the Äspö diorite is Corey's function (1954). The model calibration shows that by using this function the break-through curves in the simulation optimally reflect the measured mass flows.

In the model calibration presented below, the simulation runs are used to determine the model parameters residual gas and water saturation. Figure 3-6 shows the migration of nitrogen in a water-saturated fracture.

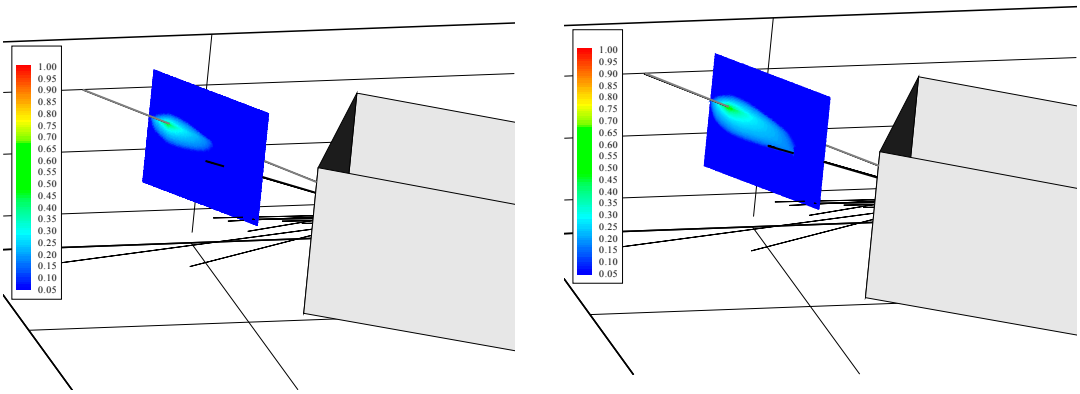

Figure 3-6. *Propagation of the gas phase after 300 and 600 seconds*

On the basis of the test, calibration was carried out to determine the residual saturations. The residual gas and water saturations were varied until the modelled and measured mass outflows of nitrogen and water corresponded. An extraction of 98 % of the injected gas masses was measured in almost all of the tests so that the residual gas saturation was fixed at 0.02. After varying the residual water saturations between 0.1 and 0.5, the simulations revealed that a residual water saturation of 0.15 was the best fit to the measured results. The calculation results shown in Figure 3-7 for the gas outflow correspond very well with the test data. The parameter selection involved did not

significantly change the size of the modelled gas outflow. The calculated water outflow was larger in these model calculations than that measured in the tests. The results show that the residual gas and water saturation parameters have only an insignificant effect on the mass balance compared to the fracture aperture. Thus, the most significant parameter is the fracture aperture, i.e., the water and gas outflows can be simulated with sufficient accuracy by varying the width of the fracture aperture. The calculations of the gas outflow are in good agreement with the test results only when the fracture aperture is between 1 and 2 mm.

A 2.5D fracture model was elaborated as part of the numerical calculations using TOUGH2. Using this program, the simulations indicate that the V2-fracture system has a permeability of $5x10^{-10}$ m^2 and a porosity of 0.5. The parameters for calculating the two-phase flow processes were determined following calibration of the model with a selected test. The best results were derived by using the Corey correlation with a residual gas saturation of 0.02 and a residual water saturation of 0.15.

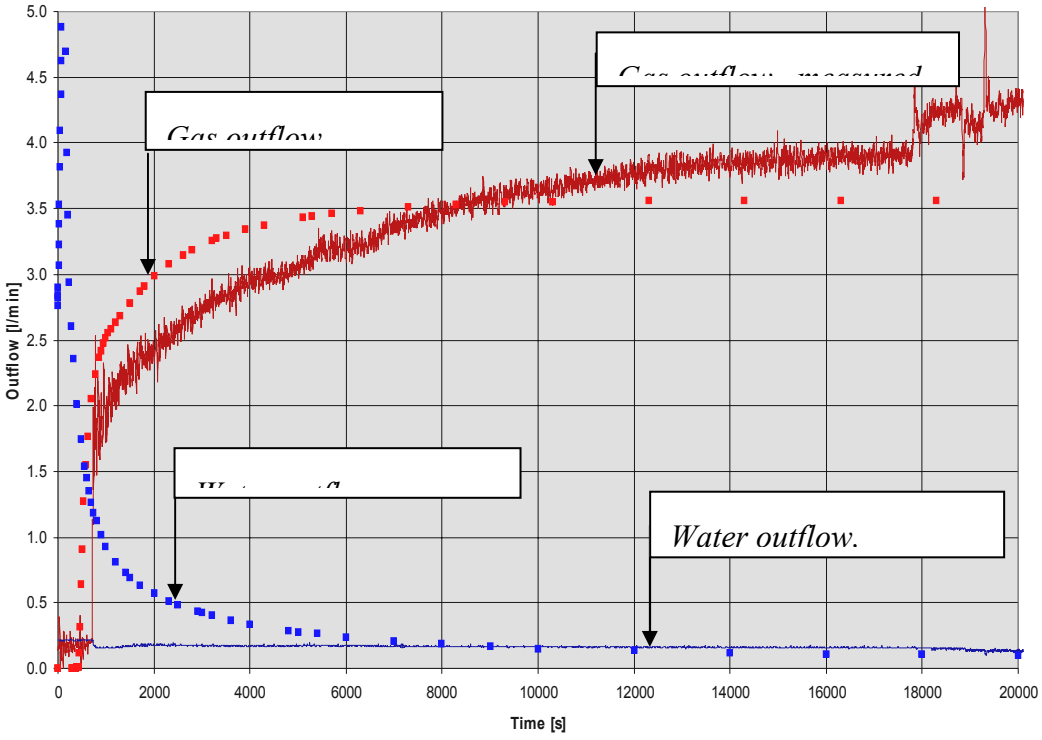

Figure 3-7*. Comparison between the calculated and the measured mass flows*

The calculations carried out with the MMTM (Multi-phase and transport model) computer program show the suitability of the program to simulate the in situ tests. The automatic time step selection for material transport calculations significantly simplifies the work involved compared to the previous program versions. The oscillations are minimised by selecting appropriate physical parameter configurations and additional development work in grid generation. Figures 3-8 and 3-9 show the calculation carried out with MMTM for one selected time step.

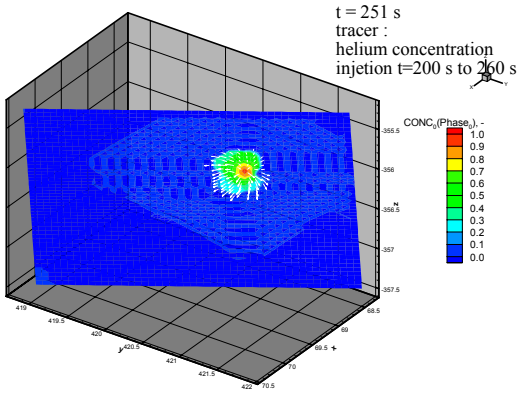

Figure 3-8. *a) Tracer distribution and flow vectors in the gas phase at t=250s*

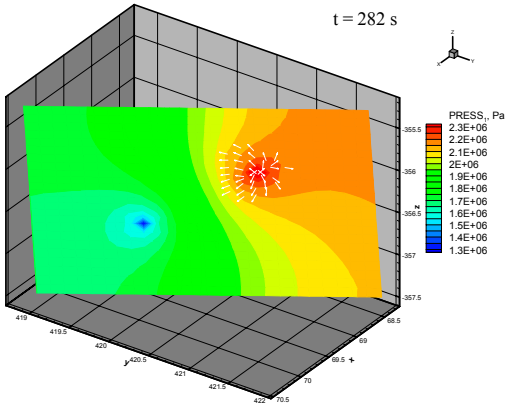

b) Water pressure distribution and flow vectors in the gas phase at t=280 s.

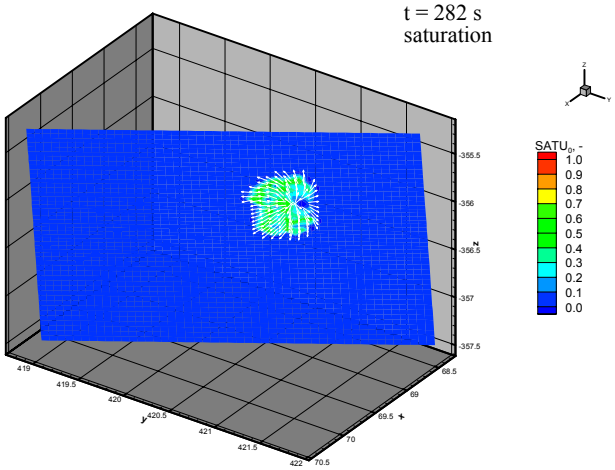

Figure 3-9. *Saturation of the gas phase at t= 282*

3.3 Modelling fluid flow (GRS)

3.3.1 Codes used

Two different codes were utilised for the flow modelling. The finite element code ROCKFLOW_SM2, version 2.22.03 (ROCKFLOW, 1988-1994) developed at University of Hanover was used to calculate all single-phase groundwater flow models. It computes hydraulic heads using the continuity equation for incompressible fluids in combination with an appropriate flow law. Darcy's law was chosen in all cases. The code allows to model combined structures of continuous regions and discrete fractures using 1D-, 2D- and 3D-elements and was therefore ideally suited to address the problems of flow in fractured porous rock. Since hydraulic heads are easily converted into pressure data this relation is implicitly used.

The two-phase flow calculations were performed with the code MUFTE_thermo version 4 (Helmig et al., 1994) developed at University of Stuttgart. It simulates the simultaneous flow of gas and water taking into account phase changes, evaporation, condensation, solution and dissolution. Darcy´s generalised law is incorporated in the two coupled continuity equations for the liquid and the gas phase. The equations are approximated by a controlled finite-element method. Like ROCKFLOW, MUFTE allows the simultaneous use of elements of different dimensionality. This proved to be useful in order to circumvent problems with the outflow boundary at the location of fluid extraction.

3.3.2 Models investigated

Regional 3D single-phase flow

At the start of the project it was not clear which geological features of the flow domain were relevant for the regional scale model. However, it was known from geological mapping that in the niche area only one series of almost vertical and parallel orientated fractures conducted a significant amount of water. One of these fractures is the V2 structure which crosses the niche. The distance between the fractures averages about 5 metres, the integral aperture width is 2.5 cm. Measurements indicated an integral water outflow of 3 litres per minute. Matrix permeability was determined in the laboratory to be about 10^{-20} m^2.

Based on this information a simplified three-dimensional single-phase flow model was constructed in order to address the following tasks:

- estimation of the fracture permeability,

estimation of matrix contribution to the flow field,
estimation of the appropriate model size and errors at the closed boundaries,
estimation of the influence of transient effects of the regional flow field,
estimation of the influence of storage in the fracture.

Advantage was taken of several symmetries. This led to a model with a vertical fracture and an adjacent rock matrix block. Both fracture and matrix were assumed to be homogeneous with different hydraulic properties. The domain size was chosen to be 500 m by 500 m and the niche was taken into account by a recess in the model. Atmospheric pressure was assigned to this recess. The remaining vertical boundaries

and the bottom boundary of the system were no-flow boundaries either due to symmetry considerations or due to the assumption that inflow over the boundaries was negligible. The top of the model was assumed to represent the level of the Baltic sea, again with fixed atmospheric pressure.

Storage of fluids in a porous medium can have different reasons like the elasticity of the rock, compressibility of the fluid, air bubbles in the liquid, etc. All these effects are condensed in the specific storage coefficient. Based on data from SKB (Rhen et al., 1997), this coefficient was estimated to 10^{-7} 1/m in the matrix and 10^{-6} 1/m in the fracture.

In the numerical model instantaneous excavation of tunnel and niche was assumed. Therefore the simulation started with a hydrostatic pressure field (or a constant hydraulic head of zero metres) for the water representing the hydraulic conditions immediately before excavation but with the atmospheric pressure boundary condition assigned to the niche. Figure 3-10 shows the hydraulic heads after a model time of one, three and ten months. After ten months the flow can be considered to be steady-state.

The model calculations yield a permeability of 10^{-12} m^2 for the fracture and provided a steady-state outflow rate of 1.59 litres per minute out of the fracture. For symmetry reasons, the flow rate was doubled because only one half of the fracture was considered in the model. This model was taken as a base case for several other calculations in order to address the tasks listed above.

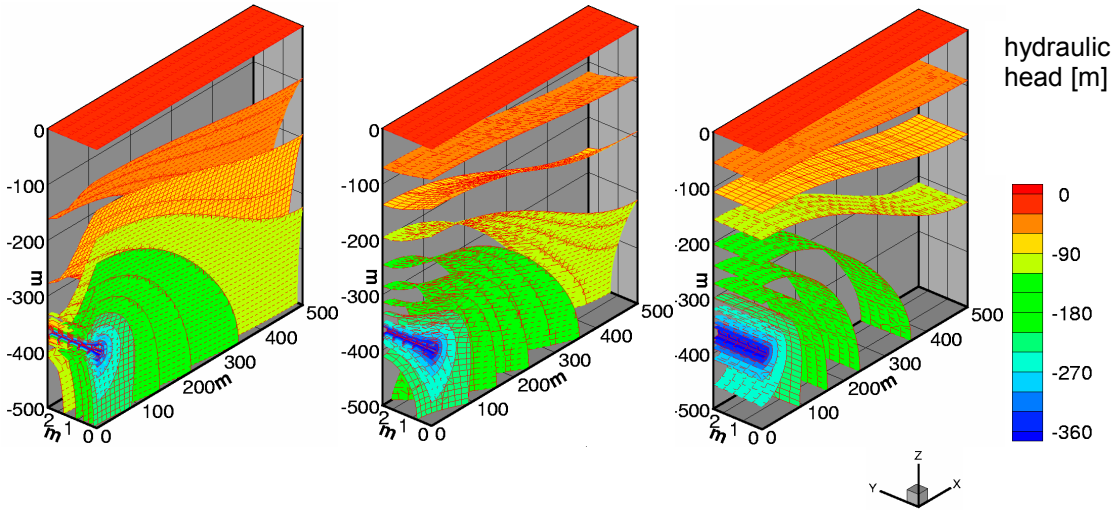

Figure 3-10. *Transient model: isoplanes of the hydraulic head at 1, 3, and 10 months; the fracture lies in the vertical plane which faces the reader.*

Local 2D homogeneous single-phase flow model

During the numerical exercise described above, the drilling of test boreholes was finished and some draw-down tests were performed. The time dependent pressure response to an instantaneous stepwise pressure drop in the fracture was measured. This time dependence of the flow is only controlled by the storage of water. The time necessary to reach steady-state conditions in the experiments can therefore be used to

verify the value of the storage coefficient chosen for the numerical model. One has simply to assign atmospheric pressure to one of the test boreholes in the model and to observe the change of pressure at the other locations over time. This check was performed for the V2-fracture with a simplified 2D model which encompasses the almost uniform high-pressure domain. For the sake of simplicity the niche as well as the undisturbed flow is not considered in this model. Hence, only a qualitative interpretation of the results was performed. (see Chapter 3.3.3)

Regional 2D inhomogeneous single-phase flow model

The measured values for the pressure in the undisturbed flow field raised doubts about the validity of the homogeneous model. The pressure values in the undisturbed flow field lay between 1.8 MPa and 1.83 MPa with two exceptions: At borehole KXP05GRS, crossing the fracture half a meter beyond the wall of the niche, a value of 0.53 MPa was measured. At borehole KXP26BGR - located furthest from the wall – a value of 1.91 MPa was measured.

The measurements of water pressure in the undisturbed flow field of the fracture were obviously in contradiction with the modelling results considered so far. The homogeneous model yielded a water pressure which increased more or less linearly with distance from the niche wall. The measured pressure distribution was characterised by two unexpected features. Firstly, a large pressure gradient in the immediate vicinity of the niche wall and secondly, a high degree of uniformity in the remaining area. Even at the test borehole KXP26BGR, the calculated pressure was only 0.5 MPa compared to the measured pressure of 1.9 MPa. Therefore, the assumption of a homogeneous permeability distribution was no longer tenable.

By assuming a narrow zone around the niche about 1m thick, the new data could consistently be explained. This zone had to be hydraulically much tighter than the neighbouring zone in which the pressure measurements were performed. Such a situation would account for the large pressure gradient. Surrounding this 1m thick zone a second zone of rather high permeability is necessary to get the almost constant high-level pressure field as well. Finally, a third outer zone with an intermediate permeability was required beyond the measurement area. In this zone the pressure had to drop from approximately 1.8 MPa in the middle zone down to atmospheric pressure at the top of the model.

In this three-zone model the permeability of each zone was varied by applying the following restrictions:

- achieve a minimum pressure gradient in the middle zone,

get a pressure level of about 1.8 MPa in the middle zone, and
maintain an outflow rate of about 3 l/min.

Considering the pressure distribution along the GRS boreholes, a thickness of one metre for the inner zone appeared to be appropriate. But there was no information available to locate the boundary between the high permeable middle zone and the intermediate permeable outer zone. A thickness of 40 m for the middle zone was therefore assumed without further reasoning.

Local 2D inhomogeneous two-phase flow

The regional-scale single-phase flow model described above was used to start the local-scale two-phase flow simulations. It provided initial and boundary conditions for the pressure which were transferred to the two-phase flow model. Some additional effort was required because the grid had to be changed due to new demands:

- Injection of fluids changes the pressure distribution compared to the undisturbed flow. These changes fade away with distance to the injection area. By an appropriate choice of the model size it had to be ensured that only minimal pressure changes occur at the boundaries of the two-phase flow model so that the pressure values taken from the single-phase flow model are still valid.

- Dipole-like flow implies strongly curved streamlines especially around source and sink, which have to be reproduced with an element grid of a resolution as high as possible. This raises on the other hand the computational effort so that an optimal element size had to be found.

The model size complying with these demands was about 30 by 30 m. Dirichlet-type boundary conditions for pressure as well as saturation along the boundary were used. The pressure values were interpolated from the single-phase flow model. The gas saturation at the boundary as well as the initial value over the whole domain was chosen to be 0.1%. Fracture porosity was assumed to be 20%. The model domain encompassed two of the three regions of the three-zone model.

A mass flux, equivalent to two litres of nitrogen per minute – as was planned while designing the two-phase flow tests - was assigned to the location of the injection borehole. At the extraction borehole the boundary needed some more attention, because the outflow rate was not known and the saturation was an unknown function of time. So, neither a Dirichlet nor a Neumann boundary condition could be applied. In order to circumvent this problem a string of one-dimensional elements was connected to the extraction borehole. The string is a sort of auxiliary construction and is only used to provide appropriate boundary conditions. The elements had a very high permeability to avoid an artificial flow resistance and the additional volume was large enough to keep the injected gas within the model domain. In other words, the simulated front of gas saturation could leave the fracture but could not reach the model boundary. This measure allowed the use of fixed pressure and saturation values at the end of the 1D-element string.

Brooks-Corey functions were used as a first approximation for the saturation dependent relative permeability and capillary pressure. From the GTHP experiment it was known that the entry pressure p_e was very low. The parameter n was chosen after experience from conventional soils. In the model the values n=2 and p_e =100 Pa were used.

3.3.3 Modelling

Regional 3D single-phase flow

The three-dimensional base case provided an integral outflow rate from the rock matrix of 1.59 10^{-6} litres per minute. Steady-state flow from the matrix is therefore negligible compared to the fracture outflow.

Despite a higher storage coefficient in the fracture than in the matrix, the fracture flow was approximately at steady-state after less than a month (model time). At that point of time mass flux out of the fracture was only 1% above the steady-state value, meaning that the matrix contributes very little to the fracture flow during transient conditions. After ten months the whole system reached steady-state conditions. Transferring the modelling results to the actual situation at Äspö means that the groundwater flow system at the Äspö-site is presently at steady-state.

Variation of the storage coefficient in the fracture confirms that the transient phase is significantly shorter in time in the fracture than in the matrix. The fracture storage capacity is not large enough to exert a long-term influence on the flow field. The transient phase in the matrix takes much longer because the matrix volume is two hundred times higher than the volume of the fracture. But even in the transient state the matrix has no noticeable effect on fracture flow. This justified firstly, to neglect the matrix for further investigation and thereby to reduce the model to of a vertical two-dimensional plane model of the V2-fracture. And secondly, it showed that it is sufficient to skip the transient phase and to do steady-state calculations only.

Local 2D homogeneous single-phase flow model

Figure 3-11 shows the measured and simulated pressure at all test locations over time for a flow test at KXP24BGR. The simulated dynamics of the pressure drop in the fracture are in good agreement with the measurements even if the steady-state pressure doesn't match well. The pressure drop was simulated for the test at KXP25BGR as well which led to the same conclusions. This confirms the estimation for the storage coefficient in the numerical model and thereby the assumption about the prevailing steady-state condition of the flow field in the fracture. It indicates further that the description of the model domain as a homogeneous medium is not appropriate.

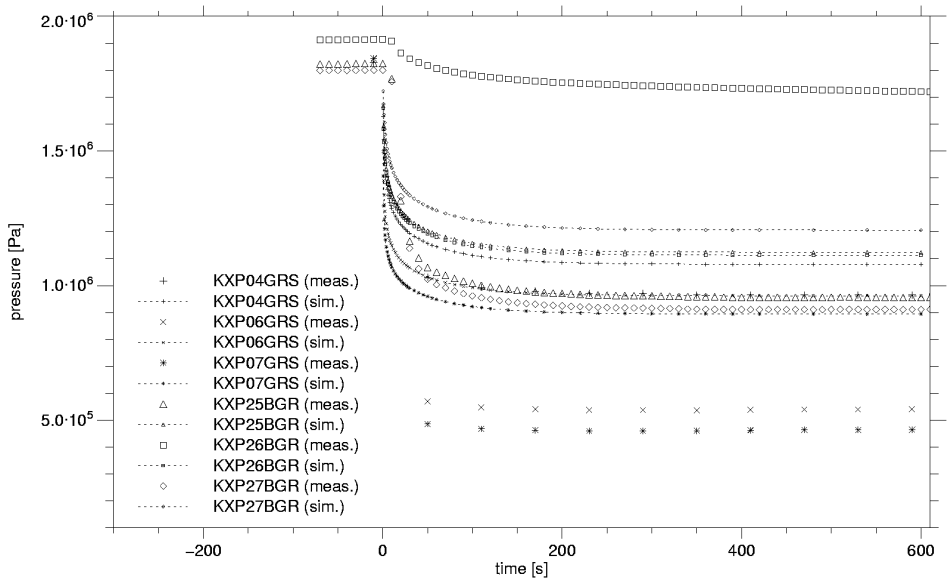

Figure 3-11. *Measured and simulated pressure after opening KXP24BGR.*

Regional 2D inhomogeneous single-phase flow model

In the three-zone model an outflow rate of 2.2 l/min is calculated using permeability values of $2 \cdot 10^{-14}$ m^2 for the inner zone, $5 \cdot 10^{-12}$ m^2 for the middle zone and $6.6 \cdot 10^{-13}$ m^2 for the outer zone. The pressure gradient in the vicinity of the test boreholes is considerably reduced. Measured and calculated pressure match fairly well at most test locations (see Figure 3-12).

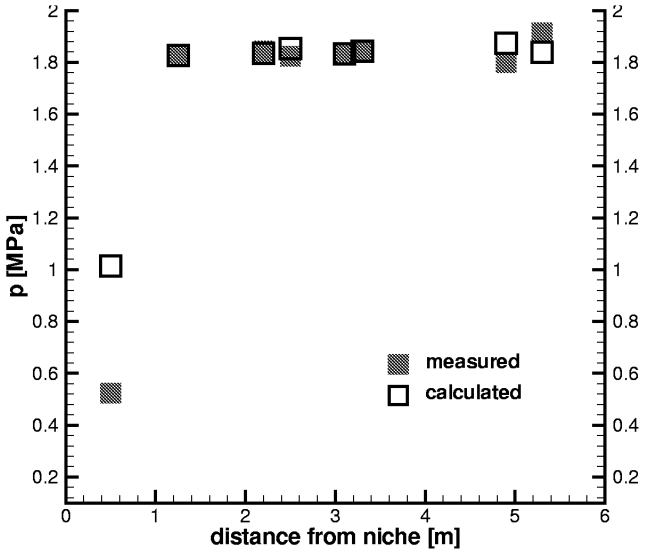

Figure 3-12. *Comparison between measured pressure values and calculated values (simulation with the three-zone model).*

The comparatively low pressure value at KXP05GRS is not well met but this is to be expected considering the following facts. The permeability in the inner zone depends strongly on the distance from the niche wall and a function for this dependency is not known. Furthermore, the size of this zone is not well known. Therefore, the calculated pressure value can be adjusted in the model by changing the permeability or the size of the inner zone. But this was not done due to the imponderabilities of the existing data and due to the fact that it would have only a minor impact on the flow field.

Local 2D inhomogeneous two-phase flow model

In Figure 3-13 the results of the two-phase flow calculations in the inhomogeneous model are presented as combined contour plots for the gas saturation and vector plots for the water velocity. To increase comprehensibility, only a representative part of the whole model domain is shown.

At the beginning of the simulation, gas mobility is low so that the injected gas accumulates and increases the pressure. An almost radial displacement of water by the gas can be observed in the very first injection phase (Figure 3-13, upper left plot). With increasing gas saturation the gas mobility increases and lower pressure is necessary to move the gas in the direction of the extraction borehole. The pressure gradient in the upstream direction becomes negative and the gas on the upstream side of the injection borehole is driven back (Figure 3-13, upper right plot).

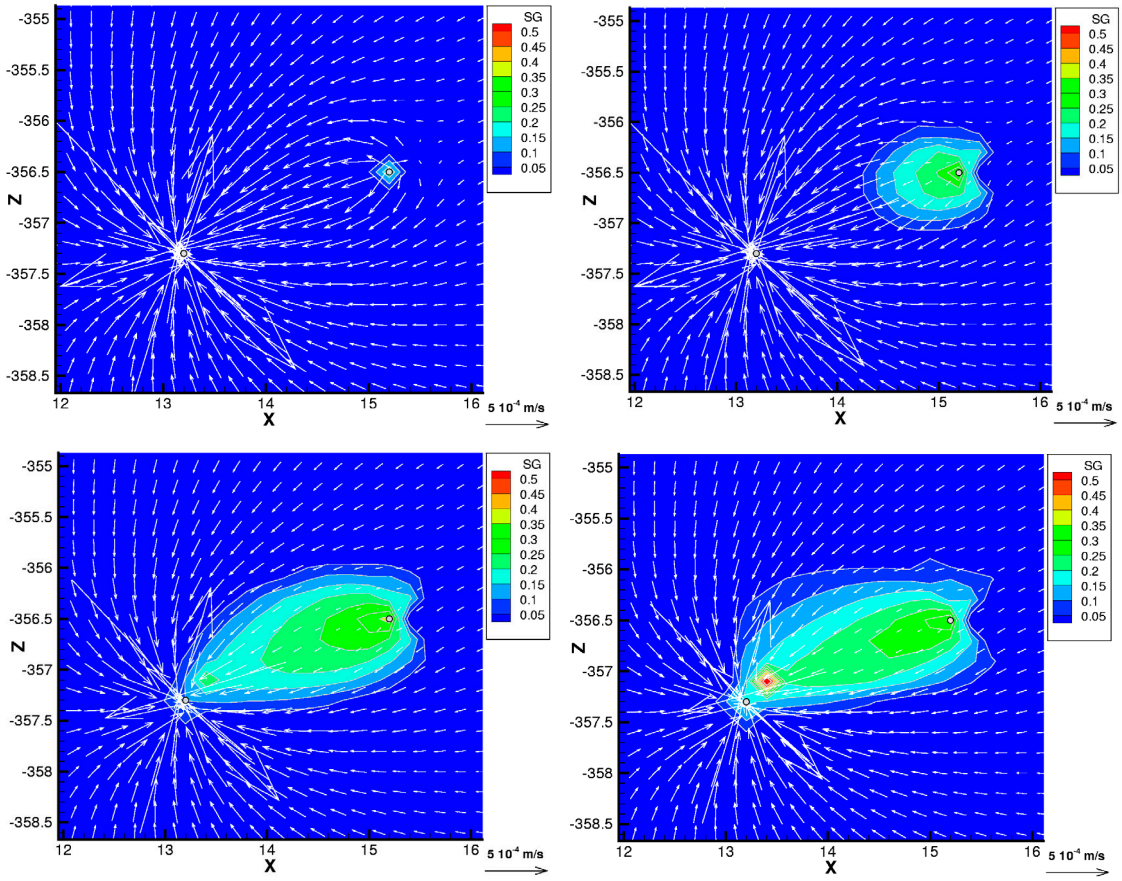

***Figure 3-13**. Gas saturation and water velocity after 10 s, 120 s, 300 s and 1200 s in the two-phase flow model.*

From that point of time, gas flow is mainly influenced by water pressure because the capillary pressure varies only negligible compared to the hydraulic pressure gradient between injection and extraction borehole. Towards the extraction borehole the gas plume is relatively narrow. A certain spreading results from the radial flow pattern at the injection borehole. Additionally, the effect of buoyancy can be observed that causes the plume to disperse more in the upward direction than downwards (Figure 3-13, lower left plot).

The extension of the gas plume changes little after the gas has arrived at the extraction borehole. Steady-state conditions are reached approximately after 900 s. The narrowness of the high-saturation area becomes even a little more pronounced (Figure 3-13, lower right plot). The saturation peak close to the extraction borehole has no physical reason but is caused by numerical difficulties.

3.3.4 Results

A 3D transient flow model of the fracture / matrix system at the niche was established which is consistent with the measured data. The appropriate model size and the errors introduced by the closed boundaries were determined numerically. The choice of the storage coefficient was evaluated with the draw-down tests performed during the project. The 3D model calculations show firstly that the flow field is presently at steady-state and secondly that the contribution of the matrix to the flow is negligible despite the fact that the matrix pore volume is much larger than the fracture volume. The matrix in the model domain as well as the storage coefficient in the continuity equation can therefore be neglected. Hence, for modelling the two-phase flow tests 2D models of the V2-structure are sufficient.

The measurements of the pressure in the undisturbed flow field revealed a high pressure gradient in the immediate vicinity of the niche and an almost uniform pressure at a rather high level in the vicinity of the measurement points. These features could be reproduced with an inhomogeneous regional 2D model assuming three zones of different permeability. The measured outflow rate was kept constant during the calibration process in order to provide reliable boundary conditions for the local two-phase flow model.

Some findings from the two-phase flow modelling should be noted: Firstly, water flow from the niche wall is not significantly influenced by the dipole test. This means that under the circumstances assumed for the model a full recovery of the injected gas can be expected.

Secondly, breakthrough occurs after 250 s model time , steady-state conditions for all practical purposes are reached after about 600 s. Accordingly, the duration for dipole tests should be a quarter of an hour.

Thirdly, comparative calculations with varied input parameters showed that even an increase of the capillary pressure by a factor of 15 has no impact on the simulation results. The same applies to some extent to the mathematical form of the relative-permeability-saturation relationship. Model results with linear functions show essentially the same saturation distribution as the results obtained with the Brooks-Corey functions.

The low sensitivity to the shape of the functions has probably the following reason. The relative permeability is increased for both phases by changing from the Brooks-Corey functions to linear functions. Effects from a higher relative permeability of one phase thereby compensate the effects from a higher relative permeability of the other phase. This problem is aggravated by the fact that in consistently derived equations of state like the Brooks-Corey functions the parameters for the relative permeability-saturation function are a subset of the parameters for the capillary pressure-saturation relationship. This means that normally the equations of state cannot be calibrated independently from each other. In other words, effects from capillary pressure would have added information to the calibration of the relative permeability-saturation relationships and thus would probably have restricted the bandwidth of possible mathematical functions.

3.4 Quantification of unsatured flow in fractured porous media (CAB and KTH)

3.4.1 Introduction

This chapter reflects the work on theoretical aspects of two-phase flow in fractured rock. It was planned to develop an improved tool for 3D-modelling of two-phase flow in fractured rock including a realistic representation of gas flow in fractures and between fractures and matrix and to apply this tool to the groundwater flow system at the test niche. However, during the in situ work of the project it became apparent that gas entry into the Äspö rock matrix is not possible due to the high entry pressure of the undisturbed rock. The techniques of the newly developed tool as well as some new developments in upscaling the saturation-dependent two-phase flow relations are nevertheless of high importance and therefore described here. Examples at the end of this chapter demonstrate the power and the possibilities of the new methods.

For simulating flow and transport processes in fractured rock, a major prerequisite is the possibility of coupling discrete fracture systems and a rock matrix (see Figure 3-14). The simulation software described here employs the concept of a porous medium for the matrix in conjunction with a discrete approximation for the fractures in view of the long-term safety of the disposal sites concerned (Helmig, 1993), (Bastian et al., 2000). A numerical code based on the finite volume method is presented for simulating two-phase-two-component flow and transport processes under the special conditions pertaining to a fractured porous medium. The code is used here to investigate a new theoretical approach for the saturation distribution in a fracture at microscopic level. This yields in combination with a description of the fracture walls by geostatistic means a modified way to quantify the equations of state for a fracture at macroscopic level, namely the relative permeability-saturation function and the capillary pressure-saturation function. First model calculations indicate not only a better agreement between the numerical results and laboratory measurements by using this new upscaling approach. Significant changes in the spreading pattern of gas in a water saturated fracture are observed also.

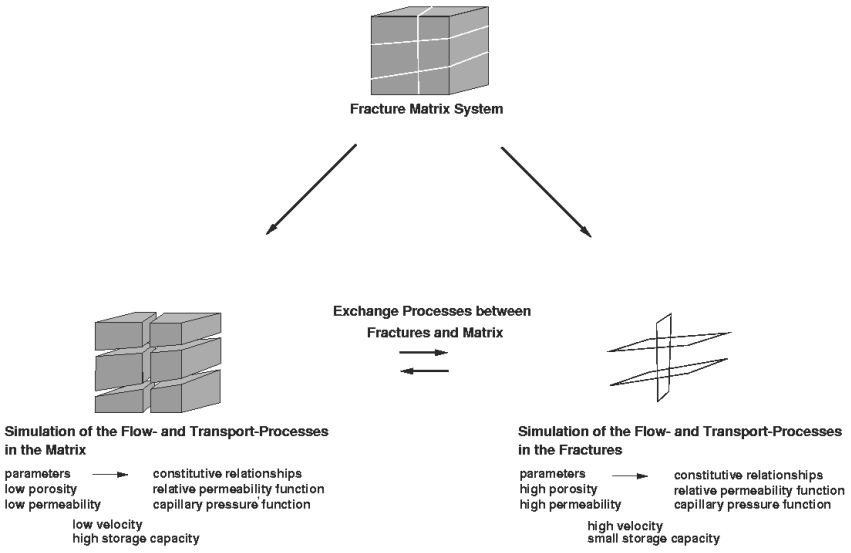

Figure 3-14. *Description of a fracture matrix system.*

3.4.2 Software description

The physical description and the discretization techniques for the considered processes within fractured porous media are coupled to the toolbox UG resulting in the simulation software MUFTE_UG (**MU**ltiphase **F**low, **T**ransport, and **E**nergy) (Helmig et al., 1994). The toolbox offers sophisticated numerical tools such as multigrid methods and adaptive refinements for unstructured grids on workstations and parallel computers (Bastian et al., 1997). Therefore MUFTE_UG is a very efficient numerical simulator for the modelling of multiphase multicomponent processes within fractured porous media (Bastian et al., 1996), (Bastian and Helmig, 1997),) (Helmig et al., 1998).

3.4.3 Considered processes

Two kinds of systems are regarded for gas water processes: the two-phase system assuming that the phases are not solvable in each other and the two-phase-two-component system, where phase transition processes are considered. The approach regarding two components assumes that thermodynamic equilibrium is reached instantaneously after change of pressure or temperature, i.e. the phase transition processes are much faster than the simulated effects. Regarding both systems advection or convection may be caused by pressure gradients as a result of boundary conditions or source and sink terms, capillary forces or by the density difference between the two phases. The two components within each phase may be also transported via diffusion due to concentration gradients of the components within each phase. The phase transfer processes which are taken into account are degassing, dissolution, evaporation, and condensation. These processes are computed via Raoult's Law, Henry's Law, Dalton's Law and the Ideal Gas Law.

3.4.4 Handling of discrete fractures

Discretization with fractures

The difficulties in describing a fractured porous medium arise as the diameter of a fracture is very small compared to the length of the system and parameter contrasts between fractures and matrix are very large. So the flow velocities are much higher in the fractures while the storage capacity of the matrix is much greater compared to the fractured system. Due to the small diameter of the fractures there are many advantages in describing them as elements of smaller dimension. In Figure 3-15 the treatment of fractures can be seen. The fracture elements are described as edges of the 2D elements. Similarly the fracture elements are described as 2D planes of the 3D elements.

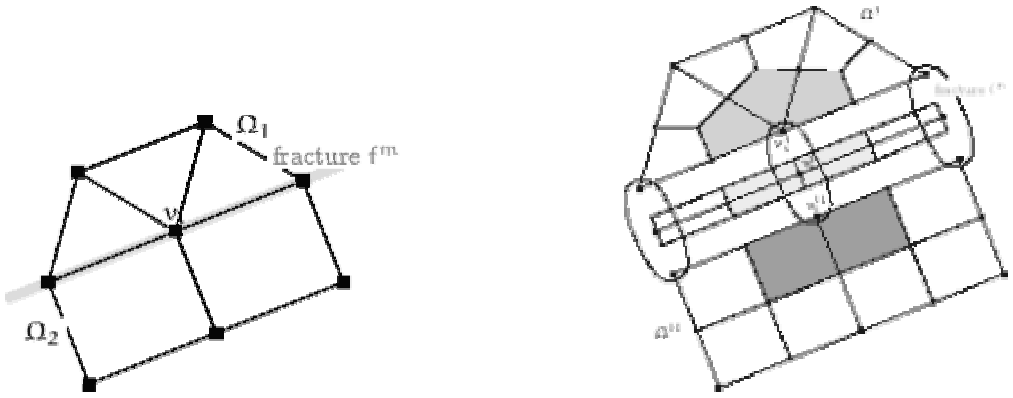

Figure 3-15. *Fracture in a grid and finite volumes for fractures*

Exchange processes between fracture and matrix

Regarding the problem of gas migration within initially fully saturated fractured porous media it had to be made sure that numerical dispersion of gas from the fracture system into the matrix system had to be prevented. As the fracture elements are of smaller dimensions it is impossible to reach a suitable refinement of the grid to achieve this. Even for the most refined grid there is still an error due to the linear interpolation between the nodes.

One solution for this problem is to use the so called **P**hase-**P**ressure-**S**aturation-**I**nterface-**C**ondition (PPSIC) where one node can have different virtual saturation values. This is achieved by computing the saturation with the inverse capillary pressure function for those domains where the capillary pressure is not minimal (see Figure 3-16). Using this interface condition the entering of a gas phase into the matrix is governed by the entry pressure of the matrix using the Brooks-Corey capillary pressure saturation relationship.

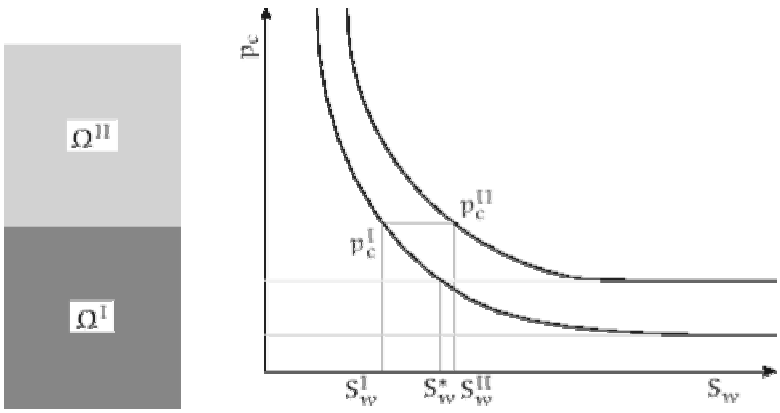

Figure 3-16. *Capillary pressure for discontinuous media.*

Fracture-system generation

With the exception of very simple fracture systems the generation of such domains is a difficult and complicated process. The input of the domain description is not only tedious, it also requires profoundly geological knowledge to create realistic models of fractured domains. A fracture generator FRAC3D was developed, that is able to generate domains based on prescribed geological properties (Hemminger et al., 1999). It creates fracture network models in 3D, where the fracture elements are represented by 2D rectangle elements and as 1D elements in a 2D clipping plane. A 3D realisation and a 2D clipping plane can be seen in Figure 3-17. It depicts that in order to avoid generating errors at the outer domain boundaries, a subdomain is cut out of the 3D and 2D domain, respectively. The generating algorithm creates fracture planes in space according to the given fracture density, spatial orientation, and trace length distribution. The information of the trace distance is not yet included.

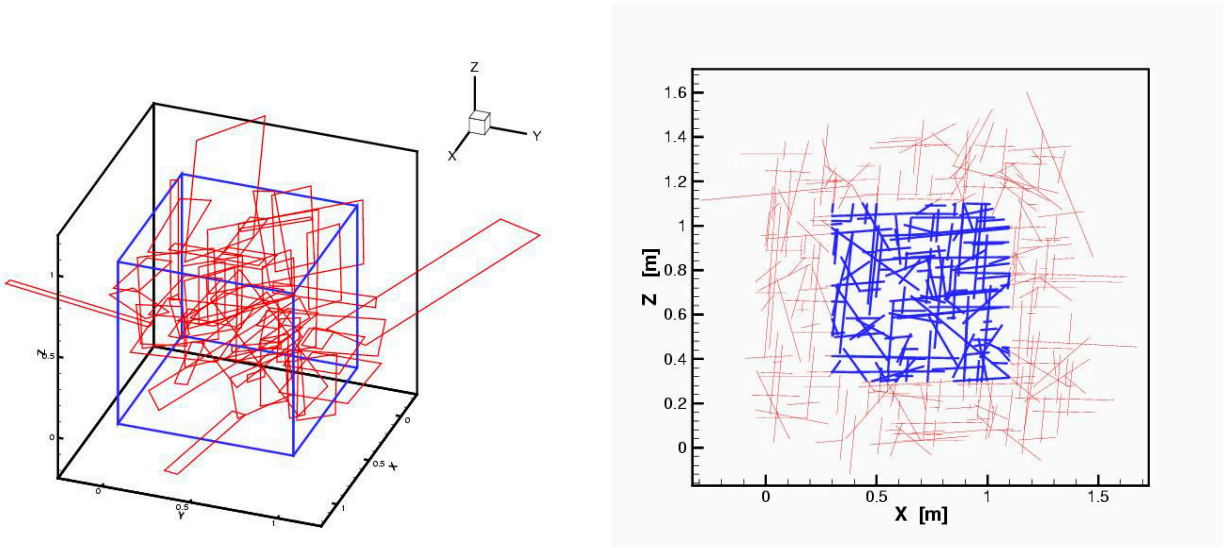

Figure 3-17. *Different fracture systems: left: 3D fracture network, fractures as 2D rectangular elements in space; right: 2D fracture network, fractures as 1D elements.*

Interface to MUFTE-UG

MUFTE-UG can directly handle the information from the fracture generator and create a boundary value problem description from it. The necessary input data include functions for fluid and media properties and boundary condition functions. They are connected to the boundaries by the property number generated by FRAC3D. The grid generator also uses the property information and retains this information in the grid description file.

The format of the grid description file is similar to the domain description. Vertices, edges (with an index number describing on which boundary it lies) and faces are the building blocks of the grid in two dimensions. MUFTE-UG can also directly read these grid files to define the finite element mesh.

Figure 3-18 shows two domains that were generated by the fracture generator and meshed with the grid generator. The configuration of the problem consists of a fully water saturated domain which is infiltrated with gas from the bottom boundary.

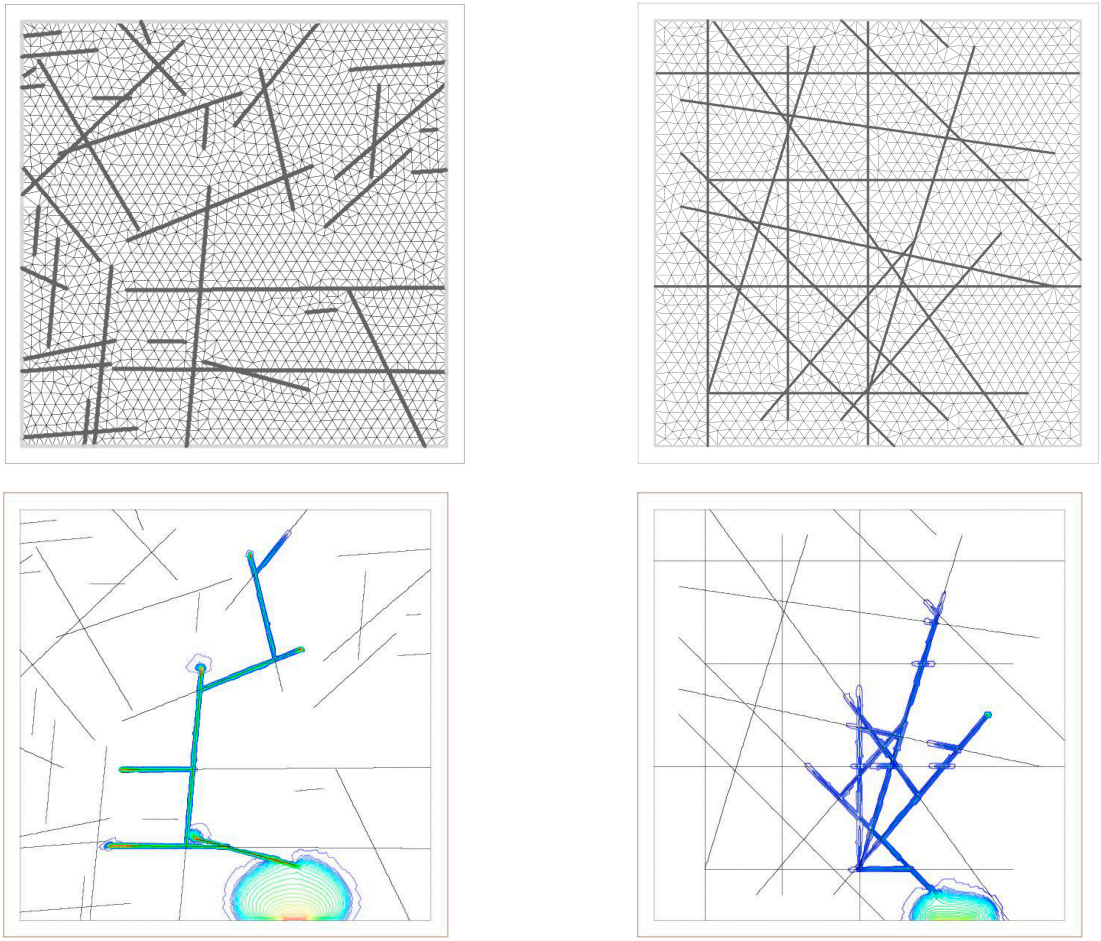

Figure 3-18. *Two domains created by the fracture generator FRAC3D and saturation plots from a gas water simulation*

3.4.5 Upscaling of gas-water flow in single fractures

The strong influence of the rough fracture surfaces on the permeability, and thus on the multiphase flow behaviour, has been realised in the last few years. The first numerical experiments on the relative permeability-saturation relation in fractures were made by Romm (1966). The results, which are based on the evaluation of two-phase flow (water-kerosene) in artificial fractures constructed of planar parallel plates, represent a linear correlation between relative permeability and saturation $k_{rw} = S_w$ and $k_{rg} = S_g$ for $0 \le k_{r\alpha} \le 1$ so that $k_{rw} + k_{rg} = 1$. This approach is applied for a large number of models for the numerical simulation of fractured oil reservoirs (Gilman and Kazemi, 1983).

More recent studies of naturally fractured rock (Pruess et al., 1990), (Persoff et al., 1991) show that the description of the relative permeability must also account for the roughness of the fracture walls, the fracture aperture, and the contact areas. The geostatistical aproach of Pruess and Tsang (1990) assumes that both phases can only flow simultaneously, if the fracture apertures are correlated anisotropically. A survey of other approaches for the description of relative permeability-saturation relations in fractures can be found in Helmig (1993).

In Pruess and Tsang (1990) rough fractures are discretised as a field of parallel plates with different averaged apertures a_{ij} (cf. Figure 3-19). So the permeability of each parallel fracture is given by $k = a^2 / 12$ as described in de Marsily (1986). As the fracture domain is normalised to a unit thickness, the transmissibility of each averaged aperture is T= a^3 / 12.

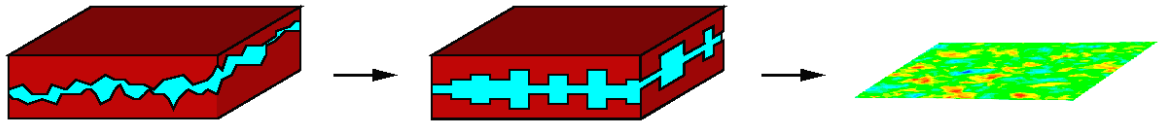

Figure 3-19. *Approximation of rough fractures with parallel plates.*

The cut-off-aperture is defined by the respective capillary $p_c = \frac{2\sigma * cos(\alpha)}{a_c}$ with the surface tension σ (cf. Figure 3-20). The contact angle α is assumed to be zero.

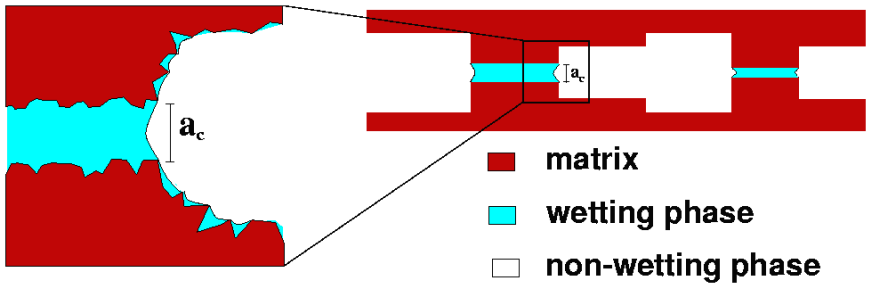

Figure 3-20. *Definition of the cut-off-aperture*

In Pruess et al. (1990), the water phase is assumed to cover all plates with an aperture lower than the cut-off-aperture. The gas phase is assumed to cover all plates with an aperture bigger than the cut-off-aperture. In Jarsjö and Destouni (1998), this approach is referred to as the separation assumption (cf. Figure 3-21).

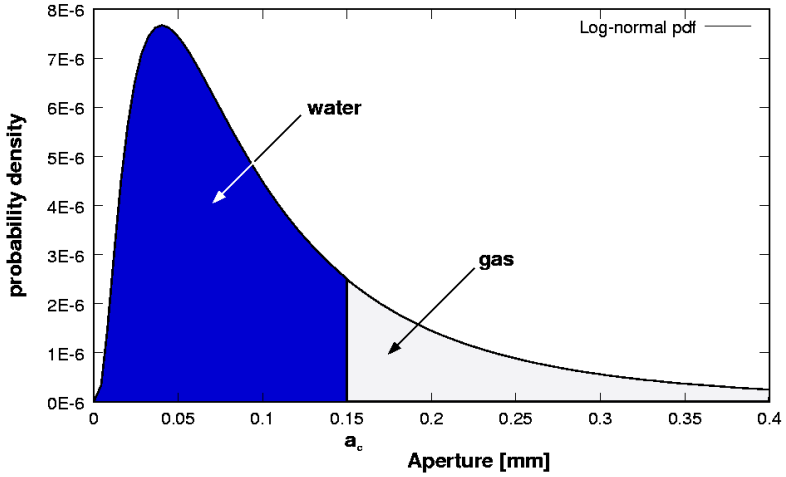

Figure 3-21. *Probability density function of aperture with separation assumption*

The saturation dependent constitutive relationships for a given cut-off-aperture can be computed only by using a given aperture distribution of the fracture. The aperture distribution used in this case was computed based on measured data given in (Jarsjö and Destouni, 1998):

$$f_{ln}(a;\mu,\sigma) = \frac{1}{a\sigma\sqrt{2\pi}} exp\left[-\frac{1}{2\sigma_\alpha^2}(ln(a)-\mu_\alpha)^2\right]$$

with the parameters $\mu_\alpha = -3; \sigma_\alpha = 0.8; \bar{a} = 0.05[mm]$. The capillary pressure for a cut-off-aperture is given in Bastian et al. (2000), the relative permeability for the wetting phase was computed via the relative transmissivity

$$T_S(a_c) = \frac{\int_0^{a_c} a^3 \cdot f_{ln}(a)da}{\int_0^{\infty} a^3 \cdot f_{ln}(a)da}.$$

The relative permeability for the gas phase was computed using the separation assumption

$$phase_s = \left\{\begin{matrix} a < a_c \rightarrow w \\ a \geq a_c \rightarrow g \end{matrix}\right\},$$

the saturation is computed using

$$S_w = \frac{\int_0^{a_c} a \cdot f_{ln}(a)da}{\int_0^{\infty} a \cdot f_{ln}(a)da}.$$

Thus, the functions for the constitutive relationships follow, as given in Figure 3-22. Observe the very steep gradient of the relative permeability - saturation function at $S_w \approx 1$. At this point, even small changes in saturation do have a big influence on hydraulic conditions within the fractures.

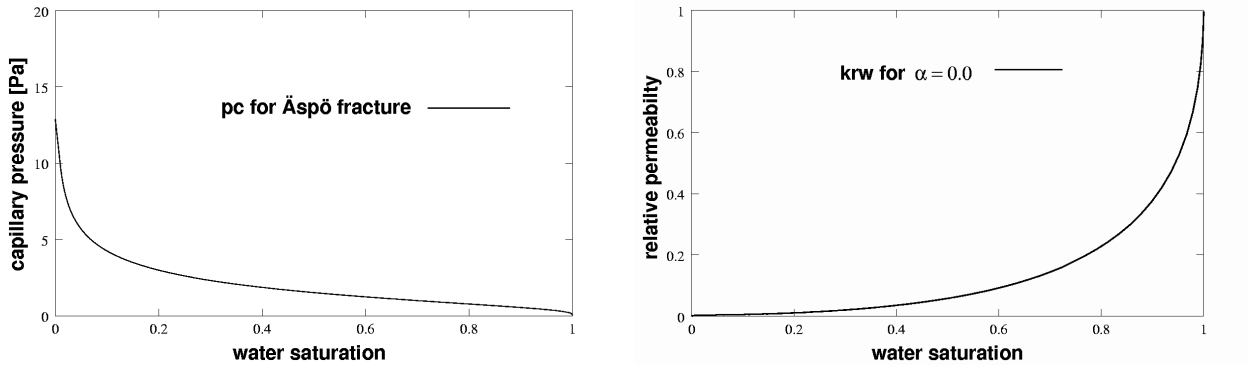

Figure 3-22. *Capillary pressure saturation function (left) and relative permeability saturation function (right) using the separation assumption*

In Jarsjö and Destouni (1998) a new upscaling aproach based on an aperture distribution is formulated using the assumption that a fraction of the plates with $S_w \approx 0$ is still covered with the water phase. This fraction is given by the factor α. They refer to this assumption as mix assumption. The results of laboratory observations of a degassing experiment published in

Jarsjö and Geller (1996) were compared with the predictions of the relative transmissibilities and the gas saturations based on the various assumptions (Jarsjö and Destouni, 1998). Better results were achieved by using the mix assumption.

Using the mix assumption

$$phase_s = \left\{ \begin{array}{c} a < a_c \rightarrow w \\ a \geq a_c \rightarrow \alpha w + (1-\alpha) g \end{array} \right\}$$

the saturation for a cut-off-aperture a_c is given by

$$S_w = \frac{\int_0^{a_c} a \cdot f_{ln}(a)da + \alpha \int_{a_c}^{\infty} a \cdot f_{ln}(a)da}{\int_0^{\infty} a \cdot f_{ln}(a)da}.$$

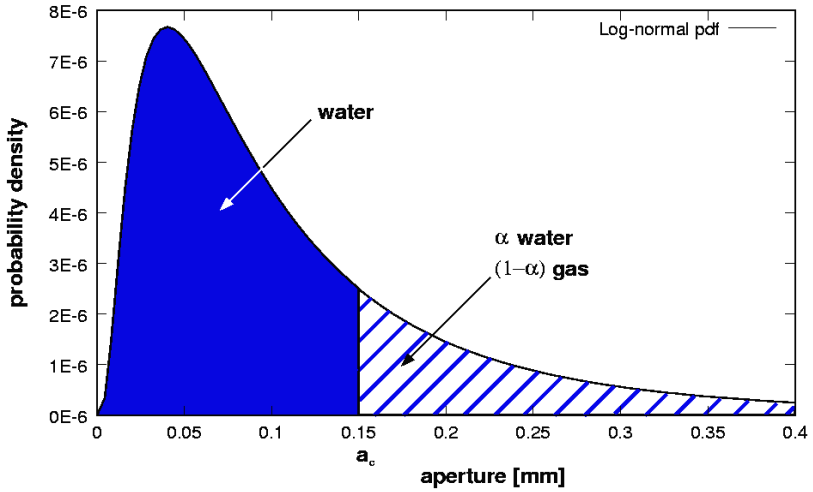

Figure 3-23. *Probability density function of aperture using mix assumption.*

Thus, different constitutive relationships follow. In (Jarsjö and Destouni, 1998) the best approximation for the mix assumption is given by $\alpha = 0.2$, which results in a residual saturation for the water phase of $S_{wr} = 0.2$. However, the steep gradient remains in these constitutive relationships.

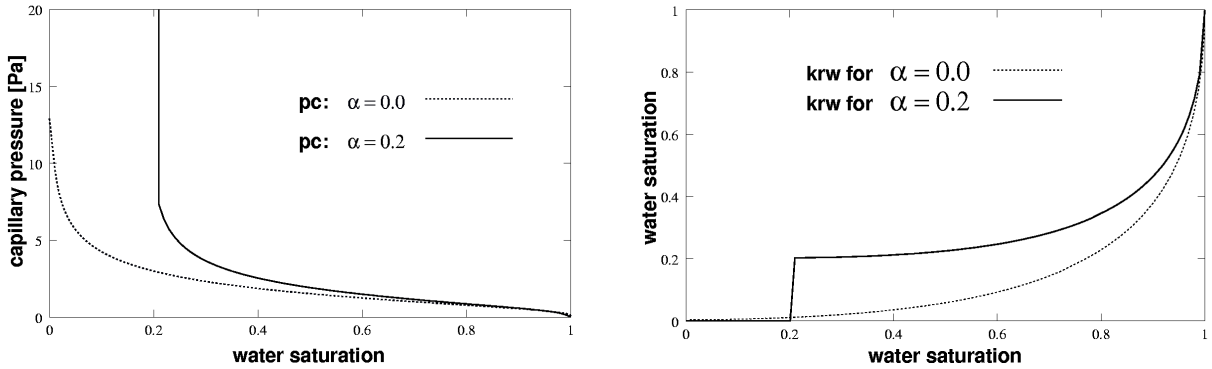

Figure 3-24. *Comparison of capillary pressure saturation function (left) and relative permeability saturation function (right) based on separation assumption (blue) and mixed assumption (red).*

Based on data published (Jarsjö and Geller, 1996), different permeability fields were generated with the geostatistical tool SIMSET. SIMSET uses the turning band method as basic approach to generate geostatistical data.

The best approximation to the measured aperture distribution given in Jarsjö and Geller (1996) was accomplished with an exponential variogram superposed with a nugget effect. Assuming the parallel plate model a permeability field was generated using the relationship $k = \frac{a^2}{12}$ for a two dimensional area of 1 x 1 m^2. In the following Table 3-2 the input parameters describing the exponential variogram with superposed nugget effect are given. These parameters are estimated based on the pictures published.

Table 3-2. Input parameters describing the exponential variogram.

Average permeability		$\log(K) = -9.0$
Variance	Proportion nugget effect	0.01
	Proportion exponential variogr.	0.30
Correlation length		0.04 m

The average permeability $\log(K) = -9.0$ corresponds to an average aperture of $\bar{a} = 0.11$ mm. This does not match with the parameters used for the computation of the constitutive relationships. Here the best approximation for the measured aperture distribution is an average aperture of $\bar{a} = 0.0087$ mm. However, the aim of these computations was to compare the influence of the two different assumptions qualitatively. Quantitative statements are not possible, since experimental results at the moment are lacking.

Based on the generated permeability field the entering of a gas phase at the bottom of the domain was simulated. The diameters of the inlet- and of the outlet-opening were given by 0.02 m. The boundary conditions can be seen in Figure 3-25. The porosity was set to $\phi = 0.4$. Both the boundary conditions and the porosity were chosen arbitrarily. The capillary pressure was upscaled for each plate via the Leverett condition (Leverett, 1941) $p_c^{elem} = p_c^{avg}\sqrt{\frac{K^{avg}}{K^{elem}}}$). For the relative permeability function no upscaling concept was established.

The input parameters for the numerical simulation of gas infiltration are summarized in Table 3-3.

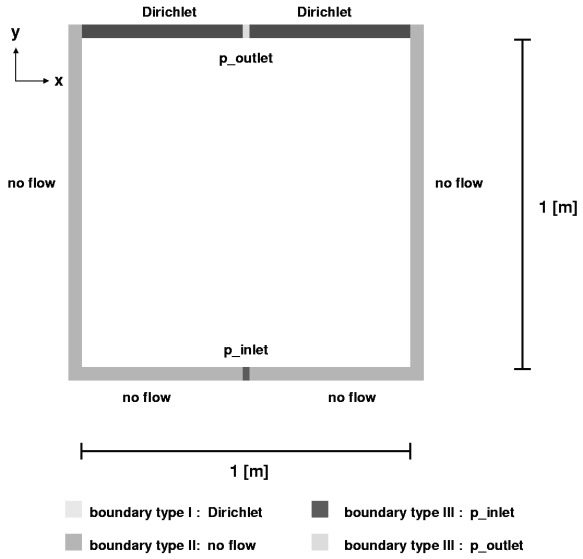

Figure 3-25. *Boundary conditions for numerical simulation of gas infiltration.*

Table 3-3. Input parameters for numerical simulation of gas infiltration

INITIAL VALUES:

$S_g(x, y) = 0.9999$

$p_g(x, y) = (1 - y) * 9810$ Pa

PHASE PROPERTIES:

Water	Gas
$\rho_w = 1000\,\text{kg/m}^3$	$\rho_g = p_g / 84149.6\ \text{kg/m}^3$
$\mu_w = 10^{-3}\,\text{Pa s}$	$\mu_w = 1.65 * 10^{-5}\ \text{Pa s}$

BOUNDARY CONDITIONS

No flow	$q_g = 0.0$	$q_w = 0.0$
Dirichlet	$p_g = 10000.0\,\text{Pa}$	$S_w = 0.9999$
P_inlet	$p_g = 30210.0\,\text{Pa}$	$q_w = 0.0$
P_outlet	$p_g = 200.0\,\text{Pa}$	$q_w = 0.0$

For both assumptions the main flow paths are given by the areas of high permeability which are slightly connected. The gas velocities shown in Figure 3-26 do not differ much, similar to the results for the effective permeability and for the pressure field. The most relevant differences occur in the saturation (Figure 3-27). The simulation using the constitutive relationships based on the mix assumption results in a wider spreading of the gas phase and in higher gradients for the gas phase. In Figure 3-28, the influence on the main flow paths is shown. The gas (dark colour) migrates through those regions with higher effective permeability.

Figure 3-26. *Velocities for relationships based on separation assumption (left) and mix assumption (right) at t=3.5 s.*

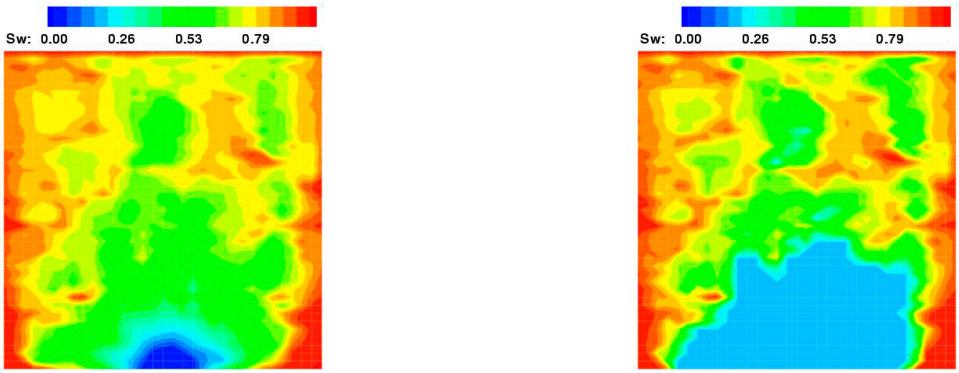

Figure 3-27. *Water saturation for relationships based on separation assumption (left) and mix assumption (right) at t=3.5 s.*

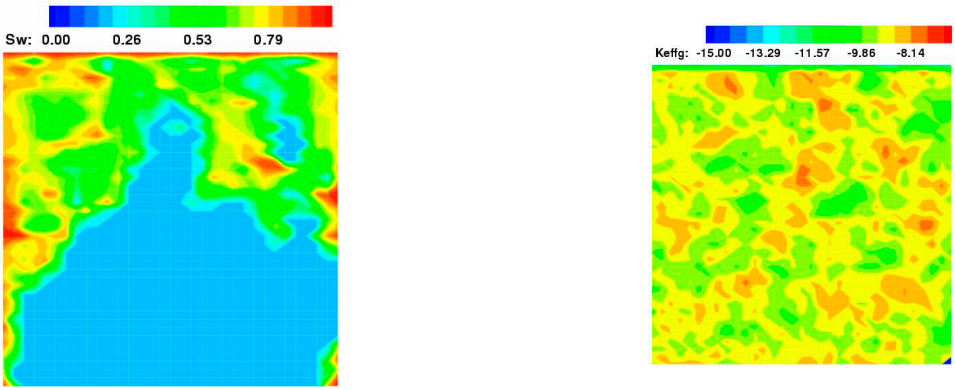

Figure 3-28. *Water saturation and filtered effective permeability for mix assumption at t=6.5 s*

3.4.6 Conclusions

The use of advanced numerical methods on high performance computers has been established for the simulation of gas water flow and transport processes. This approach allows the implementation of geostatistic data fields in two and three dimensions to identify uncertainties with e.g. Monte Carlo methods.

Due to the implementation of fractures as hyper-planes the entering of gas from the fracture into the matrix system was considered carefully. Therefore the Phase-Pressure-Saturation-Interface-Condition (PPSIC) has been established for the fracture formulation. In a synthetic example for gas intrusion into a fractured porous medium it was shown that the PPSIC eliminates numerical dispersion of gas from the lower dimensional fracture into the matrix.

First approaches have been presented to get effective parameters which are necessary for a reliable simulation of gas water processes in fracture matrix systems. Firstly, a fracture generator (Hemminger at al., 1999) was integrated into MUFTE_UG so that reasonable stochastic or deterministic fracture fields could be included into the simulation process. Secondly, a new upscaling concept for two-phase flow parameters in a single fracture was formulated.

Based on the geostatistical data for Äspö rock, a model for a fracture with variable aperture and variable permeability was created. The fracture was assumed to be fully water saturated and a gas intrusion into this fracture was simulated using MUFTE_UG. The constitutive relationships for the two-phase flow were derived with the conventional upscaling scheme on one hand and with the new approach on the other hand. A comparison of the results shows significant differences in the saturation distribution. Apparently, further research is necessary to investigate the implications of this new upscaling concept.

3.5 Comparison of modelling approaches and results

The modelling work can be divided into two categories: (1) theoretical work related to developing the constitutive relationships and to improving the simulation tools as described in Chapter 3.4 and (2) simulation of groundwater and two-phase flow at Äspö as described in Chapters 3.2 and 3.3.

The investigations started with single-phase regional flow models aimed at understanding the larger flow system before the local system was studied more closely. Both BGR and GRS use the ROCKFLOW code for modelling regional flow but they use different special features of this code. BGR models the complex regional fracture system with a system of nine planar fractures which intersect each other as well as the tunnels of the Äspö HRL. Additionally, the fractures are connected by a horizontal plane at about 700 m depth (see Figure 3-4). GRS concentrates more on a possible matrix influence on the groundwater flow, uses a number of more simplifying assumptions on the conceptual model resulting in a model with only one vertical fracture which substitutes the complicated fracture system. This fracture crosses the test niche and is coupled to an adequate rock matrix volume. GRS model calculations indicate that the matrix does not play a significant role in the groundwater flow system at Äspö, neither in terms of water conduction nor in terms of storage effects. Subsequently, the matrix part of the model is not considered any further.

Each fracture in the BGR fracture network model has a width of 1 mm. In the GRS model the fracture network is substituted by a single 25-mm-wide fracture. In the BGR model all fractures except one are directly connected to the Baltic sea. Each of these fractures is larger than the 500 m x 500 m fracture in the GRS model. The total area of the fracture openings to the sea lies on the same order of magnitude in both models. Using the measured outflow rate out of the niche for calibration of the single-phase flow models yields permeability values which differ not more than one order of magnitude. In this respect the capability of both models to simulate the characteristics of the regional flow is good.

For integrating the permeability changes at the niche into the model, BGR uses almost uniform element meshes and therefore needs an intermediate scale model. This is accomplished by GRS with the help of a locally highly refined grid at the niche using the regional scale model for the fracture.

Two-phase flow is modelled by GRS with the MUFTE code and by BGR with two-phase flow module MMTM of ROCKFLOW. Supporting two-phase flow calculations are performed by BGR with TOUGH2. Whereas GRS conducts predictive calculations based on actual test design data available before test performance, BGR models a specific test, namely the GWTR6 test. BGR uses the models to fit the necessary parameters to the measured data while GRS performs a sensitivity analysis in order to back up the predictions.

Both groups use a vertical or subvertical 2D fracture model to model the two-phase flow dipole test. While the influence of the dip on the fracture flow is negligible, the models differ in several more significant aspects:

- model size
- boundary conditions
- injection rates
- pressure at the dipole
- fracture permeability
- parameters for the relative permeability-saturation function
- use of capillary pressure-saturation function

The models used and the input parameters are summarised in Table 3-4. The ROCKFLOW and the TOUGH2 model use a homogeneous permeability and are much smaller (3-m scale) than the MUFTE model (30-m scale). In the MUFTE model the reduced permeability as well as the well defined boundary conditions at the niche wall are considered, in the ROCKFLOW and the TOUGH2 models the niche is not included.

In the ROCKFLOW model constant pressure boundary conditions are used and in the TOUGH2 model constant water flow conditions along each of the model edges. For the MUFTE model the pressure boundary conditions are gained from the regional scale model. Because the boundary conditions determine the flow patterns of the velocity field, the undisturbed groundwater flow is represented quite differently in the three models. In the TOUGH2 model a horizontal parallel flow field is implicated by the Neumann boundary conditions. Somewhat more complicated is the flow field in the ROCKFLOW model due to the assumption of different, but constant pressure values along the model boundaries. In the MUFTE model the water pressure was directly transferred from the larger scale single-phase flow model to the two-phase flow model. For this reason the undisturbed-flow boundary condition in that two-phase flow model seems to be better corresponding to single-phase flow of the regional scale model.

In the MUFTE model only gas is injected. In the other two models simultaneous gas and water injection is simulated. Gas injection rates are 2 l/min (MUFTE), 2.9 l/min (ROCKFLOW) and 0.082 l/min (TOUGH2). Water injection into the TOUGH2 model is indirectly handled by applying a pressure boundary condition at the injection point. In the ROCKFLOW model 0.051 l/min water are injected. Water pressure at the extraction point is constant. In the MUFTE model atmospheric pressure is assumed and in the ROCKFLOW and the TOUGH2 models an elevated pressure value is used according to the actual test.

The pressure difference between the poles of the dipole influences the flow velocity. This difference is higher in the ROCKFLOW model than in the other two models. Another flow controlling factor is the fracture permeability. In the TOUGH2 model it is significantly higher than in the other models. A relative permeability-saturation function after Brooks and Corey is used in the MUFTE model and in the TOUGH2 model. A similar approach is used in the ROCKFLOW model. In the MUFTE model a capillary pressure-saturation relationship is included.

In order to compare the modelling results, the distribution of gas saturation after about 5 minutes as shown in the graphical presentations of the modelling groups is used in the following as basis.

Despite the different model set-up, the shape of the gas plume is rather similar in the MUFTE and the TOUGH2 model (see Figure 3-13 and Figure 3-6). The maximum gas saturation is about 40% at the injection location and decreases with the distance to the source. The plume appears to be stretched in the direction towards the extraction point which results in an ellipsoidal shape.

In contrast to that, the plume in the ROCKFLOW model has an almost circular shape with the injection point located near to the plume boundary (see Figure 3-9). The maximum gas saturation amounts to about 40% as well but it is more or less equally distributed over the gas filled area with the exception of several local spots with lower concentrations. The saturation distribution seems to be disturbed by some large oscillations which could be due to the steep saturation gradient at the boundary of the gas filled area. This gradient is much steeper than in the other two models.

The summary of the features in the models is given in Table 3-4.

Table 3-4. Description of the models

Modeller	BGR		GRS
Evaluation	Test GWTR6		Predictive
Model	ROCKFLOW (MMTM)	TOUGH2	MUFTE
Fracture model	subvertical 2D fracture	Vertical 2D fracture	
TPF model	3.6 m x 2 m, niche not included	3 m x 3 m, niche not included	32 m x 32 m, niche included
Boundary conditions	constant pressure	Constant water flow	variable pressure from regional scale
Injected fluids	simultaneous gas/water injection		gas injection
Water pressure at extraction point	1.3 MPa	1.825 MPa	0.1 MPa
Pressure difference between poles	1 MPa	0.5 MPa	0.3 MPa
Fracture permeability	$5\ 10^{-13}\ m^2$	$5\ 10^{-10}\ m^2$	$5\ 10^{-12}\ m^2$
Relative permeability-saturation function	similar to Brooks/Corey	Brooks/Corey	
Residual water saturation	10%	14%	9%
Residual gas saturation	5%	2%	0%
Comparison	distribution of gas saturation after about 5 minutes		
Shape of gas plume	Max 40%, equally distributed, circular	40%-peak at injection point, ellipsoidal	
Gas breakthrough	600 sec		250 sec

Another important difference between the results can be found in the travel time of the gas plume. In the MUFTE model, the gas plume moves faster than in the ROCKFLOW and TOUGH2 models. MUFTE predicts gas breakthrough after 250 s whereas according to ROCKFLOW and TOUGH2 calculations breakthrough occurs after 600 s.

In order to understand the reason for these differences, the following factors controlling the spreading of the gas plume are to be taken into account:

- pressure gradient,
- effective gas permeability,
- capillary pressure,
- injection rates,
- pore volume.

In principal, the gas flow is proportional to the pressure gradient multiplied by the effective permeability. The effective permeability depends on the absolute permeability - a single parameter - and the relative gas permeability which is calculated from a relative permeability-saturation function. Thus, for an estimation of the gas flow the actual saturation distribution along the flow path has to be taken into account.

Water displacement by the injected gas is proportional to the injection rate. Additionally, the spreading of the gas plume is dependent on the fracture width. The larger the aperture the bigger the volume into which the gas expands and the slower the progress of the saturation front. The same applies for the porosity value of the fracture. Finally, the average gas saturation and the average pressure in the plume have to be considered because these values, too, are proportional to the amount of gas mass in the pore space. Furthermore, gas spreading is influenced by the amount of injected water. The extent to which the injected water - and the gas carried with the water - flows from the injection point in the upstream direction and perpendicular to the dipole axis is proportional to the injection rate.

This compilation of interacting effects explains the difficulties in comparing the two-phase flow models. If possible at all, the reason for the discrepancies can only be clarified in terms of qualitative considerations. Here, a rough consistency check of the models is performed which is based on the idea that the time period until breakthrough is mainly dependent on the rate at which the pore space is filled with gas. This rate is measured in filling time per fracture area and requires a set of parameters as given in Table 3-5. Such a consistency check is made between the MUFTE and the ROCKFLOW model.

Table 3-5. Parameters for a consistency check between the MUFTE and the ROCKFLOW model

Parameter	unit	MUFTE	ROCKFLOW
Gas injection rate	l/min	2	2,9
Water injection rate	l/min	0	0,051
Average gas pressure	MPa	0,25	2,2
Aperture	mm	25	1
Porosity	-	0,20	1,00
Average gas saturation	-	0,20	0,40

Based on the data of Table 3-5 it takes 75 s in the MUFTE model and 131 s in the ROCKFLOW model until one square metre of the fracture is filled up to the maximum with gas. The rates differ about a factor of less than 2 while the difference in the breakthrough times – 250 s in the MUFTE model and 600 s in the ROCKFLOW model - is about 2.5. Considering the imponderabilities in the data, the agreement between the calculation results is satisfying.

The remaining discrepancy could be due to the fact that no water injection is considered in the MUFTE model. This may explain the differences in shape of the gas plume as well as in the saturation distribution. If the naturally flowing water in the fracture is completely displaced by the injected water, the gas saturation would remain constant in the whole range of the displaced water. Gas could thereby be transported from the injection point in the upstream direction as well as perpendicular to the dipole axis as was observed in the ROCKFLOW model. In contrast to that, the gas source in the MUFTE model is mostly overflown by water and thus the gas plume gets the ellipsoidal shape. The fact that the shape in the TOUGH2 model is ellipsoidal as well indicates that only little water is injected into the TOUGH2 model compared to the injection into the ROCKFLOW model.

A comparison between numerical simulation and measurements is given for the TOUGH2 model. In Figure 3-7 the measured outflow rate of gas is fairly well matched by the calculated flow rate in terms of breakthrough time and the steady-state flow rate. The outflow rate of water is measured with a rather low resolution. However, a constant rate of 0.21 l/min is measured until gas breakthrough. Breakthrough is marked by an almost instantaneous decrease to 0.16 l/min, but subsequently the rate increases again to a steady state flow rate of 0.17 l/min during the first 1000 seconds after gas breakthrough. In the model the same steady-state flow rate is calculated after the gas flow reaches steady-state. This takes more than 10 000 s and is therefore not completely satisfying.

The short peak in the outflow rate at the very beginning of the simulation is not understood. It may have to do with the rather unusual set-up of the constant flow boundary conditions and the source/sink descriptions in a domain which is closed for flow otherwise.

3.6 Conclusions from modelling work

From the modelling results the conclusion can be drawn that fracture flow is dominant in a fractured porous rock similar to that at Äspö. In the fracture the entry pressure is very low and the fracture permeability is rather high. On the other hand, in the matrix the water flow is negligible and the entry pressure is high. Therefore it can be expected that gas entering the rock will flow along the fractures and will not enter the rock matrix. The fracture system is open against the atmosphere at sea level and therefore gas will be transported to the atmosphere and not be stored in the rock. Gas production in a repository will therefore not lead to exceedingly high pressures in the rock.

For a regional fracture model, calibration of integral single-phase flow parameters can be accomplished with reasonable accuracy. Local deviations in the parameters average so that no detailed description is required on a regional scale. But, the smaller the model domains are the more important the influence of those local deviations becomes. One example is the unexpected low permeability zone around the niche walls which calls for a more detailed model description in order to sustain the reliability of the small scale models.

However, even in these small scale models the properties of the fracture are homogenised over a comparatively large area. On an even smaller scale – a scale which resolves the variable fracture aperture - flow channels become apparent. If and how far a detailed description of these features in a model is necessary depends on the problem at hand and is subject to further investigations. The detailed models developed in the present work of KTH and CAB may be powerful tools to determine appropriate parameters for upscaled models.

For modelling two-phase flow, models with very different properties were implemented, particularly as far as size and boundary conditions are concerned. However, from a comparison of the results the following general conclusions can be drawn:

The two-phase flow ROCKFLOW and TOUGH2 models are 3.6 x 2 m^2 and 3 x 3 m^2 in size, respectively, and have constant boundary conditions along each boundary. They do not include the niche with its special properties providing easily definable boundary conditions. This approach requires great care in selecting the boundary conditions. Additionally, it must be ensured that the transient flow processes induced by the fluid injection are not influenced by the constant conditions on the model boundary. Therefore, the MUFTE model has a model size of 32 x 32 m^2 due to an of extensive grid refinement and uses pressure boundary conditions from the regional scale model. The grid resolutions in the region surrounding the dipole are on the same order of magnitude for all three models. This means, that the physical processes are simulated on the same scale in the area of interest, even if the fracture area covered by the MUFTE model is one hundred times larger than in the two other models.

A comparison between measured and calculated data is presented for the TOUGH2 model. Since, as shown in Chapter 3.5, fairly good agreements were reached between the results of the TOUGH2 model and the ROCKFLOW model and between the results of the TOUGH2 model and MUFTE model, respectively, this comparison can, to a certain extent, be used for the overall modelling results.

While a rather good correspondence exists between measured and calculated gas outflow rates, larger differences exist between the water outflow rates. This can be explained by the fact that even single-phase flow parameters like fracture aperture and porosity varied in the models considerably. Moreover, some observations during the in situ tests indicated more local pathways and permeability inhomogeneities in the region surrounding the test boreholes. However, a further refining of the models was not possible. On the other hand, the sensitivity analysis based on the MUFTE model shows a low dependence of the results on the relative permeability-saturation function. These items lead to the conclusion that for providing the parameter values required for two-phase flow calculations the single-phase flow must be characterised in much greater detail than for simulating groundwater flow.

4 Conclusions

4.1 Knowledge gained

On macroscopic scale the flow field in the Äspö underground is – except for faults of extreme extension like the NE-2 – generally influenced by structures of equal orientation and with high spatial frequency as the investigated V2-fracture at the niche 2715. These structures are not real planar fractures but complex fault systems of limited extension consisting of major faults, splays and steps. The geometry of these features varies to a certain extent and consequently also the hydraulic properties.

Therefore, investigation of the water pressure distribution, the starting point of field data collecting, and the time dependent changes in the flow field are of high importance. For example, while the observed water pressure and the measured water flow rates in the V2-fracture show evidence that the flow field around the niche has become stationary, the pressure and flow values did not match the theoretically expected data coming from a homogeneous isotropic model. This phenomenon is probably a result of excavation effects, of the development of a disturbed zone, and in some cases a result of two-phase-flow phenomena.

The gas entry pressure in the matrix was found to be above the measurements detection limit (5 MPa). Gas will therefore enter the matrix only at gas pressures of at least 5 MPa. At pressures lower than 5 MPa, gas will not migrate into the matrix as a separate phase but rather as a solved component in the water phase.

Not yet fully understood is the role of the tight rock matrix with respect to the water flow. Obviously, capillary effects determine the water exchange between matrix and fractures if the rock is not fully saturated. Gas which has evolved in the matrix due to a pressure drop – for example from excavation – is stuck in the matrix pore spaces and reduces the effective water permeability to approximately zero. It is still open to what extent this effect will be relevant for long-term considerations.

Since natural gas solved in the fracture water was detected, too, degassing effects can occur in the fractures as well. Gas can therefore interfere with the determination of the water permeability to a significant extent. Additionally, the heterogeneity within a fracture system leads to a broad distribution of the water permeability values. It has therefore to be kept in mind that pointwise information about the permeability can be misleading due to the natural spread on the local scale when using this information for macroscopic considerations or further numerical calculations.

In the test field, fracture apertures are too big to form a serious obstacle against gas flow. On the other hand, the experiments have revealed that the entry pressure of the undisturbed matrix is very high. Therefore, it can be concluded that gas located in a fracture cannot enter the matrix even at gas generation rates as expected under the operating conditions of a repository. Since the entry pressure represents the lowest value in the capillary pressure-saturation relationship, gas flow in the rock matrix is not possible. Thus, in a granitic rock like that at Äspö, gas transport is restricted to the fractures where gas flow is not hindered by capillary pressure. Gas production in a repository will therefore not raise the gas pressure in the host rock significantly above

the hydrostatic level.The results of the modelling exercise confirmed the following conclusions of earlier investigations into the groundwater flow in the Äspö host rock: The granite contains large scale fracture systems which are well interconnected. This overall fracture systems reaches from the Baltic sea down to the horizon of the Äspö HRL. In the rock matrix, steady-state water flow is negligible due to the very low permeability of the undisturbed rock and due to its very low storage capacity. After tunnel excavation or any other major change in the flow domain, a transient phase of the groundwater flow can not be expected to last more than several months. Consequently, effects of the tunnel excavation on the flow field are not traceable anymore. The undisturbed groundwater movement is therefore dominated by steady-state fracture flow.

The rather low value of the capillary pressure in the fracture which was measured in the field implies that the impact of the capillary pressure on the two-phase flow is of secondary importance in the in situ experiment. The maximum capillary pressure is on the order of 100 Pa or less and can therefore cause only negligible pressure gradients compared to the hydraulic pressure gradient of several hundred kPa/m in the in situ test. Thus, no conclusive results concerning the capillary pressure-saturation function can be given.

However, the modelling results as well as the measurements show clearly that the experiments result in a pronounced two-phase flow. Injection pressure at the dipole and gas inflow rate, respectively, were in a range in which a complete displacement of water by gas was not possible. No two-phase flow model produced a gas saturation exceeding a value of 40 %.

It must be noted that the spreading of the gas plume looks rather similar in the MUFTE model and in the TOUGH2 model, despite all the differences concerning model geometry, boundary conditions, and flow parameters as listed in Chapter 3.5. Even the most obvious difference, obtained in the travel time, amounts to a factor of about 2 only. It remains to be investigated if the results are not very sensitive to the above mentioned differences or if effects of the differences cancel each other.

Taking the findings about the saturation-dependent equations of state into account, it is recommended to follow the theoretical work of KTH concerning the means of upscaling two-phase flow parameters. The advantage of this approach is that the saturation dependent parameters are a function of measurable geostatistic data from the fractures. If successful, it will provide alternative means of identifying two-phase flow parameters. Further investigations are required to study the applicability of this method.

The application of newly derived constitutive relationships to real fracture-matrix domains was further improved by the work of CAB. A new approach which virtually eliminates numerical dispersion from a fracture into the matrix was incorporated in the MUFTE_UG code. It allows more realistic representations of two-phase flow phenomena in fractured rock than conventional continuum models. Due to the ability to handle geostatistical data the code seems to be ideally suited to be utilised in the new upscaling approach of KTH.

4.2 Problems encountered and lessons learned

The pressure measurements around the niche indicate that a narrow zone of comparatively low permeability exists around the niche. This finding is in contrast to the assumption of an increased permeability in the excavation damaged zone. The reason for this effect is not clear and remains to be investigated further. Another uncertainty became apparent during the draw-down tests. The pressure responses indicate further inhomogeneities of the V2 fracture within the region of the test locations. From the available data base generated from the in situ tests it was not possible to obtain sufficient information to further refine the models.

The extent to which the flow domain must be characterised for a two-phase flow simulation exceeds by far the demands for single-phase flow simulations. Small scale permeability changes due to a variable fracture aperture average out for single-phase flow and deviations from the average fracture aperture lead to calculation errors in the permeability in the range of the uncertainties. However, in two-phase flow the variable fracture width controls the saturation dependent constitutive relationships and, therefore, spreading of a second phase strongly depends on the fracture width. During the project performance it became evident that these demands could not be met sufficiently by the data base generated from the in situ tests.

Depending on the theoretical approach, different mathematical functions – the equations of state – can be chosen to describe the saturation dependent permeability like the functions of Brookes-Corey or van Genuchten. For a given function the optimal parameter set can be calibrated using measurements as was demonstrated by BGR. But the more ambitious task to determine the appropriate underlying function cannot be achieved in this case, where the influence of the capillary pressure is missing. Capillary effects in the two-phase flow would have added information for the calibration of the relative permeability-saturation relationship. In the absence of significant capillary pressure, the modelling results of GRS, based on linear and exponential functions, showed no significant differences so that no conclusions concerning the shape of the relative permeability-saturation function can be drawn.

Downscaling of the models for two-phase flow calculations was performed differently in each of the three models. But in all three cases the undisturbed water flow field was used as the basis for the two-phase flow models. In the light of the findings concerning the necessary accuracy of the single-phase flow field it is recommended for future exercises to focus not only on the two-phase flow simulations but on the underlying undisturbed flow in the downscaled model as well. This should improve the understanding and comparison of different models.

5 References

Bastian P, Helmig R, Huber R, Braun C, 1996. Modelling and efficient solution technique for multiphase flow in porous media, Technical report, SFB 404 Mehrfeldproblem in der Kontinuumsmechanik

Bastian P, Helmig R, 1997. Fully-Coupled Solution Techniques for Two Phase Flow in Porous Media. 1, Multigrid solution and large scale computing Advances in Water Resources

Bastian P, Birken K, Lang S, Johannsen K, Neuß N, Rentz-Reichert H, Wieners C, 1997. UG: A flexible software toolbox for solving partial differential equations, Computing and Visualization in Science, 1:27-40

Bastian P, Chen Z, Ewing R, Helmig R, Jakobs H, Reichenberger V, 2000. Numerical Simulation of Multiphase Flow in Fractured Porous Media, Numerical Simulation of Multiphase Flow in Porous Media, Lecture Notes in Physics, Springer Verlag

Corey A T,1954. The Interrelation between Gas and Oil Relative Permeabilities, Producer´s Monthly, Vol. 9, No. 1: 38-44

De Marsily G, 1986. Quantitative Hydrogeology, Academic, Berkeley, Cal.

Flach D, Jockwer N, Kull H, Komischke M, Rothfuchs T, 1997. Preliminary investigations for the characterization and selection of a test field for a two-phase flow experiment in the Äspö Hard Rock Laboratory, GRS-145

Gilman J A, Kazemi H, 1983. Improvements in Simulation of Naturally Fractured Reservoirs, Society of Petroleum Engineers Journal, 8:695 - 707

Helmig R, 1993. Theorie und Numerik der Mehrphasenströmungen in geklüftet-porösen Medien. Technical report, Institut für Strömungsmechanik und Elektronisches Rechnen im Bauwesen, Universität Hannover

Helmig R, Braun C, Emmert M, 1994. MUFTE - A numerical model for simulation of multiphase flow processes in porous and fractured-porous media, Programmdokumentation (HG 208), Technical Report 94/3, Institut für Wasserbau, Universität Stuttgart

Helmig R, Class H, Huber R, Sheta H, Ewing J, Hinkelmann R, Jakobs H, Bastian P, 1998. Architecture of the modular program system MUFTE-UG for simulating multiphase flow and transport processes in heterogeneous porous media, Mathematische Geologie, Band 2,

Hemminger A, Neunhäuserer L, and Helmig R, 1999. The Reliability of a Stochastic Fracture Generator, in F. Stauffer, W. Kinzelbach, K. Kovar, and E. Hoehn, editors, IAHS Publication, number 265, Wallingford, Oxfordshire, UK

Jarsjö J, Geller J, 1996. Groundwater degassing: Laboratory experiments in rock fracture replicas with radial flow, SKB HRL Progress Report HRL-96-13

Jarsjö J, Destouni G, 1998. Groundwater degassing in fractured rock, SKB TR 98-17

Jarsjö J, Destouni G, Gale J, 2001. Groundwater degassing and two-phase flow in fractured rock: Summary of results and conclusions during the period 1994-2000, SKB TR-01-13.

Leverett M C, 1941. Capillary Behavior in Porous Solids, Transactions of the AIME, 142:152 - 169

Liedtke L, Shao H, Alheid H J, Sönnke J, 1999. Material transport in fractured rock / Rock characterization in the proximal tunnel zone, Federal Institute for Geosciences and Natural Resources (BGR), Archiv-Nr, 119006, Hannover

Marschall P, Fein E, Kull H, Lanyon W, Liedtke L, Müller-Lyda I, Shao H, 1999. Conclusions of the Tunnel Near-Field Programme (CTN), Nagra TR 99-07

Persoff P, Pruess K, Myer L, 1991. Two-Phase Flow Visualization and Relative Permeability Measurement in Transparent Replicas of Rough-Walled Rock Fractures, Technical report, University of California

Pruess K, Cox B, Persoff P, 1990. A Casting and Imaging Technique for Determining Void Geometry and Relative Permeability Behavior of a Single Fracture Specimen, Lawrence Berkeley Laboratoy

Pruess K, Tsang Y, 1990. On Two-Phase Relative Permeabilitiy Capillary Pressure of Rough-Walled Rock Fractures, Water Resources Research, 10

Rhén I, Gustafson G, Stanfors R, Wikberg P, 1997. ÄSPÖ HRL – Geoscientific evaluation 1997/5 – Models based in site characterization 1986-1995, SKB, TR-97-06

ROCKFLOW 1988 – 1994. Theorie und Benutzeranleitung zum Programmsystem ROCKFLOW, Teil 1: J. Wollrath / R. Helmig: SM2 - Strömungsmodul für inkompressible Fluide, Institut für Strömungsmechanik und Elektronisches Rechnen im Bauwesen, Universität Hannover

Rodwell W R, Harris A W, Horseman P, Lalieux P, Müller W, Ortiz Amaya L, Pruess K, 1999. Gas migration and two-phase flow through engineered and geological barriers for a deep repository for radioactive waste. EUR 19122 EN

Romm E S, 1966. Fluid Flow in Fractured Rocks, Moscow (translated by W. R. Blake, Bartlesville, OK)

Thiem G, 1906. Hydrogeologische Methoden, Leipzig

Weltest 200, 1997. User Guide Schlumberger, Geoquest , 97A

Wikman H, Kornfeldt K-A, 1995. Updating of a lithological model of the bedrock of the Äspö area, SKB, PR 25-95-04

Witherspoon P A, Wang J S Y, Iwai K, Gale J E, 1980. Validity of Cubic Law for Fluid Flow in a Deformable Rock Fracture.- Water Resource Research, vol. 16, no6, p.1016-1024